

Unveiling Causal Links, Temporal Patterns, and System-Level  
Dynamics of Freshwater Salinization Using Transit Time  
Distribution Theory

Shantanu V. Bhide

Dissertation submitted to the Faculty of the  
Virginia Polytechnic Institute and State University  
in partial fulfillment of the requirements for the degree of

Doctor of Philosophy  
in  
Civil Engineering

Stanley B. Grant, Chair

Kevin J. McGuire

Todd Schenk

John C. Little

September 22, 2023

Manassas, Virginia

Keywords: Freshwater salinization, sodium, transit time distribution, One Water,  
social-ecological systems

Copyright 2023, Shantanu V. Bhide

# Unveiling Causal Links, Temporal Patterns, and System-Level Dynamics of Freshwater Salinization Using Transit Time Distribution Theory

Shantanu V. Bhide

## ABSTRACT

Inland freshwater salinity is rising worldwide and threatens the quality of our water resources, a phenomenon called the freshwater salinization syndrome (FSS). Simultaneously, the practice of indirect potable reuse (IPR) that augments critical water supplies with treated wastewater to enhance water security presents complexities in water quality management. This dissertation explores the complex interplay between FSS and IPR in the Occoquan Reservoir, an important drinking-water source in the Mid-Atlantic United States, within its diverse environmental, social and political contexts. Using extensive data collected over 25 years, this research quantifies contributions of multiple salinity sources to the rising concentration of sodium (a major ion associated with the FSS) in the reservoir and the finished drinking water. These sources encompass two rapidly urbanizing watersheds, a sophisticated water reclamation facility and the drinking water treatment utility. The novel application of unsteady transit time theory reveals that stream salinization can be linked to watershed salt sources using stream water age as a master variable and provides a real-time prediction model for sodium concentration in the reservoir. These results identify substantial opportunities to mitigate sodium pollution and help set the stage for stakeholder-driven bottom-up management by improving the predictability of system dynamics, enhancing knowledge of this social-ecological system and supporting the development of collective action rules.

# Unveiling Causal Links, Temporal Patterns, and System-Level Dynamics of Freshwater Salinization Using Transit Time Distribution Theory

Shantanu V. Bhide

## GENERAL AUDIENCE ABSTRACT

The global rise in freshwater salinity, termed as the freshwater salinization syndrome (FSS), poses a significant threat to water quality in our freshwater resources. The practice of indirect potable reuse (IPR), which involves reusing treated wastewater to supplement and secure our water supplies presents significant challenges in managing water quality. This dissertation delves into the intricate relationship between FSS and IPR, focusing on the Occoquan Reservoir—a vital drinking water source in the Mid-Atlantic United States—within its multifaceted environmental, social, and political contexts. This study uncovers the contributions of various sources of salinity to rising sodium ion concentrations (a key FSS-associated ion) in the reservoir and in finished drinking water. Sodium ions are contributed by road salts, chemicals used in water and wastewater treatment, commercial and industrial discharges, household products (e.g., laundry detergents) and human excretion. An innovative approach of examining the age of water in the stream and in the reservoir outflow enables us to trace origins of salinity within the watershed and predict the concentration of sodium ions in the reservoir, respectively. These findings reveal promising avenues for effectively addressing sodium pollution at this site. Furthermore, this research underscores the significance of convergence research, bringing diverse stakeholders together to develop collaborative strategies to manage freshwater salinization using a bottom-up approach.

# Dedication

*Dedicated to my beloved grandparents, Aaji and Aba, whose unwavering love and support would have filled my heart with pride as I achieve this significant milestone in my life.*

*Your spirit lives on in every step I take.*

# Acknowledgments

I would like to thank my advisor, Stanley Grant, for his continuous guidance, support and unwavering faith in me. Thank you to Todd Schenk for directing the incredible STEP program, for stimulating my interest in science policy and for bringing a social science dimension to this work. Thank you to Kevin McGuire for always being available to help with hydrologic analyses, answer questions and for thought provoking conversations. Finally, thank you to John Little for valuable discussions and feedback that informed this dissertation.

Thank you to my loving wife, Meghana, for her unconditional love and support, and most importantly for always believing in me.

Thank you to my parents, my sister and my family for all the emotional support and encouragement along the way.

I'm incredibly grateful for all the friends and colleagues I gained in graduate school. These valuable relationships make all the hard work worthwhile.

I would like to thank all my co-authors who contributed their time, energy, and brilliant insight to my manuscripts.

I would like to acknowledge several funding sources that made my research possible: US National Science Foundation Growing Convergence Research (GCR) Program (award #2021015), Metropolitan Washington Council of Governments award to S.B.G. and S.K. (contract #21-

001). I would also like to gratefully acknowledge support from Virginia Tech's Graduate Research Development Fellowship, Virginia Water Environment Association's Sonny Roden Memorial Graduate Scholarship, American Water Works Association's Dr. Robert C. Hoehn Graduate Scholarship, Virginia Tech Civil and Environmental Engineering's Thomas J. Grizzard, Jr. Graduate Fellowship and Virginia Tech Policy Destination Area's Science, Technology and Engineering in Policy Graduate Fellowship.

Finally, I would also like to thank Bob Angelotti, Brian Owsenek, Shannon Curtis, Greg Prelewicz, Niffy Saji, Anne Spiesman, Sarah Sivers and all the stakeholders and members of the Executive Committee on the Occoquan System, for providing data and valuable feedback that informed this dissertation.

# Attribution

Several colleagues aided in the writing and research presented in this dissertation. A brief description of their contributions is included here.

Chapter 2: Addressing the Contribution of Indirect Potable Reuse to Inland Freshwater Salinization

S.B. Grant, E.A. Parker, M.A. Rippy, A.N. Godrej, S.S. Kaushal, G. Prelewicz, N. Saji, S. Curtis, P. Vikesland, A. Maile-Moskowitz, M. Edwards, K.G. Lopez, T.A. Birkland and T. Schenk served as co-authors on this paper and assisted with analysis and editing.

Chapter 3: Stream Water Age Reveals Hydrological and Human Drivers of Freshwater Salinization

S.B. Grant, S.S. Kaushal, K. McGuire, K. Prestegard, T. Schenk, S. Curtis, J. Webber, J. Jastram, A. Sekellick served as coauthors on this paper and assisted with analysis and editing. J. Gomez-Velez, E.R. Hotchkiss, M.A. Rippy, P. Vikesland, S. Saxena served as coauthors on this paper and assisted with editing.

Chapter 4: Transit Times Link Sodium Sources to Drinking Water Quality in a One Water System

S.B. Grant and M.Stacy served as co-authors on this paper and assisted with analysis and editing. M.A. Rippy, B. Laursen, H. Whitley, S. Misra, T. Schenk, S.S. Kaushal, T.A. Birkland, P. Vikesland, B. Roston and A. Monofy served as coauthors on this paper and assisted with editing.

# Contents

<b>List of Figures</b>	<b>xii</b>
<b>List of Tables</b>	<b>xvi</b>
<b>1 Introduction</b>	<b>1</b>
<b>2 Indirect potable reuse and freshwater salinization</b>	<b>5</b>
2.1 Introduction . . . . .	5
2.2 Field Site . . . . .	9
2.3 Results . . . . .	11
2.3.1 MLR models for sodium concentration . . . . .	11
2.3.2 Time series of sodium mass load and concentration . . . . .	12
2.3.3 Influence of weather on sodium mass loading . . . . .	14
2.3.4 Sources of wastewater salts . . . . .	16
2.4 Discussion . . . . .	17
2.5 Methods . . . . .	21
2.5.1 Historical monitoring data . . . . .	21
2.5.2 Daily average time series of sodium concentration and mass loads . . . . .	22
2.5.3 Construction of bivariate distributions and conditional probabilities . . . . .	24

2.5.4	Stationarity . . . . .	26
<b>3</b>	<b>Stream Water Age Reveals Drivers of Freshwater Salinization</b>	<b>27</b>
3.1	Introduction . . . . .	27
3.2	Hydrologic and Transit Time Frameworks . . . . .	29
3.3	Stream Water Age and Snowmelt Fraction . . . . .	35
3.4	Conceptual Model of Salinity Sources and Physical and Geochemical Processes	41
3.5	Deicer Application Rates and Stream Salinity . . . . .	44
3.6	Extensibility of Model and Site Observations . . . . .	44
3.7	Conclusions . . . . .	47
<b>4</b>	<b>One Water: transit times, sodium sources and water quality</b>	<b>50</b>
4.1	Introduction . . . . .	50
4.2	The Occoquan One Water System . . . . .	53
4.3	Sources of Sodium along One Water flow paths . . . . .	56
4.4	Transit time model of the reservoir . . . . .	57
4.4.1	Step 1: Define the Control Volume . . . . .	59
4.4.2	Step 2: Perform Water Budget . . . . .	59
4.4.3	Step 3: Select a StorAge Selection (SAS) function . . . . .	61
4.4.4	Step 4: Solve the Age Conservation Equation . . . . .	62
4.4.5	Step 5: Predict Sodium Concentrations . . . . .	62

4.5	Transit time model calibration and performance . . . . .	63
4.6	Second-Level Variable RS7: System Predictability . . . . .	66
4.7	Second-Level Variable A7: Knowledge of the Social-Ecological System . . . . .	67
4.8	Second-Level Variable GS6: Collective Choice Rules . . . . .	69
4.9	Conclusions and Future Directions . . . . .	72
4.10	Methods . . . . .	73
4.10.1	Daily sodium mass loading to the reservoir . . . . .	73
4.10.2	TTD solution, model calibration and validation . . . . .	75
<b>5</b>	<b>Conclusions and Future Directions</b>	<b>78</b>
	<b>Bibliography</b>	<b>84</b>
	<b>Appendices</b>	<b>127</b>
	<b>Appendix A Supplementary Information for Chapter 2</b>	<b>128</b>
A.1	MLR Model Validation and Stationarity Analysis . . . . .	128
A.2	Supplementary Tables and Figures . . . . .	130
	<b>Appendix B Supplementary Information for Chapter 3</b>	<b>137</b>
B.1	HBV Model . . . . .	137
B.2	Hydrologic Model . . . . .	138
B.3	Transient-Transit Time Distribution (T-TTD) Model . . . . .	142

B.3.1	Deriving Solutions for the Mean Age of Water . . . . .	142
B.3.2	Mean Age of Water Leaving a Generic Control Volume . . . . .	143
B.3.3	Mean Age of Water in Interflow . . . . .	146
B.3.4	Mean Age of Water in Groundwater . . . . .	147
B.3.5	Snow Melt Fraction . . . . .	149
B.4	Model Calibration . . . . .	151
B.4.1	Data Sources . . . . .	151
B.4.2	Parameter Inference . . . . .	152
B.5	Estimating Deicer Application Rates . . . . .	153
B.6	Inferring Chloride Concentrations from Specific Conductance . . . . .	155
B.7	Groundwater Specific Conductance in the Mesozoic Lowland HGMR . . . . .	156
B.8	Deconvolution Framework . . . . .	160
<b>Appendix C Supplementary Information for Chapter 4</b>		<b>164</b>
C.1	TTD model calibration procedure . . . . .	164
C.1.1	Evaluation of Water Balance Error . . . . .	164
C.1.2	Shifted-uniform SAS . . . . .	165
C.1.3	Gamma distribution SAS . . . . .	166
C.2	Identifying deicer wash-off events . . . . .	167
C.3	Supplementary Tables and Figures . . . . .	167

# List of Figures

1.1	The Occoquan Reservoir is a vital drinking water source for more than 1 million people across multiple jurisdictions in Northern Virginia. . . . .	3
2.1	Both IPR and human activities in the Bull Run and Occoquan River watersheds contribute to salinization of the Occoquan Reservoir in Northern Virginia, USA. . . . .	9
2.2	Annualized sodium load and concentration in outflow from the Occoquan River, Bull Run and UOSA water reclamation facility. . . . .	12
2.3	Daily sodium load and concentration in outflow from the Occoquan River, Bull Run and UOSA water reclamation facility for an illustrative two-year period (2012–2013). . . . .	15
2.4	Probability density functions of the percentage sodium mass load entering the Occoquan Reservoir from the Occoquan River, Bull Run and UOSA conditioned on rate of flow into the reservoir. . . . .	16
2.5	Sources of sodium discharged by the UOSA water reclamation facility. . . . .	19
3.1	Site map of Flatlick Branch and its location in the Chesapeake Bay watershed.	30
3.2	Conceptual representation of the (a) hydrologic model and (b) transient-transit time distribution (T-TTD) model, along with (c,d) posterior distributions and top-model values for the hydrologic model’s six parameters . . . . .	31

3.3	Comparison of model-predicted and measured timeseries for an illustrative seven months of the validation period. . . . .	34
3.4	Probability distributions of model-predicted stocks and flows. . . . .	36
3.5	Stream water age is a master variable for stream salinization. . . . .	39
3.6	Individual snow melt and rain events. . . . .	40
3.7	A conceptual model for changing salinization patterns. . . . .	43
3.8	Cause-and-effect relationship at Flatlick Branch. . . . .	45
4.1	Change in sodium ion concentrations along flow paths through the Occoquan “One Water” system. . . . .	54
4.2	Daily water balance for the Occoquan reservoir. . . . .	60
4.3	Transit time model predictions. . . . .	65
4.4	Sodium addition by Griffith treatment plant. . . . .	68
4.5	A theory of change for the bottom-up management of sodium ions in the Occoquan Reservoir. . . . .	71
5.1	Role of biofilters in transporting road salts from impervious surfaces to either groundwater or MS4s. . . . .	80
5.2	A grand vision for an integrated transit time model for salt transport in the Occoquan One Water system. . . . .	82
A.1	Schedule of sodium concentration measurements available at ST10, ST45 and UOSA, respectively for the period 2010–2018. . . . .	134

A.2	Calculated and predicted sodium mass loads at ST10 and ST45. . . . .	135
A.3	Measured and predicted sodium concentrations at ST10 and ST45. . . . .	136
B.1	Conceptual representation of the catchment hydrologic model and transit time distribution model. . . . .	139
B.2	Probability distributions for catchment inflow intensities for summer (June, July, August), winter (December, January, February) and all days of the study period. . . . .	141
B.3	Median age of subsurface flow discharged to streams in the Chesapeake Bay watershed. . . . .	148
B.4	Model-predicted median subsurface flow age discharged to Flatlick Branch for different choices of passive groundwater storage depth. . . . .	150
B.5	Master recession curve for the Flatlick Branch watershed. . . . .	153
B.6	Comparison of actual and model predicted winter weather mobilization levels in Northern Virginia for a two-year period. . . . .	154
B.7	Measured chloride vs in-stream specific conductance at Flatlick Branch. . . .	156
B.8	Example of HBV model's limitation. . . . .	161
B.9	Seasonal patterns in model-predicted storage (monthly averaged) in the catch- ment subsurface (vadose zone + active groundwater). . . . .	162
B.10	Model-predicted fraction of snowmelt in groundwater for the validation period.	162
B.11	Illustrative examples of misalignment between peaks in measured specific con- ductance and reductions in the mean stream water age. . . . .	163

C.1	Population density in the Occoquan Reservoir watershed. . . . .	170
C.2	Sodium mass load balance in the Occoquan Reservoir. . . . .	171
C.3	TTD model predictions. . . . .	172
C.4	TTD model residuals. . . . .	173
C.5	Identifying deicer washoff. . . . .	174
C.6	Annually averaged contributions from different sources to sodium mass load in Griffith’s finished drinking water for the years 2014-2020. . . . .	175
C.7	Fraction of UOSA’s flow in daily reservoir inflow and outflow. . . . .	176

# List of Tables

3.1	Definitions and Inferred Values for Hydrologic Model Parameters . . . . .	32
A.1	Top-ranked MLR models of Sodium Concentration at ST10, ST45, and UOSA.	131
A.2	Characteristics of the two watersheds. . . . .	131
A.3	Steps during the drinking water treatment process that introduce sodium and alternative low-sodium or sodium-free methods or compounds. . . . .	132
A.4	External (hold-out) validation metrics. . . . .	133
A.5	ADF, PP and KPSS test results. . . . .	133
B.1	HBV model parameter values. . . . .	138
B.2	Salt Institute’s standard road salt (as NaCl) application rates . . . . .	155
B.3	Groundwater Specific Conductance for Wells in the Mesozoic Lowland HGMR Reported in Posner and Zenome, 1983 . . . . .	157
B.4	Groundwater Specific Conductance for Wells in the Mesozoic Lowland HGMR Reported in Froelich and Zenome, 1985 . . . . .	158
B.5	Groundwater Specific Conductance for Wells in the Mesozoic Lowland HGMR in Virginia from the National Groundwater Monitoring Network ( <a href="http://cida.usgs.gov/ngwmn">cida.usgs.gov/ngwmn</a> )	159
C.1	Rating curve for the Occoquan Reservoir. . . . .	168
C.2	Top-ranked MLR models of Sodium Concentration at ST10 and ST45. . . . .	168

C.3 Optimal SAS function based on RMSE. . . . . 169

# Chapter 1

## Introduction

Inland freshwater salinization, once perceived as a challenge limited to arid and semi-arid climates [42, 219], has transcended geographical boundaries to establish its presence in unexpected regions [59, 103, 105, 199]. This phenomenon, also known as the freshwater salinization syndrome (FSS), is characterized by concurrent trends in rising pH, alkalinity, specific conductance and base cation concentrations in Earth's freshwaters [105]. The FSS has permeated diverse landscapes, impacting ecosystems, communities, and water resources in ways unforeseen. Regions renowned for their humid subtropical, humid continental and humid temperate climates, including the Mid-Atlantic, Northeastern and Midwestern parts of the United States, respectively, have witnessed salinity-related issues in the last two decades [34, 49, 81, 110, 151, 155]. Globally, countries from Canada to Iran have experienced the growing footprint of freshwater salinization [106]. This abrupt and rapid expansion warrants a careful examination of the drivers, patterns, impacts, and management strategies associated with FSS.

Central to this phenomenon is a complex interplay between human activities and natural processes. Anthropogenic actions like road salt use [47, 53, 128, 142], wastewater and industrial discharges [198, 208], and accelerated urban development [54, 141, 204, 220], have emerged as significant contributors to freshwater salinization. These activities release ions (e.g., sodium, calcium, chloride, etc.) into freshwater systems, disrupting their natural chemical balance. Concurrently, natural processes like weathering and erosion are influenced by

shifting climate patterns that further complicate the issue [137, 218]. As temperatures and precipitation patterns evolve, hydrologic pathways shift, altering the fate and transport of salt ions [107]. This complex interplay forms the cornerstone of the FSS, necessitating a holistic investigation that connects human practices, climatic shifts, and their combined impacts.

This dissertation explores freshwater salinization across multiple dimensions, including (1) examining its implications for crucial sustainability goals (Chapter 2), (2) identifying patterns that modulate different salt sources, the associated risk factors for legacy salt pollution and relevant policy and engineering interventions (Chapter 3), and (3) addressing the complex challenges it poses for effective management of salt pollution (Chapter 4), by using the Occoquan Reservoir in Northern Virginia as a test-bed. The Occoquan Reservoir is a vital drinking water source for approximately 1 million people [84] served by the local water purveyor Fairfax Water’s Griffith water treatment plant (orange shading in Figure 1.1). For the past two decades, the reservoir has been grappling with rising salinization, most notably in the form of increased sodium ion concentrations, which now frequently exceeds the United States Environmental Protection Agency’s (EPA) health advisory and lower taste thresholds (20 and 30 mg/L, respectively, see details in Chapter 2) [32]. What further adds to the complexity of this issue is that the Occoquan Reservoir is also the United States’ first large-scale deliberate indirect potable reuse (IPR) system for surface water augmentation [32, 84], i.e., a significant portion of the water in the reservoir is treated wastewater or “reclaimed water” that is discharged from a wastewater treatment plant upstream [32, 84]. Fairfax Water also draws raw water from the Potomac River for its Corbalis water treatment plant, that serves another  $\approx 1$  million people in the Northern Virginia (green shading in Figure 1.1). However, Fairfax Water has the ability to transfer water across the two water distribution systems, for example, during periods of high demand or during events when water quality at either of

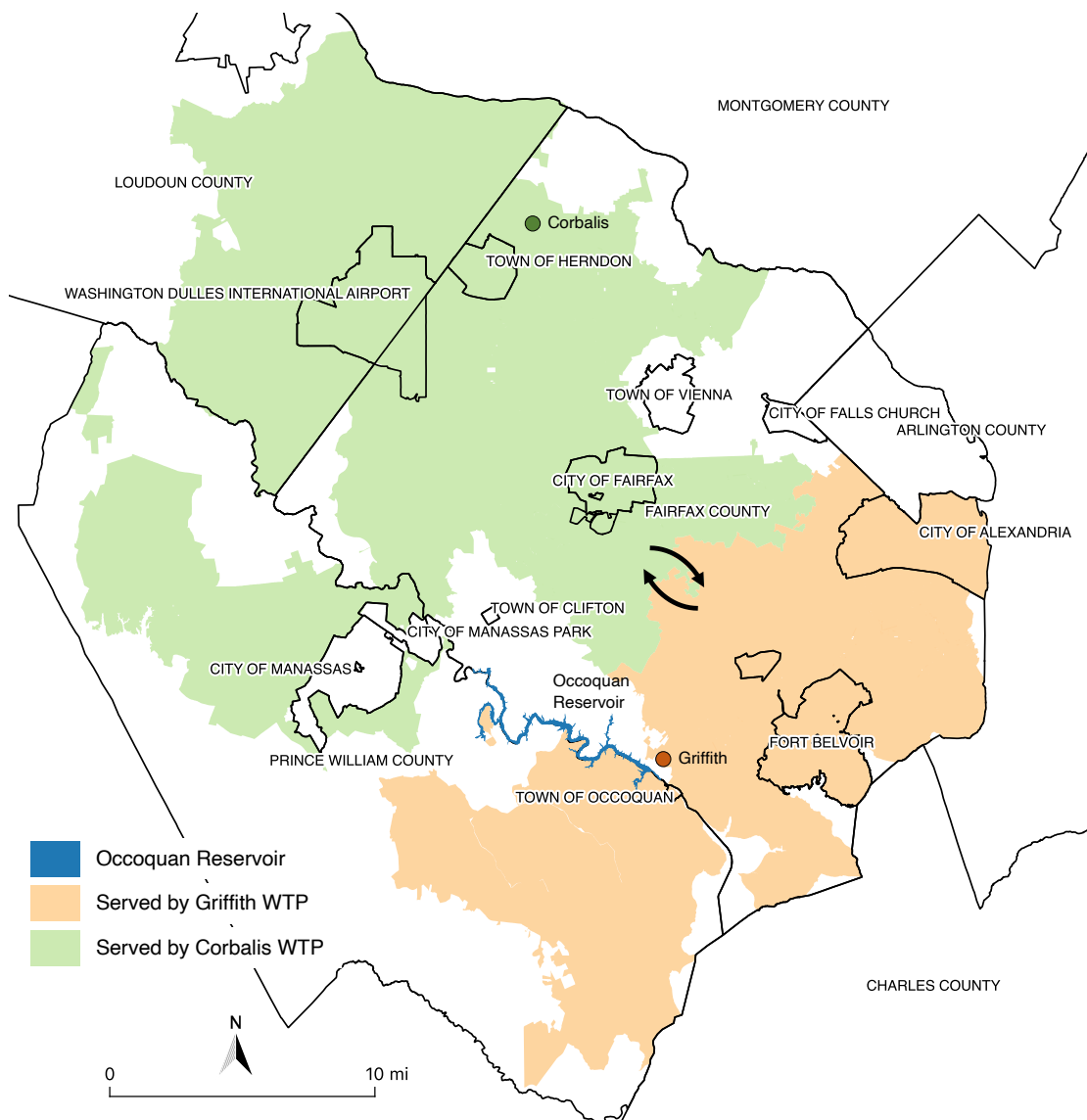


Figure 1.1: The Occoquan Reservoir is a vital drinking water source for more than 1 million people across multiple jurisdictions in Northern Virginia. Shaded polygons depict the geographical area served by each of Fairfax Water’s drinking water treatment plants (closed circles).

the two sources is compromised (see black arrows in Figure 1.1) [35, 144]. Hence, the Occoquan Reservoir’s raw water could potentially serve a much larger population than originally intended. Thus, the Occoquan Reservoir offers a perfect setting to explore the interplay between human activities and the natural environment, making it a prime candidate for

studying and understanding the intricate dynamics of freshwater salinization.

In this dissertation, I first describe a study that explores a potential conflict between two important sustainability goals [32]: (1) minimizing or reversing the FSS and (2) augmenting water supplies through IPR i.e., through the addition of highly treated wastewater to reservoirs and groundwaters [5] (Chapter 2). Results from this study underscore the substantial impact of treated wastewater as a weather-modulated contributor of sodium to the Occoquan Reservoir, and mark a pivotal advancement in comprehending the nuanced challenges associated with managing salt pollution amid escalating water scarcity concerns. Furthermore, these findings pave the way for developing locally tailored interventions to mitigate freshwater salinization. Second, I describe the benefit of mean stream water age as a metric to identify salt sources over multiple timescales in a complex urban watershed that ultimately drains into the Occoquan Reservoir (Chapter 3). This study presents a novel framework that couples hydrologic and transit time models to parse out end members of stream salinity. Third, I present a mechanistic assessment of the upstream sources of sodium, their temporal dynamics and how these sources, both individually and collectively influence the sodium ion concentration in the Occoquan Reservoir and in the final drinking water produced from the Occoquan system (Chapter 4). The results of this study, firmly rooted in unsteady transit time distribution (TTD) theory, provide a real time prediction model for sodium in the Occoquan Reservoir and can serve as a basis for catalyzing stakeholder engaged bottom-up management of sodium in the Occoquan Reservoir and more generally, other unregulated contaminants. Finally, I offer conclusions and suggestions for future research to build on the work presented here.

# Chapter 2

## Addressing the Contribution of Indirect Potable Reuse to Inland Freshwater Salinization

### 2.1 Introduction

While historically a problem only in areas with arid and semi-arid climates, poor agricultural drainage practices, sodic soils and saline shallow groundwater [42, 219], inland freshwater salinization is on the rise across many cold and temperate regions of the United States [59, 103, 105, 199]. The trend is particularly notable in the densely populated Northeast and Mid-Atlantic [34, 81, 110] and agricultural Midwest [49, 151, 155] regions of the country. Globally, inland freshwater salinization has been reported in Canada, Finland, France, Greece, Italy, Iran and Russia [106]. The ions driving inland freshwater salinization vary by location and source but generally include a subset of the so-called major ions (defined here as  $\text{Na}^+$ ,  $\text{Ca}^{2+}$ ,  $\text{Mg}^{2+}$ ,  $\text{K}^+$ ,  $\text{Cl}^-$  and  $\text{SO}_4^{2-}$ ) [103]. Freshwater salinization is part of a broader change in the

---

*This chapter reprinted with permission from:* Bhide, S.V., Grant, S.B., Parker, E.A., Rippey, M.A., Godrej, A.N., Kaushal S., Prelewicz, G., Saji, N., Curtis, S., Vikesland, P., Maile-Moskowitz, A., Edwards, M., Lopez, K.G., Birkland, T.A., & Schenk, T. (2021). Addressing the contribution of indirect potable reuse to inland freshwater salinization. *Nature Sustainability*, 4 699-707.

chemistry of many of Earth’s inland freshwaters—including rising pH, alkalinity and base cation concentration—known as the ‘freshwater salinization syndrome’ (FSS) [105]. Human drivers include the use of deicers on roads and parking lots [14, 34, 47, 53, 128, 142, 195], water softener use [155, 208] wastewater and industrial discharges [198, 208], the weathering of concrete [34, 54, 141, 204, 220] and the accelerated weathering of geologic materials from the release of strong acids and human excavation of rock, which currently exceeds natural denudation processes by an order of magnitude [137, 218] In a recent modelling study, Olson [151] predicted that specific conductance (one measure of salinity) will increase >50% in more than half of US streams by 2100.

The FSS threatens freshwater ecosystem health and human water security. Chloride enrichment of streams is associated with declines in pollution-intolerant benthic invertebrates and loss of critical freshwater habitat [186]. Stream-borne salts can mobilize, through biogeochemical processes, previously sequestered contaminants (for example, nutrients and heavy metals) into sensitive ecosystems and drinking-water supplies [87, 106, 128, 193] potentially reversing hard-won pollution reductions. Salinization of drinking-water supplies can mobilize lead, copper and other heavy metals from ageing drinking-water infrastructure through cation exchange and corrosion [95, 147, 199]. It can also alter the perception of potability— at high enough concentrations, sodium and other salts degrade the taste of drinking water [56]. The World Health Organization and the US Environmental Protection Agency (EPA) have set taste thresholds for the concentration of sodium in drinking water of 200 mg/L NaCl (about 78.6 mg/L Na) and between 30 and 60 mg/L Na, respectively [2, 4]. An EPA drinking-water health advisory of 20 mg/L Na applies to individuals on sodium-restricted diets [4, 56].

In this study, we explore a potential conflict between two important sustainability goals: (1) minimizing or reversing the FSS and (2) augmenting water supplies through the addition of

highly treated wastewater to reservoirs and groundwaters, a practice referred to as ‘indirect potable reuse’ (IPR) [5]. While the number of IPR facilities is modest at present [8, 143], the EPA recently released a draft national Water Reuse Action Plan [12, 131] that promotes IPR and other forms of water reuse and recycling to address, where appropriate, expected water supply shortfalls over the next ten years in 40 of 50 US states [7]. More common is unplanned water reuse, which occurs, for example, when treated wastewater is discharged to surface waters upstream of a drinking-water intake [5]. Rice and Westerhoff [173] estimated that wastewater contributes >50% of the flow in 900 streams across the contiguous United States. Even in water-rich areas of the country, such as Indiana, unplanned water reuse constitutes a sizeable fraction of the water supply (3–134%, with the larger end of the range referring to circulation of wastewater through multiple water systems as it flows downstream) [216].

Human health and ecological concerns associated with IPR and unplanned water reuse typically focus on the impacts of discharged pathogens, nutrients, micropollutants and endocrine disruptors on receiving water quality [5, 64, 91, 173]. These water reuse practices also have the potential to exacerbate the FSS. This is because salt entering a sewage collection system, or added during the treatment process, is not removed by conventional wastewater treatment processes. However, according to the literature, the contribution of treated wastewater to the FSS appears to be strongly context dependent. For example, in a study of salt retention in a rural watershed in New York State, “salt used for deicing accounted for 91% of the sodium chloride input to the watershed, while sewage and water softeners accounted for less than 10% of the input” [110]. By contrast, a study of sodium and chloride surface-water exports from the Dallas/Fort Worth region of Texas found that “the single largest contributor was wastewater effluent” [198]. A reasonable inference from these and other studies is that treated wastewater is a dominant source of freshwater salinity in warmer climates while

deicers drive freshwater salinization in colder climates that receive snowfall [53, 150, 208]. This conclusion is supported by the strong south-to-north increasing trend in stream-specific conductance along the US east coast [142]. However, untreated wastewater drives the FSS across all climates, for example, as documented by the contribution of ageing sanitary infrastructure to stream chloride concentrations in Baltimore and Puerto Rico [104, 165].

We hypothesize that two common methodological shortcomings in the literature may obscure the contribution of IPR and unplanned water reuse to the FSS in colder climates: (1) the focus is often on characterizing salt mass loads (salt mass per time) discharged from wastewater treatment plants, whereas many endpoints of human and ecological concern are concentration based (for example, EPA acute and chronic criteria for in-stream chloride concentrations [3] and the taste thresholds and health advisory for sodium concentrations in drinking water [2, 4, 56]); and (2) salt mass loads discharged from wastewater treatment plants are typically aggregated to monthly or longer period averages, thereby removing higher frequency processes (for example, day-to-day stream-flow variability) that can strongly influence the dilution of wastewater flows in inland freshwaters [5].

We test this hypothesis by analysing a >25-year time series of flow and sodium concentration measurements in the tributaries and highly treated wastewater (reclaimed water) that collectively drain to a regionally important drinking-water reservoir in Northern Virginia. Using regression and a copula-based conditional probability analysis [145] we demonstrate that, of the three sources evaluated here, reclaimed water dominates sodium mass loading to the reservoir during dry weather periods and has the highest sodium concentration year-round. To minimize the potential conflict raised earlier—between managing the FSS and augmenting water supplies through IPR—we suggest a set of locally tailored interventions that collectively increase a region’s salt productivity, defined here as the goods and services produced per unit of salt discharged to inland freshwaters.

## 2.2 Field Site

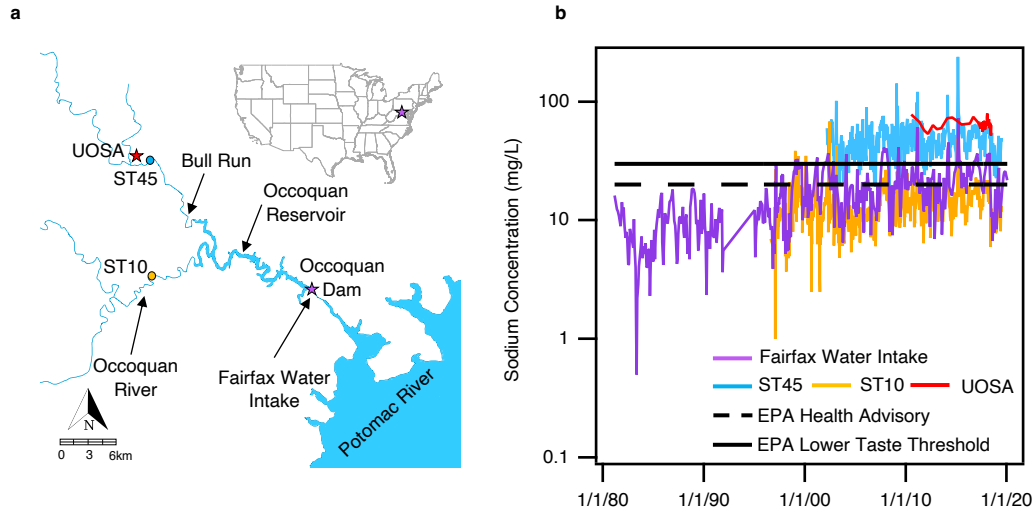


Figure 2.1: **Both IPR and human activities in the Bull Run and Occoquan River watersheds contribute to salinization of the Occoquan Reservoir in Northern Virginia, USA.** **a**, More than 95% of freshwater inflow to the reservoir is from the Occoquan River and Bull Run, which drain mixed undeveloped, agriculture, ex urban and urban landscapes. Shown are key geographical features, including the Occoquan Dam (where Fairfax Water sources its raw water), ion- and flow-monitoring sampling sites on the Occoquan River and Bull Run (monitoring stations ST10 and ST45), and the location on Bull Run where reclaimed water is discharged from the UOSA. Water from the Occoquan Reservoir is treated by Fairfax Water, the water wholesaler, and from there passes to various water distributors. **b**, Forty years of sodium concentration measurements at the Fairfax Water intake and upstream stations (ST10, ST45) and the final reclaimed water discharged by UOSA. Also shown are the EPA health advisory and lower taste threshold for sodium.

The Occoquan Reservoir, located approximately 30 km southwest of Washington DC in Northern Virginia, is one of two primary sources of water supply for nearly 2 million people in Fairfax County, Virginia, and surrounding communities (Fig. 2.1a). Sodium concentration in the reservoir began increasing around 1995 (purple curve in Fig. 2.1b) and now frequently exceeds the EPA's lower taste and health advisory thresholds (horizontal black solid and dashed lines). This trend prompted the local water purveyor, Fairfax Water, to explore planning-level options to address the rising sodium concentration in the reservoir, including

the possible construction of a reverse osmosis treatment upgrade. The irony of desalinating freshwater and the estimated cost (US\$1 billion, not including operating and maintenance costs and a vastly higher carbon footprint [60]) makes identifying, and ideally mitigating, sources of sodium in the reservoir a top regional priority.

On an annual basis, approximately 95% of the water flowing into the reservoir comes from its Occoquan River and Bull Run tributaries. Water from Bull Run includes baseflow and stormwater runoff from the Bull Run watershed ( $1.94 \times 10^8 \text{ m}^3 \text{ yr}^{-1}$ ) together with highly treated wastewater discharged from a water reclamation facility (Upper Occoquan Service Authority, UOSA) ( $3.28 \times 10^7 \text{ m}^3 \text{ yr}^{-1}$ ) located approximately 1.5 km upstream of Bull Run's confluence with the reservoir (red star in Fig. 2.1a). One of UOSA's missions is to improve drinking-water security in the region by augmenting stream flow into the Occoquan Reservoir with a high-quality and drought-proof source of water. Conceived and built in the 1970s, UOSA was the United States' first planned application of IPR for surface-water augmentation and a model for the design and construction of similar reclamation facilities around the world [5]. Water discharged from the Occoquan River comes primarily from baseflow and stormwater runoff from the Occoquan River watershed ( $3.43 \times 10^8 \text{ m}^3 \text{ yr}^{-1}$ ). Thus, possible sources of rising sodium concentration in the reservoir include deicer use and other land-based anthropogenic sodium sources in the rapidly urbanizing Occoquan River and Bull Run watersheds, which have experienced population increases of around 200,000 and 220,000 residents, respectively, over the past 20 years, and salt added to UOSA's sewershed from its >350,000 residential and commercial connections [9]. Indeed, sodium concentration measured in daily flow-weighted composite samples of UOSA's reclaimed water are consistently higher than sodium concentrations measured in grab samples collected downstream on the Bull Run at station ST45 and on the Occoquan River at station ST10 (Fig. 2.1b). Possible sources of sodium within UOSA's sewershed include the down-drain disposal

of sodium-containing drinking water and sodium-containing household products [205], use of water softeners in commercial and residential locations [155, 208], and permitted and non-permitted sodium discharges from industrial and commercial customers. The sodium concentration in UOSA’s effluent may also be elevated due to structural and non-structural water conservation measures that concentrate salts in wastewater [187].

## 2.3 Results

### 2.3.1 MLR models for sodium concentration

Multiple linear regression (MLR) models of sodium concentration generated for each monitoring station (ST10, ST45 and UOSA) were ranked by Bayesian information criterion (BIC) and then validated, depending on the length of the data record, using either leave-one-out cross validation (LOOCV) or the hold-out method (see Section 2.5 and Appendix A for details). The top-ranked MLR models (Table A.1) are significant ( $p < 0.001$ ) and capture between 31% and 87% of the measured variance in log-transformed sodium concentration (adjusted  $R^2$  values and other model statistics are reported in Table A.1). The top-ranked MLR model for sodium concentration at ST45 captures the most variance ( $R^2 = 87\%$ , hold-out  $R^2 = 81\%$ ), and its predictor variables include in situ specific conductance (positive correlation), maximum snow depth over the previous two weeks (positive correlation), log-transformed flow (negative correlation) and season (higher sodium concentration during the winter season). The top-ranked MLR model for sodium concentration in UOSA’s reclaimed water captures the second-most variance ( $R^2 = 54\%$ , LOOCV- $R^2 = 51.6\%$ ) and has as its only predictor variable specific conductance measured on flow-weighted composite reclaimed water samples (positive correlation). The top-ranked MLR model for sodium concentration

at ST10 explains the least variance ( $R^2 = 31\%$ , hold-out  $R^2 = 15\%$ ), presumably because in situ specific conductance measurements were not available at this station. Predictor variables for sodium concentration at ST10 include log-transformed flow (negative correlation), maximum snow depth over the previous two weeks (positive correlation) and number of days below freezing in the previous two weeks (positive correlation). In summary, sodium concentration at these three stations is (1) positively correlated with specific conductance measured either in situ (ST45) or on flow-weighted composites of the reclaimed water (UOSA); (2) positively correlated with environmental variables (antecedent snow, freezing weather and winter season) likely to be associated with deicer use (ST10 and ST45); and (3) negatively correlated with flow (ST10 and ST45), implying that stormwater tends to dilute in-stream sodium concentration.

### 2.3.2 Time series of sodium mass load and concentration

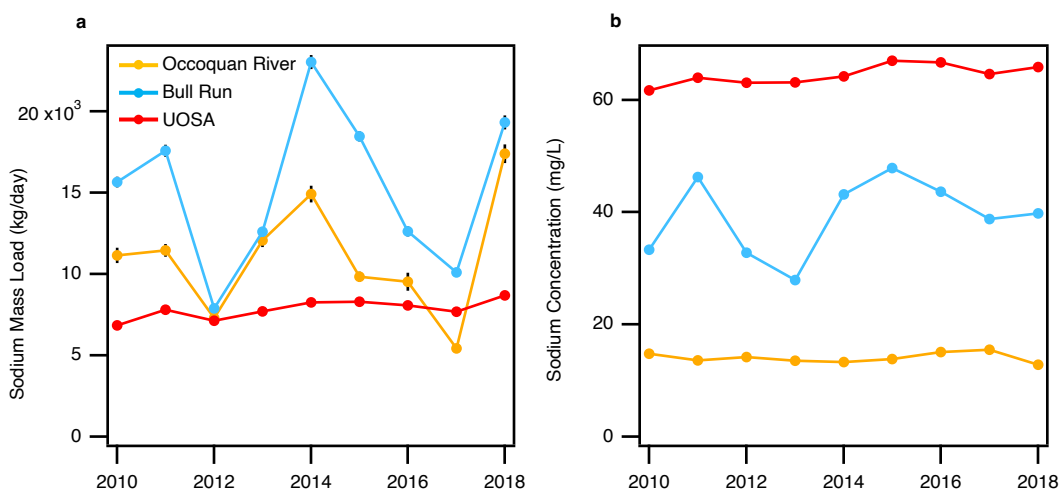


Figure 2.2: **Annualized sodium load and concentration in outflow from the Occoquan River, Bull Run and UOSA water reclamation facility.** **a**, Sodium mass loads. **b**, Sodium concentration. Error bars represent 95% prediction intervals (in some cases, too small to be visible).

Synthetic time series of sodium concentration (generated using the top-ranked and validated MLR models described in the preceding) were combined with daily flow measurements at ST10, ST45 and UOSA to generate daily predictions (from 2010 through 2018) of sodium mass load and concentration in flows from the three putative sources evaluated in this study—Occoquan River watershed, Bull Run watershed and UOSA water reclamation facility (Section 2.5.2). When these daily predictions are aggregated to annual averages, the results are in line with previous reports for regions that experience seasonal snowfall; namely, annual mass loading of sodium to the Occoquan Reservoir is dominated by the two watershed sources, not by UOSA (Fig. 2.2a). Consistent with Fig. 2.1b, however, the annualized sodium concentration in UOSA’s reclaimed water ranges between 60 and 70 mg/L, well above EPA’s lower threshold for taste (30 mg/L) and >1.5 and >4.5 times above the annualized sodium concentration in flow from the Bull Run and the Occoquan River watersheds, respectively (Fig. 2.2b).

These annualized results could be interpreted to imply that UOSA’s reclaimed water contributes a relatively minor portion of sodium mass loading to the Occoquan Reservoir. However, the story is more nuanced when evaluated on a day-by-day basis (Fig. 2.3). During extended periods of reduced precipitation, sodium mass load from UOSA’s reclaimed water frequently exceeds mass loads from either the Occoquan River or Bull Run watershed (see four vertical grey stripes, Fig. 2.3b). During wet weather, however, sodium mass loads from the two watersheds consistently exceed those from UOSA, often by >200-fold (note that the sodium mass load axis in Fig. 2.3b is logarithmic). Spikes in wet weather sodium mass loading from the two watersheds dominate the annual load estimates, giving the potentially misleading impression that UOSA’s reclaimed water is a minor contributor to sodium in the reservoir (compare with Fig. 2.2a). These daily and annual sodium mass load estimates should be relatively robust to uncertainty in the MLR-generated synthetic sodium

concentration time series because most of the variance in the daily mass load predictions ( $R^2 = 66\%$ ,  $91\%$  and  $82\%$  for Occoquan River watershed, Bull Run watershed and UOSA, respectively) is attributable to measured daily average flow at each station.

Consistent with the annualized results (Fig. 2.2b), on a day-to-day basis the sodium concentration in UOSA’s reclaimed water is nearly always higher than the sodium concentration in outflows from the Occoquan River and Bull Run watersheds (Fig. 2.3d). Sodium concentration in outflow from the Bull Run watershed is generally higher than in outflow from the Occoquan River watershed, consistent with the latter’s greater impervious surface fraction (Table A.2).

### 2.3.3 Influence of weather on sodium mass loading

Application of a copula-based conditional probability analysis to daily predictions of sodium mass load for the period 2010–2018 (Section 2.5.3) confirms that UOSA’s reclaimed water dominates the sodium mass load entering the reservoir from the Occoquan River and Bull Run during dry and median weather conditions (Fig. 2.4). UOSA’s percentage contribution to sodium mass loading varies from 60% to 80% during dry conditions (corresponding to cumulative flow from the Occoquan River and Bull Run of  $\langle Q_{Total} \rangle = 2.55 \text{ m}^3 \text{ s}^{-1}$ ), 30% to 50% during median conditions ( $\langle Q_{Total} \rangle = 6.91 \text{ m}^3 \text{ s}^{-1}$ ) and 5% to 25% during wet conditions ( $\langle Q_{Total} \rangle = 31.0 \text{ m}^3 \text{ s}^{-1}$ ). The Occoquan River and Bull Run watersheds exhibit the opposite pattern, contributing a greater percentage of the overall sodium load during wet weather periods. During wet weather, sodium mass loading from the Bull Run watershed is, on average, higher than sodium mass loading from the Occoquan River watershed, consistent with the land-use data in Table A.2.

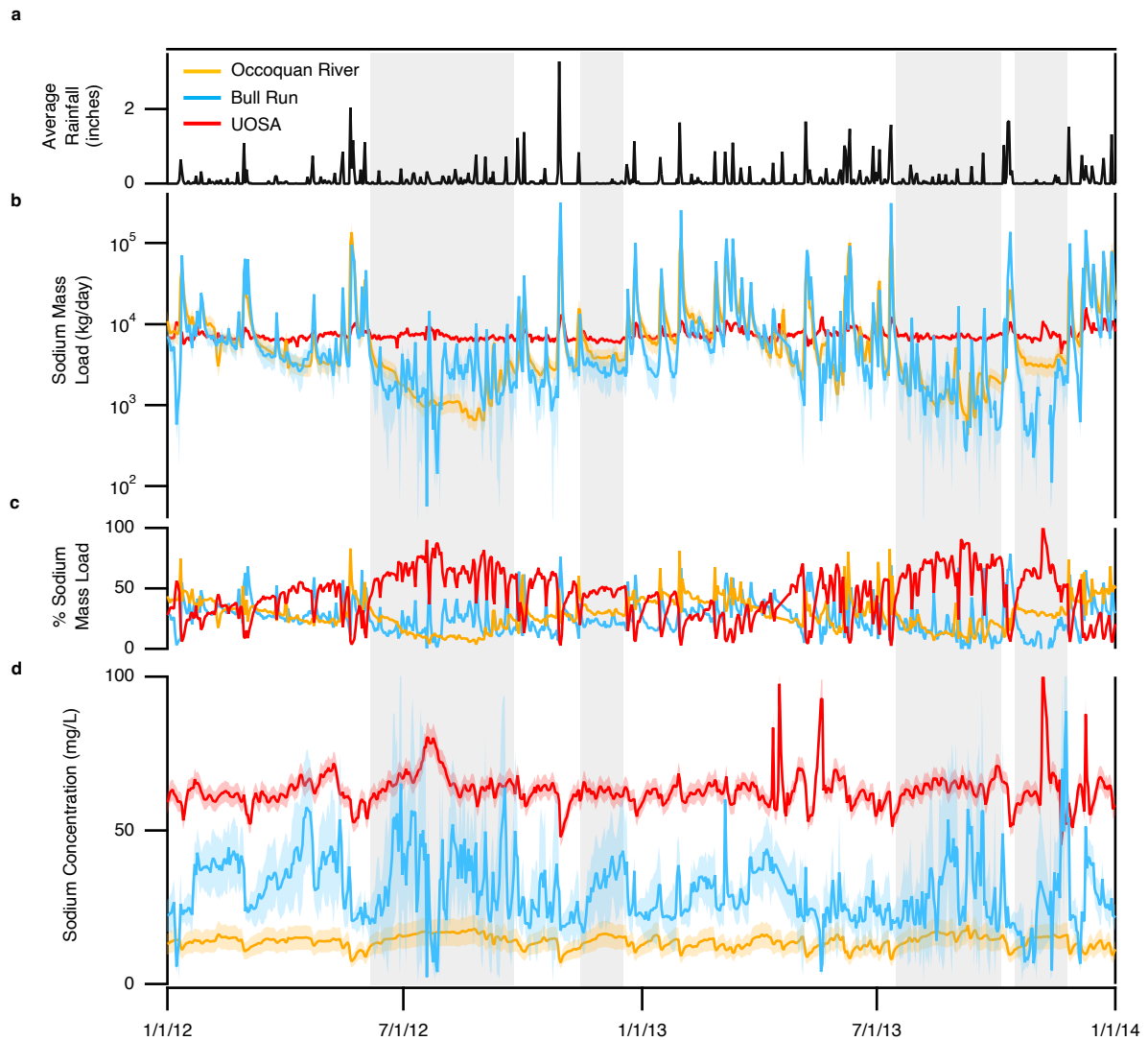


Figure 2.3: **Daily sodium load and concentration in outflow from the Occoquan River, Bull Run and UOSA water reclamation facility for an illustrative two-year period (2012–2013).** **a**, Daily average rainfall in the watershed calculated using the Thiessen polygon method. **b**, Daily sodium mass load entering the reservoir from each source (Occoquan River, Bull Run and UOSA). **c**, Percentage of daily sodium mass load entering the reservoir from each source. **d**, Daily sodium concentration in each source. Grey vertical stripes indicate extended periods of reduced precipitation. Coloured ribbons represent 95% prediction intervals.

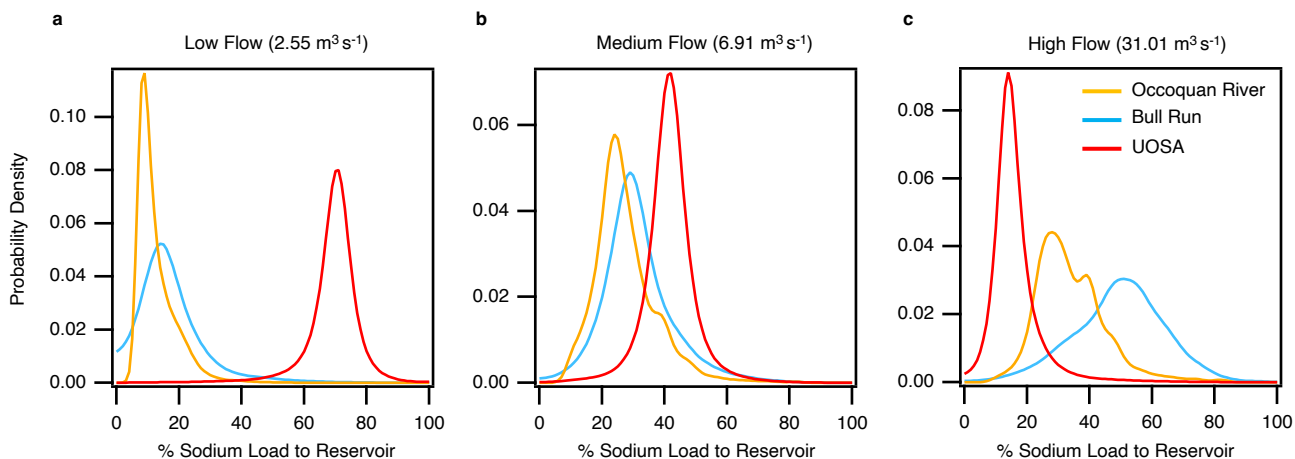


Figure 2.4: **Probability density functions of the percentage sodium mass load entering the Occoquan Reservoir from the Occoquan River, Bull Run and UOSA conditioned on rate of flow into the reservoir.** **a**, Low flow ( $2.55 \text{ m}^3 \text{ s}^{-1}$ ). **b**, Medium flow ( $6.91 \text{ m}^3 \text{ s}^{-1}$ ). **c**, High flow ( $31.0 \text{ m}^3 \text{ s}^{-1}$ ). The salient feature of each curve is the range of values on the horizontal axis for which there is non-zero probability density. The peak height of each curve is determined by the unit area of each probability density function.

### 2.3.4 Sources of wastewater salts

The results presented in the preceding subsection support our hypothesis that, when evaluated on a day-to-day basis, discharge from water reclamation facilities can be an important component of the freshwater sodium budget even in colder climates, such as the Mid-Atlantic US, where deicers are a well-documented cause of inland freshwater salinization [14, 34, 47, 53, 81, 128, 142, 195]. Where is the sodium in UOSA’s reclaimed water coming from? UOSA water reclamation facility serves as a conduit through which sodium from myriad sources (watershed deicers, water treatment processes, household products, commercial and industrial discharges, drinking water treatment, and wastewater treatment) are focused into a single point source discharge (Fig. 2.5a). On the basis of data provided by the utility, we estimate that, on an annual average, 36% of the daily sodium mass load in UOSA’s reclaimed water ( $7,600 \pm 590 \text{ kg d}^{-1}$ ) is partitioned between chemicals used in water and wastewater treatment (for pH adjustment, chlorination, dechlorination and odour control),

a single permitted discharge from a microfabrication facility and human excretion (human excretion was estimated by multiplying UOSA's service population (351,906) [9] by a mean per-person urine excretion rate of  $3.608 \text{ g Na}^+ \text{ d}^{-1}$  (ref. [44]) (Fig. 2.5b)). The source of the remaining 64% is unknown but presumably includes contributions from the down-drain disposal of sodium-containing drinking water (  $2.5 \text{ mg/L Na}$ ) from Lake Manassas, the Potomac River and the Occoquan Reservoir, as well as sodium-containing household products that eventually end up in the sanitary sewer system.

## 2.4 Discussion

Given these results for the Occoquan Reservoir, how can the potential conflict between (1) minimizing freshwater salinization; and (2) promoting water security through IPR be addressed? One possible conceptual framework, borrowed from soft-path approaches for enhancing human water security [79, 82] focuses on a variety of behavioural and technological interventions, applied at various scales, for increasing the goods and services produced per unit of salt discharged to inland freshwater; that is, improving salt productivity. As applied to sodium, we envision at least four ways in which salt productivity can be improved: (1) reduce watershed sources of sodium that enter the water supply (such as from deicer use); (2) enforce more-stringent pre-treatment requirements on industrial and commercial dischargers; (3) switch to low-sodium water and wastewater treatment methods; and (4) encourage households in the sewershed to adopt low-sodium products. These are considered in turn.

Because potable water supply and sewage collection systems are inextricably linked (Fig. 2.5a), factors that contribute salt to the former ultimately contribute salt to the latter as well. As mentioned earlier, many different sources (apart from treated wastewater) contribute salt to inland freshwaters, most notably deicer use in northern climates but also

untreated sewage (such as from failing sanitary sewer systems [165]) and erosion of civil infrastructure (such as from concrete drainages [220]). With respect to deicers, their use on roadways can be curtailed without a reduction in public safety (for example, through the development of advanced pavement materials [125]). However, interventions at the watershed scale raise many questions across various domains, including human behaviour (how do we induce residents to be more conservative about their use of deicers on parking lots and driveways, and what is the ‘right amount’ of deicer they should be using?); hydrology (what are the hydrologic pathways by which salt moves through watersheds, and what are their timescales?); ecology (how do the changing concentrations and compositions of salinized waters alter biological communities and ecosystem processes?); and engineering design (are we unintentionally creating legacy salt pollution by adopting stormwater best management practices that transfer road salts to groundwater?). In such complex socio-hydro-ecological systems, well-intended interventions can have adverse consequences and so-called aggregation effects in which “desirable outcomes at a larger scale conceal inequalities and, as such, distributional injustices at the local scale” [22]. For example, deicer use might be reduced by lowering expectations for clean roads and public transportation during winter storms, but such actions could also limit access to free and subsidized school breakfast and lunch programmes for low-income children and thereby exacerbate child hunger [201].

Alternatively, more-stringent pre-treatment requirements can be imposed on commercial and industrial activities that discharge to the sewershed [91], although this will inevitably raise questions about potential economic trade-offs. For example, nearly 14% of the annual sodium load discharged by UOSA can be traced to a single chip fabrication facility (Fig. 2.5b). While imposing more-stringent sodium discharge limits on the facility would certainly reduce sodium loading to the reservoir, it might also curtail plans to expand the facility and add up to 1,000 high-tech jobs to the local economy [11].

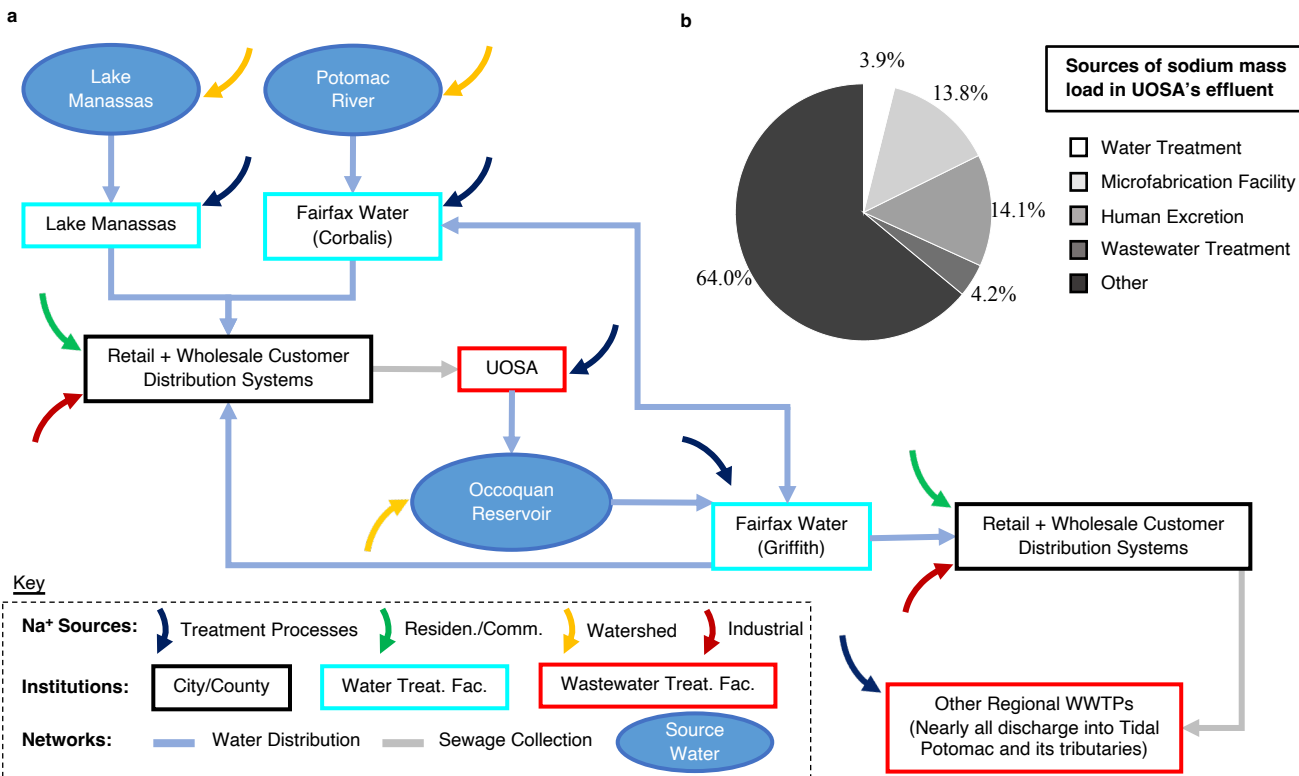


Figure 2.5: **Sources of sodium discharged by the UOSA water reclamation facility.** **a**, Schematic representation of the interdependent drinking-water distribution and sewage collection networks in the Occoquan watershed and surrounding area. Under normal conditions, the portion of the sewage network draining to UOSA receives water from the Fairfax Water Corbalis and the Lake Manassas water treatment plants, although some water from the Fairfax Water Griffith water treatment plant may also contribute to UOSA's inflow (forming a system-scale semi-closed loop for the circulation of sodium through the Occoquan Reservoir). **b**, Source breakdown for the annual sodium mass load in UOSA's reclaimed water. WWTP: wastewater treatment plant.

Changes in centralized water and wastewater treatment practices are also possible. Chlorine is a cost-effective and well-established method for destroying viruses, bacteria and protozoa, including those responsible for waterborne human disease [5]. Wastewater treatment plants that use chlorine for disinfection must also dechlorinate to prevent harm to downstream aquatic life. Dechlorination is typically achieved through the addition of sulfur dioxide or sulfite salts, including sodium sulfite, sodium bisulfite and sodium metabisulfite, thereby increasing the sodium content of the water [121]. Dechlorination dosages depend on the

compound used; for example, sodium sulfite, sodium bisulfite and sodium metabisulfite require 1.8–2.0, 1.5–1.7 and 1.4–1.6 mg/L of chlorine residual, respectively [55]. Therefore, judicious choice of a dechlorinating agent or the use of alternative disinfectants (for example, ultraviolet light) can help reduce sodium mass loading from wastewater treatment. Interestingly, the use of ultraviolet light for disinfection might also reduce micropollutant concentrations in the reclaimed water [177].

Likewise, there are multiple steps in the drinking-water treatment process where sodium can be introduced. Drinking-water facilities should identify which of their processes contribute sodium and what alternative chemicals or processes might be adopted (see Table A.3), while being mindful of potential unintended consequences. As an example of a potential unintended consequence, adoption of the coagulant ferrous sulfate for drinking-water treatment, while potentially minimizing the addition of sodium, could accelerate the corrosion of downstream sewer infrastructure [169]. As with the chip fabrication facility example, economic constraints, as well as a risk-averse public service culture [166], may limit what can be achieved in practice. Finally, improvements in salt productivity are possible at the household scale. Most research on household product ionic composition has been conducted in countries interested in greywater recycling as a water conservation strategy. For example, in 2008 a comprehensive study of sodium mass loads from household products in Melbourne, Australia, reported that [205] (1) laundry and dishwashing products contribute orders of magnitude more to sodium mass loads than do other household products; (2) median sodium mass loads from household products are 58–300% higher than those from human excretion; (3) mass loads of sodium can vary across product brands, which leads to high variability in the salinity of household sewage; and (4) product switching has the potential to reduce sodium mass loading to the sewershed. Assuming human excretion accounts for about 14% of the UOSA sodium mass loads (Fig. 2.5b), these Australian results suggest that household

products could account for another 10–51%; notably, the upper limit would nearly close UOSA’s annual sodium mass balance. Educational and social marketing campaigns aimed at informing consumers and manufacturers about the FSS, with the goal of fostering product and behavioural changes, could ultimately reduce salt loading from common household products such as detergents [136].

## 2.5 Methods

### 2.5.1 Historical monitoring data

To characterize the relative sodium contributions of the Bull Run watershed, the Occoquan River watershed and UOSA’s reclaimed water to the Occoquan Reservoir, we utilized data from a long-term (>25 years) sampling program that was originally established to monitor the effects of UOSA’s water reclamation activities on water quality in the reservoir. We focused specifically on a 12-year period, 2006–2018, during which discrete surface-water samples were collected weekly or semi-weekly from the Occoquan River and the Bull Run monitoring stations (ST10 and ST45,  $N = 395$  and  $338$ , yellow and blue circles, Fig. 2.1a) and analysed for a suite of water-quality parameters, including sodium concentration. Continuous measurements ( $f=1 \text{ hr}^{-1}$ ) of specific conductance ( $N=106,708$  at ST45) and flow ( $N=160,446$  and  $170,179$  at ST10 and ST45, respectively) were also available during this time frame. Daily average measurements of discharge from UOSA were provided by the utility for the period 2010–2018 ( $N=2,941$ ), along with measurements of specific conductance ( $N=2,943$ ) and sporadic measurements of sodium concentration ( $N=68$ ) on daily flow-weighted composite samples of their reclaimed water.

## 2.5.2 Daily average time series of sodium concentration and mass loads

From the monitoring data described in the preceding, we set out to evaluate the relative contributions of three key sources—the Occoquan River watershed, the Bull Run watershed and UOSA—to sodium mass load (mass per time) and concentration (mass per volume) entering the Occoquan Reservoir under various weather and environmental conditions. Several limitations with the monitoring data had to be overcome (cf. ref. [216]): (1) flow and sodium concentration measurements at ST45 reflect the combined inputs from the Bull Run watershed and the UOSA water reclamation facility; (2) at ST10 and ST45, sodium concentrations were measured on grab samples, whereas sodium concentrations reported by UOSA were measured on daily flow-weighted composites of their final product water; (3) the sampling schedules at ST10 and ST45 were asynchronous (grab samples were collected at different times on any given day, or on different days); and (4) while sodium measurements at ST10 and ST45 were collected every other week for the entirety of the study period (2010–2018), sodium measurements on UOSA’s composite samples were sporadic and infrequent (Fig.A.1).

To address these challenges, for the period 2010–2018 (for which all of the required data resources were available), we constructed synthetic daily time series of average sodium mass load and concentration at the three monitoring locations as follows: (Step 1) at each monitoring station, an MLR model of log-transformed sodium concentration (dependent variable) was prepared (glmulti package [41] in R Statistical Software, R Core Team) by adopting, on the basis of stakeholder recommendations, the following set of potential environmental covariates (independent variables): (1) hourly stream flow (ST45 and ST10) or daily average reclaimed water discharged to Bull Run (UOSA), (2) maximum daily rainfall in the preced-

ing two weeks, (3) maximum daily snow depth in the preceding two weeks, (4) number of days below freezing in the preceding two weeks, (5) season (as represented by sine and cosine functions with annual periodicity), and (6) either hourly in situ measurements of specific conductance (ST45) or measurements of specific conductance on daily flow-weighted composites of the reclaimed water (UOSA). For model validation we used the hold-out method at ST10 and ST45 and LOOCV at the UOSA station (see Supplementary Information for details); (Step 2) the populations of MLR models generated for each monitoring station in Step 1 were ranked according to BIC to identify the most parsimonious model, accounting for the trade-off between model fit and model complexity [188]. If the top-ranked models for a given station were within two BIC units, they were further ranked by LOOCV root mean squared error; (Step 3) the final top-ranked MLR model for each station from Step 2 was then used to generate an eight-year (2010–2018) synthetic time series of hourly (ST10 and ST45) or daily (UOSA) sodium concentration; and (Step 4) the synthetic sodium concentration time series from Step 3 were combined with hourly (ST10 and ST45) or daily (UOSA) flow measurements at each station and then aggregated to daily and annual sodium concentration and mass load using the `aggregateSolute` command in the USGS software package `Loadflex` (for error propagation we adopted the default data correlation structure, which assumes a unit correlation if two samples are collected on the same calendar date and zero correlation otherwise; cf. ref. [17]). The result was three fully aligned eight-year synthetic time series of daily and annual average sodium mass load and concentration (denoted here by the symbols  $\langle L \rangle$  and  $\langle C \rangle$ , respectively) and associated prediction intervals at each of the three monitoring stations. As noted, ST45 receives water and sodium from both the Bull Run watershed and the UOSA water reclamation facility. The contribution of the Bull Run watershed to daily average sodium concentration and mass load was therefore isolated by mass balance where  $\langle Q \rangle$  denotes daily average flow measurements and the subscript ‘BR’ refers to the Bull Run watershed:

$$\langle C_{BR} \rangle = \frac{\langle L_{ST45} \rangle - \langle L_{UOSA} \rangle}{\langle Q_{ST45} \rangle - \langle Q_{UOSA} \rangle} \quad (2.1a)$$

$$\langle L_{BR} \rangle = \langle L_{ST45} \rangle - \langle L_{UOSA} \rangle \quad (2.1b)$$

From these synthetic time series, we constructed daily time series for the percentage contribution of the Occoquan River watershed ('OccRiv'), Bull Run watershed ('BullRun'), and UOSA reclaimed water ('UOSA') to the total sodium mass entering the reservoir from the Occoquan River and Bull Run (which, as noted earlier, contributes 95% of freshwater flow into the reservoir):

$$\%Load_{OccRiv} = 100 \frac{\langle L_{ST10} \rangle}{\langle L_{ST10} \rangle + \langle L_{ST45} \rangle} \quad (2.2a)$$

$$\%Load_{BullRun} = 100 \frac{\langle L_{BR} \rangle}{\langle L_{ST10} \rangle + \langle L_{ST45} \rangle} \quad (2.2b)$$

$$\%Load_{UOSA} = 100 \frac{\langle L_{UOSA} \rangle}{\langle L_{ST10} \rangle + \langle L_{ST45} \rangle} \quad (2.2c)$$

### 2.5.3 Construction of bivariate distributions and conditional probabilities

Equations 2.2a - 2.2c provide daily predictions for the relative contribution of each source to sodium mass discharged to the reservoir from the Occoquan River and Bull Run. How are these predictions modulated by local weather conditions? To answer this question, we adopted the cumulative daily discharge of water flowing into the reservoir from the Occoquan River and Bull Run as a proxy of local weather conditions:  $\langle Q_{Total} \rangle = \langle Q_{ST10} \rangle + \langle Q_{ST45} \rangle$ .

Marginal probability distributions of percentage sodium mass load from Equations 2.2a - 2.2c ( $\%Load_{OccRiv}$ ,  $\%Load_{BullRun}$ ,  $\%Load_{UOSA}$ ) and log-transformed values of cumulative stream flow from the Occoquan River and Bull Run ( $\ln\langle Q_{Total} \rangle$ ) were then joined by a copula to yield three bivariate cumulative distribution functions of the form  $F_{LQ}(l, q) = C[F_L(l), F_Q(q)]$ , where  $L$  and  $Q$  are random variables for the percentage sodium mass load from a particular source and cumulative discharge from the Occoquan River and Bull Run, respectively,  $l$  and  $q$  are specific values of these random variables, and  $C$  is the cumulative distribution function form of the copula function [129]. The copula was selected on the basis of BIC ranking of the Plackett and Archimedean copula families optimized to our daily time series of percentage mass load (from Equations 2.2a - 2.2c) and measured daily cumulative discharge from the Occoquan River and Bull Run using the MATLAB software package MvCAT [181]. The probability density function (PDF) of percentage sodium mass load from each of the three sources conditioned on a specific cumulative discharge was then calculated as follows [129]:

$$f_{L|Q}(l|q) = c[F_L(l), F_Q(q)]f_L(l) \quad (2.3)$$

Here, the function  $c$  is the PDF form of the copula function and  $f_L(l)$  is the PDF form of the marginal distribution for the percentage of sodium mass load to the Occoquan Reservoir from a particular source. We focused on three conditioning events corresponding to low (10th percentile), medium (50th percentile) and high (90th percentile) cumulative discharge ( $\langle Q_{Total} \rangle = 2.55 \text{ m}^3 \text{ s}^{-1}$ ,  $6.91 \text{ m}^3 \text{ s}^{-1}$  and  $31.0 \text{ m}^3 \text{ s}^{-1}$ , respectively). These three conditioning events represent dry, average and wet weather conditions, respectively.

### 2.5.4 Stationarity

The time-series data used for the copula analysis and to generate the MLR models were tested for stationarity (tseries package in R Statistical Software, R Core Team [167]) using the Augmented Dickey-Fuller test, the Phillips-Perron test and the Kwiatkowski-Phillips-Schmidt-Shin test (Table A.5 and Section A.1). These test statistics indicate that measured sodium concentration and all independent variables included in our analysis are stationary over the period for which the MLR and copula analyses were conducted (2010–2018).

# Chapter 3

## Stream Water Age Reveals Hydrological and Human Drivers of Freshwater Salinization

### 3.1 Introduction

Inland freshwater salinity is rising across many regions of the United States as well as globally, a phenomenon called the freshwater salinization syndrome [105]. Salinization of water supplies affects the taste of drinking water [56] and accelerates the leaching of heavy metals, such as lead, from water plumbing and water pipes through dezincification and galvanic corrosion [161]. Freshwater salinization mobilizes heavy metals, nutrients and radionuclides along hydrologic flow paths [87, 106], and is associated with declines in pollution-intolerant benthic invertebrates in streams [186]. The ecosystem-level impacts of freshwater salinization are just beginning to be understood [93]. Many hydrologic systems have long memories [118], which can lead to legacy pollution [207], wherein salt and other contaminants continue to be released to sensitive receiving waters days-to-centuries after all inputs have ceased [86, 215].

Evidence points to the application of deicers, such as sodium chloride (or “rock salt”), on roads and parking lots as a primary cause of freshwater salinization in cold and temperate

climates all across the world, particularly in the Mid-Atlantic, Northeastern, and Northern regions of the United States [94], Canada [63], Sweden [128], United Kingdom [178] and the Alps [148]. Identifying context-specific cause-and-effect relationships between deicer application and inland freshwater salinization (e.g., with the goal of informing engineering and policy solutions) is complicated, however, by the spatially and temporally variable flow paths that transport deicers from their points of application to impacted water bodies. These flow paths include conventional stormwater drainage systems in regions with substantial impervious land cover [109], as well as natural flow paths through the vadose zone and shallow and deep groundwater [97]. Interpretation of freshwater salinity patterns is further complicated by the tendency of some ions to undergo ion exchange [108] and the contribution of diffuse ion sources beyond deicers, including septic systems [102], wastewater discharges [32], mineral dissolution along subsurface flow paths [15], and leaking sewage collection systems [70].

We hypothesized that in a complex urban catchment, insight into the sources and processes that influence stream salinity can be revealed by combining high-frequency measurements of in-stream salinity with high-frequency estimates of stream water age and snow melt fraction. Here, stream water age is defined as the elapsed time an average water parcel spends moving along surface and subsurface flow paths before reaching a stream, while snow melt fraction is the fraction of streamflow that can be attributed to one or more previous snow melt events. To test this hypothesis we developed and implemented a generalizable modeling framework, based on transient transit time distribution (T-TTD) theory [97], to estimate the time-varying mean age of water in Flatlick Branch, a deicer-impacted stream draining a 10.9 km<sup>2</sup> urban catchment (32% impervious cover in 2016) located in the Mesozoic Lowland hydrogeomorphic (HGMR) province, also known as the Triassic Lowland province of Northern Virginia (Figure 3.1) [71, 120, 214]. Flatlick Branch is tributary to the Occoquan Reservoir,

a critical source of drinking water for up to 1 million people in Northern Virginia. Sodium concentrations have been rising steadily in the reservoir over the last two decades and now routinely exceed EPA drinking water guidelines for taste ( $30 \text{ Na}^+ \text{ mg/L}$ ) and sodium intake for individuals on a severely restricted salt diet ( $20 \text{ Na}^+ \text{ mg/L}$ ) [32, 84].

Our study examines the utility of model-predicted stream water age and snow melt fraction for identifying: (1) salt sources responsible for the variation in stream salinity over timescales ranging from hours to decades; (2) risk factors for long-term build-up of deicer salt in groundwater and consequent legacy salt pollution; (3) deicer application rates from routine measurements of stream flow and specific conductance; and (4) policy and engineering interventions that could help mitigate the contribution of deicers to inland freshwater salinization.

## 3.2 Hydrologic and Transit Time Frameworks

Hourly estimates for the mean age of water in Flatlick Branch, along with the fraction of streamflow contributed by snow melt, were estimated using the modeling approach outlined by Benettin et al. [23] for chloride travel times through the comparably sized  $3.7 \text{ km}^2$  Upper Hafren catchment in Wales, UK. The two main differences between our modeling framework and Benettin et al. [23] is that we allow for the direct input of runoff to the stream (e.g., through community drainage systems that are typically built in urbanized catchments to protect against flooding [185]), and we track the accumulation and melting of snow over time (because deicers are often released to a catchment in snow melt [48, 195]). We linked three sub-models (Sections B.1, B.2 and B.3): (1) hourly estimates of rainfall and snow melt entering the catchment from the Hydrologiska Byråns Vattenbalansavdelning (HBV) model (top of Figure 3.2a) [28, 139]; (2) hourly contributions of direct runoff, interflow

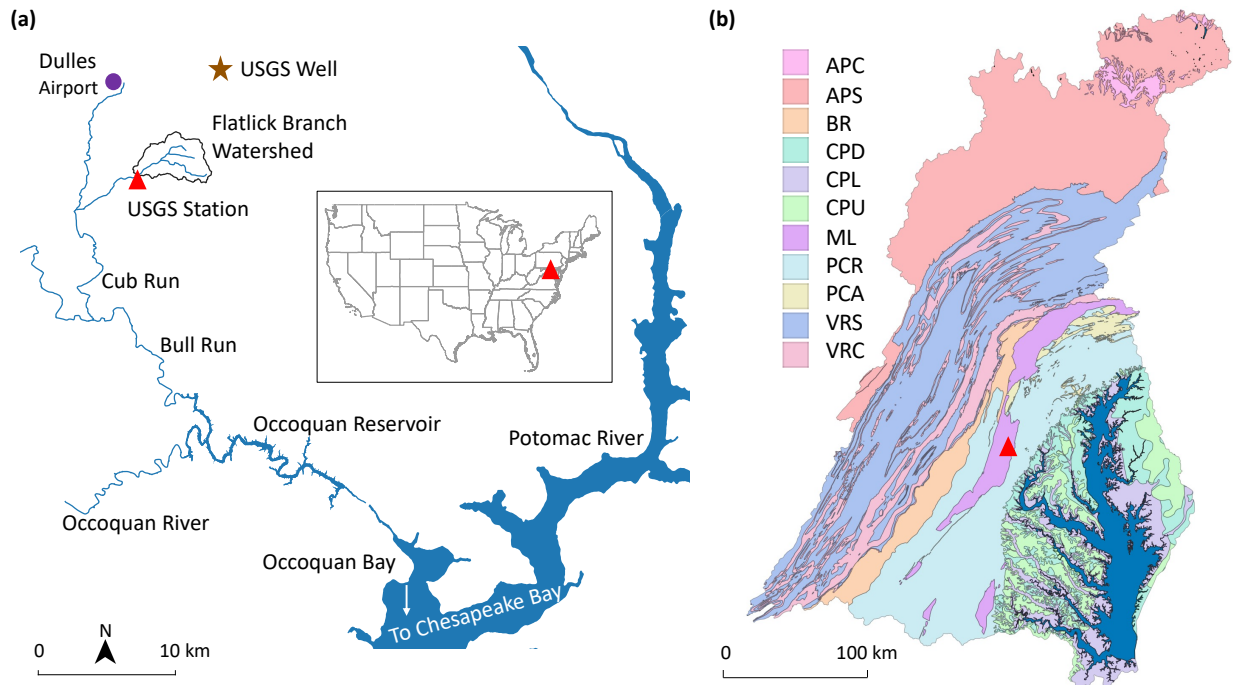


Figure 3.1: (a) Flatlick Branch drains an urban watershed in Northern Virginia, and is tributary to the Occoquan Reservoir, where rising sodium concentrations threaten a critical water supply for up to 1 million people; (b) Flatlick Branch is located in the Mesozoic Lowland hydrogeomorphic region (HGMR) of the Chesapeake Bay watershed (APC/APS: Appalachian Plateau Carbonate/Siliciclastic, BR: Blue Ridge, CPD/CPL/CPU: Coastal Plain Dissected Uplands/Lowlands/Uplands, ML: Mesozoic Lowlands, PCR/PCA: Piedmont Crystalline/Carbonate, VRS/VRC: Valley and Ridge Siliciclastic/Carbonate).

and groundwater to stream flow from a dynamic water balance over a three flow-path model representation of flow entering the stream from direct runoff (e.g., through urban stormwater drainage systems), interflow and groundwater (middle and bottom of Figure 3.2a); and (3) hourly estimates of mean stream age, along with the fraction of streamflow originating as snowmelt, from the T-TTD theory, adopting a uniform sampling function for outflow from the vadose zone and groundwater storages in the dynamic water balance [25, 83, 90] (Figure 3.2b). As noted by Benettin et al. [23] and also discussed later, the storage selection function for the overall system (including direct runoff, interflow and groundwater) is non-uniform, time varying, and will bias toward younger water, especially during snow melt and rain

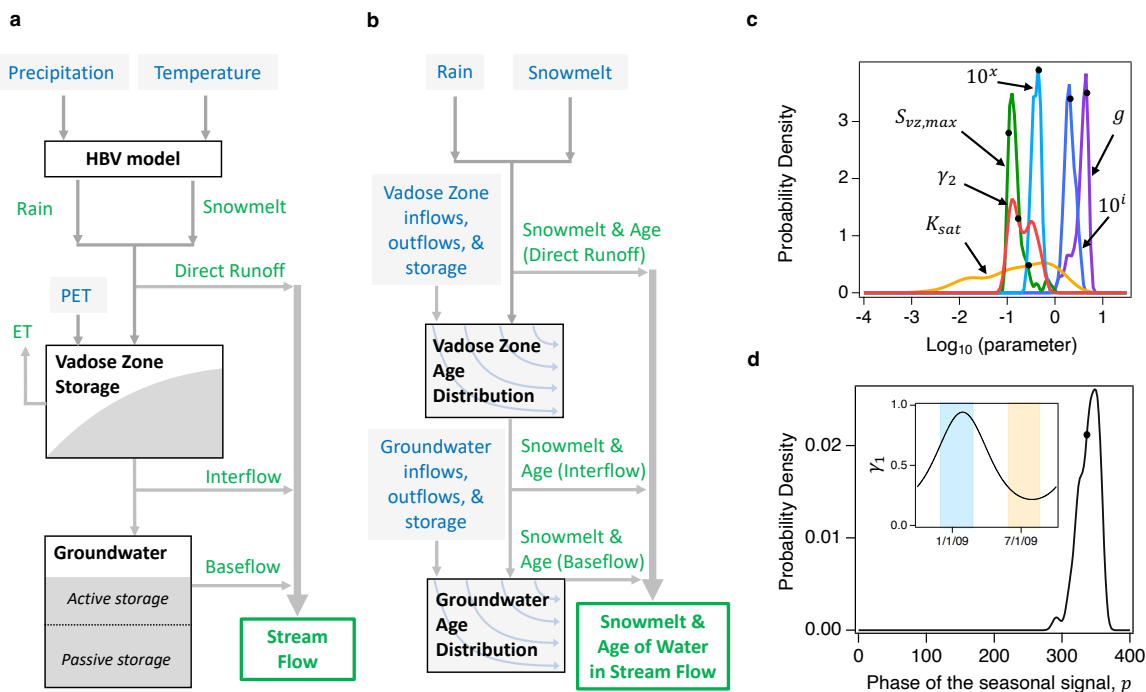


Figure 3.2: Conceptual representation of the (a) hydrologic model and (b) transient-transit time distribution (T-TTD) model, along with (c,d) posterior distributions and top-model values (closed circles) for the hydrologic model’s six parameters (defined in Table 3.1). The color coding in panels (a,b) indicates model inputs (blue) and outputs (green). Note that outputs of the hydrologic model (a) become inputs to the T-TTD model (b). “PET” is NASA Land Surface Model estimates of potential evapotranspiration, while “ET” is model-predicted evapotranspiration, accounting for vadose zone storage. The curving and flat water surfaces in (a) represent non-linear and linear discharge-storage relationships in the vadose zone and groundwater, respectively. “Active groundwater” refers to the portion of groundwater storage that directly influences stream flow, whereas “passive groundwater” does not influence stream flow but is still hydrologically connected to the stream and available for salt mass storage. The blue and yellow stripes in the inset (d) correspond to winter and summer periods, respectively.

events.

The hydrologic model (Figure 3.2a) was calibrated as described in Section B.4. Briefly, 10-years of hourly stream flow measurements on Flatlick Branch were divided into a model break-in period (water years 2008 and 2009); a calibration period (water years 2010 and 2011); and a validation period (water years 2012-2017). Hourly stream flow was then simu-

lated with the model for the first four water years  $10^5$  times, each time with a different set of parameter values drawn randomly from uniform distributions spanning a credible range of values (Table 3.1). The simulations were subsequently ranked based on the root mean squared error (RMSE) between log-transformed simulated and measured stream flow (over the calibration period), and posterior distributions for each parameter were generated from the top 100 models with the lowest RMSEs. The parameter set for the top-ranked model (i.e., with the lowest RMSE) was used for all subsequent water balance simulations (see Table 3.1 for top-ranked model parameter set).

Table 3.1: Definitions and Inferred Values for Hydrologic Model Parameters

Parameter	Variable [units]	Lower, Upper Bound	Top Model Value**
Annual average infiltration fraction*	$x$ [-]	-1, 0	-0.34
Magnitude of the seasonal signal*	$i$ [-]	0, 1	0.32
Phase of the seasonal signal*	$p$ [day of year]	170, 360	336
Maximum depth of the vadose zone	$S_{vz,max}$ [m]	0.1, 2	0.105
Power-law exponent	$g$ [-]	1, 5	4.73
Saturated hydraulic conductivity	$K_{sat}$ [m h <sup>-1</sup> ]	0.001, 1.8	0.28
Fraction of flow to groundwater	$\gamma_2$ [-]	0.1, 1	0.17

\*Seasonal infiltration fraction is represented as:  $\log_{10} \gamma_1(t) = x + i \sin \frac{2\pi(d+p)}{365}$ , where  $d$  is the day of the water year ( $d=1$  corresponds to 1<sup>st</sup> October in the calendar year).

\*\*Top model values are indicated by closed circles in Figure 3.2c,d.

With the exception of the active groundwater response rate (which was set equal to  $k_{gw} = 0.11 \text{ day}^{-1}$  based on an analysis of the master recession curve, see Section B.3.4), the calibration step converged to a set of well-constrained parameter values, as evidenced by their mostly uni-modal posterior distributions (Figure 3.2c,d). From the inferred values of  $i$ ,  $x$ , and  $p$  (Table 3.1), the fraction of rainfall or snow melt that infiltrates into the vadose zone,  $\gamma_1(t)$ , is 52% on an annual basis, but varies seasonally between 24 and 88% in summer (June, July, August) and winter (December, January, February), respectively (inset in Figure 3.2d). Put another way, direct runoff to the stream varies between 12 and 76% in the

winter and summer, respectively. Canopy interception can account for about 10% of the reduced summer-time infiltration [92], while the rest is likely due to the increased frequency of intense storms and consequent runoff generation during the summer compared to the winter (see the sequence of intense summer rain events toward the end of the timeseries in Figure 3.3a, and discussion of Figure B.2). Once water infiltrates, the model predicts that, on average, between 4 and 56% of water entering the vadose zone is returned to the atmosphere by ET in the winter and summer periods, respectively (results not shown).

Stream flow predicted from the top-ranked model closely reproduces measured stream flow in the validation period (Figure 3.3b), including the timing and magnitude of storm flows (which can exceed  $10 \text{ mm hr}^{-1}$ ), recessional flows (which can fall below  $0.01 \text{ mm hr}^{-1}$ ) and recession shape; note that all flows and volumes have been normalized by the area of the catchment. Model performance metrics in the validation period are within acceptable ranges (Nash-Sutcliffe Efficiency = 0.24, Kling-Gupta Efficiency = 0.56, RMSE = 0.98, and percent bias = 0.9%, all calculated based on hourly log-transformed measured and modeled flow [43]).

While daily inflow to the catchment is relatively evenly distributed throughout the year (Gini Index of 0.87 [159]), the seasonal nature of storm intensities, infiltration fraction and ET (see Figure 3.2d and discussion of  $\gamma_1(t)$  above) drive seasonal patterns in model-predicted stocks and flows. During winter, when the infiltration fraction is high and ET is low, daily average storage volumes in the vadose zone and groundwater are higher (blue curves in panels a and b, Figure 3.4) and consequently interflow and groundwater contribute substantially to streamflow during both wet and dry weather (blue curves in panels c, d and e, Figure 3.4). During summer, when the infiltration fraction is lower and ET is higher, daily average storage volumes in the vadose zone and groundwater are lower (yellow curves in panels a and b, Figure 3.4) and the daily average stream flow during the summer consists primarily of direct

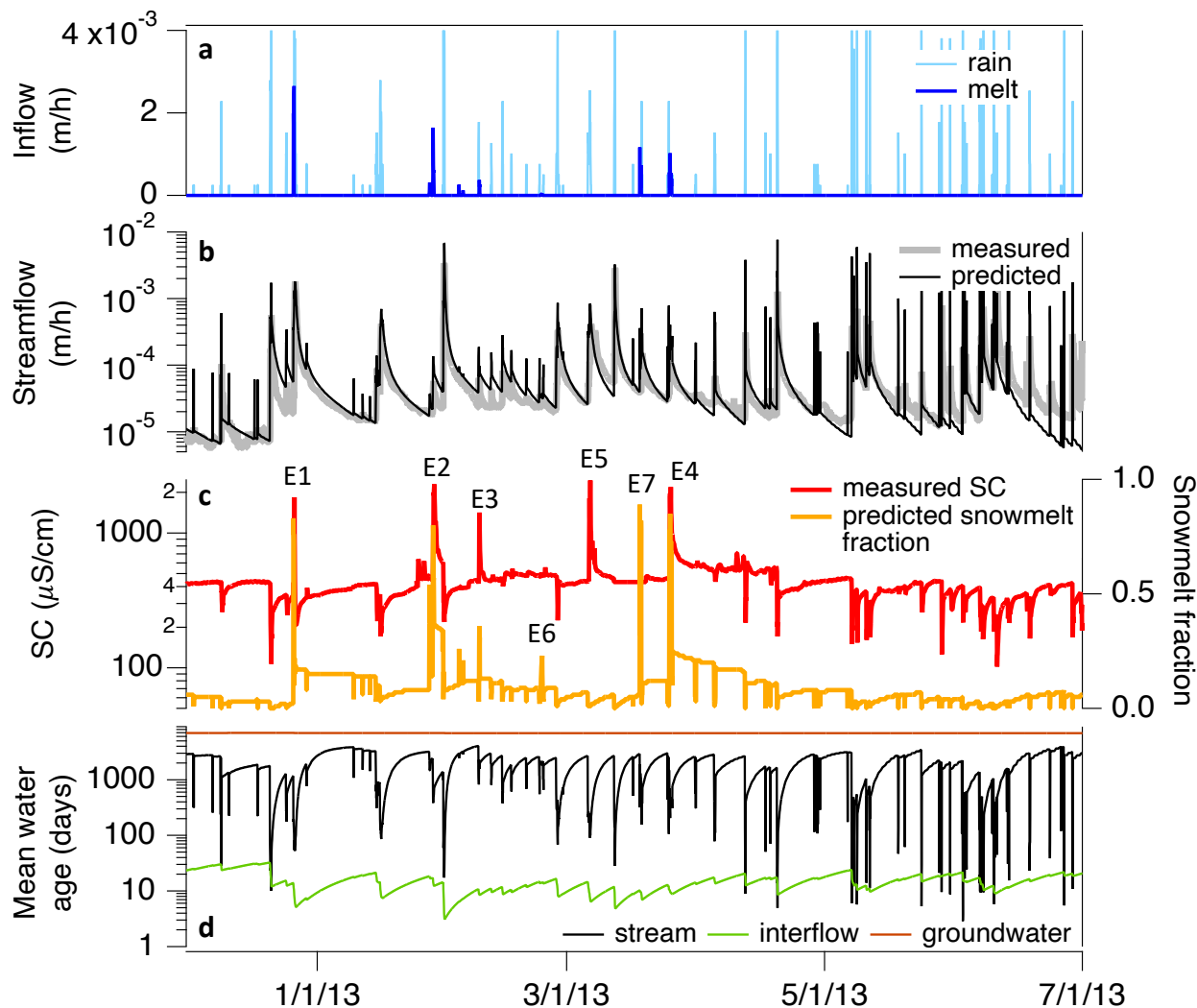


Figure 3.3: Comparison of model-predicted and measured timeseries for an illustrative seven months of the validation period, including (a) HBV model predictions of rainfall and snow melt; (b) measured and hydrologic model-predicted streamflow; (c) measured specific conductance (SC, a measure of salinity) and T-TTD model-predicted fraction of stream flow from snow melt; and (d) T-TTD model-predicted mean water age of interflow, groundwater and stream flow.

runoff (as evidenced by the emergence of a storm-associated mode at  $\frac{\langle Q_{run} \rangle}{\langle Q_{stream} \rangle} \approx 100\%$ , yellow curve in Figure 3.4c. Daily average evapotranspiration is  $< 20\%$  of daily average stream flow during the winter and up to  $300\%$  of daily average streamflow during the summer (Figure 3.4f). The seasonality of model-predicted storage in the vadose zone and groundwater is

consistent, although slightly phase lagged, with groundwater levels measured in a nearby well, which are generally higher and lower during winter and summer months, respectively (Figure B.9).

Note that the distributions of groundwater depths plotted in Figure 3.4b include both active groundwater (which is hydrologically connected to the stream and therefore contributes to streamflow) and passive groundwater (which is not hydrologically connected to the stream but influences solute transport). The depth of passive groundwater was inferred from the transit time modeling exercise presented in the next section, based on previously reported estimates of median subsurface flow age at this site [13]. The very small model-inferred depths of active groundwater ( $<3$  cm) are consistent with the local hydrogeology, which consists of a thin veneer of soil and saprolite overlaying fractured bedrock [71, 72, 133]. The small active storage estimates are also consistent with the hydrologic classification of the Flatlick Branch watershed as a surface flow dominated catchment (i.e.,  $k_{gw} = 0.11 \text{ day}^{-1}$  [182]).

### 3.3 Stream Water Age and Snowmelt Fraction

The mean water age and snow melt composition of the stream can be calculated directly from the hydrologic model results presented above using T-TTD theory, after specifying the age of water in direct runoff,  $T_{run}$ , and the depth of the passive portion of groundwater,  $S_{gw,p}$  (Section B.3). The former was set to zero,  $T_{run} = 0$ , on the premise that the delivery of direct runoff to streams (e.g., by community storm water drainage systems) is nearly instantaneous (ca., minutes to hours), compared to transport times through the vadose and groundwater (ca., days to decades or longer) [212]. The median age of subsurface flow discharged to the stream in the Flatlick Branch watershed is  $\approx 5.2$  years (see Figure B.3) [13], which for our

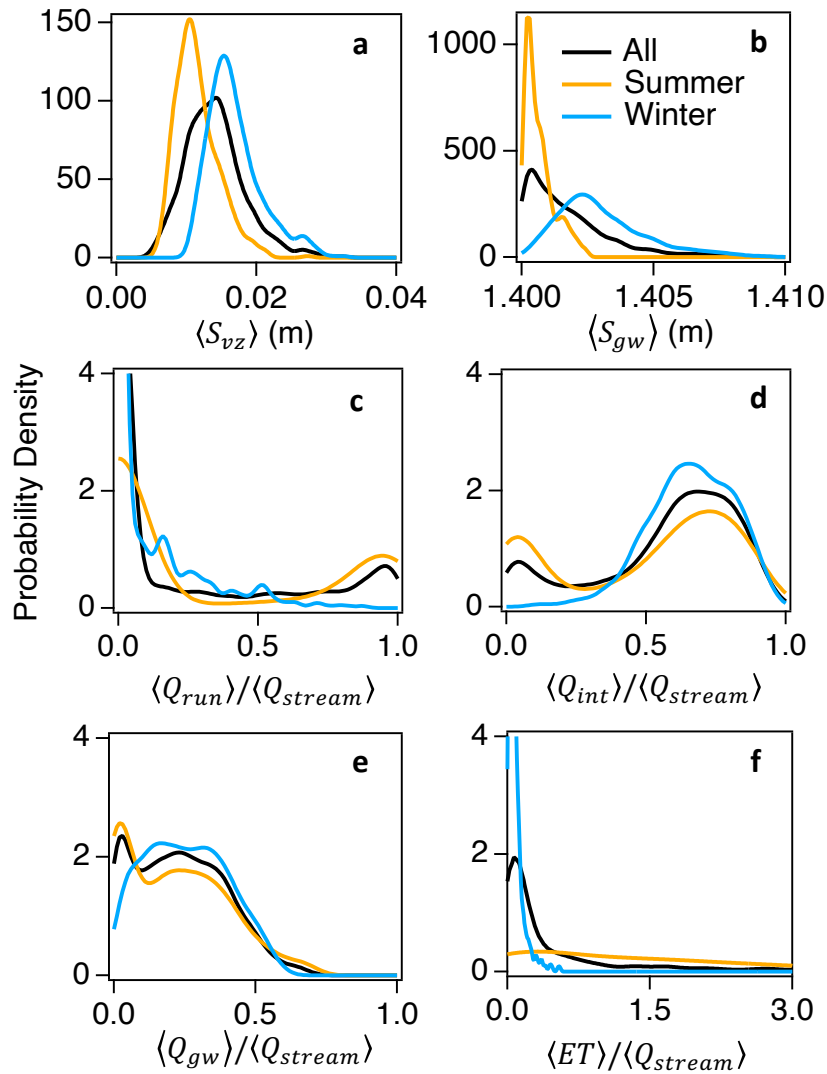


Figure 3.4: Probability distributions of model-predicted stocks and flows for summer (June, July, August), winter (December, January, February) or all days of the six-year validation period, including: daily average water stored in the (a) vadoso zone ( $\langle S_{vz} \rangle$ ) and (b) groundwater ( $\langle S_{gw} \rangle$ ); daily average fraction of streamflow from (c) direct runoff ( $\langle Q_{run} \rangle / \langle Q_{stream} \rangle$ ), (d) interflow ( $\langle Q_{int} \rangle / \langle Q_{stream} \rangle$ ), or (e) groundwater ( $\langle Q_{gw} \rangle / \langle Q_{stream} \rangle$ ); and daily average (f) evapotranspiration normalized by the daily average stream flow ( $\langle ET \rangle / \langle Q_{stream} \rangle$ ).

model corresponds to a passive groundwater depth of  $S_{gw,p} = 1.4$  m (see Section B.3.4 and Figure B.4).

Periods of high salinity on Flatlick Branch (corresponding to specific conductance values in excess of  $1000 \mu\text{S cm}^{-1}$ ) frequently align with periods of time when our T-TTD analysis predicts that stream flow contains a high fraction of snow melt (25 – 100%, compare yellow and red curves during events E1, E2, E3, and E4, Figure 3.3c). There are also cases where measured salinity is high and our model predicts a low fraction of snow melt in the stream (event E5) and conversely when the predicted contribution of snow melt to the stream is high but the measured salinity is low (events E6 and E7). Over the eight-year calibration and validation period, measured spikes in stream salinity aligned with model-predicted snow melt events 77% of the time, model-predicted snow melt events occurred in the absence of measured spikes in stream salinity 15% of the time, and measured spikes in stream salinity occurred in the absence of model-predicted snow melt events 8% of the time (data not shown). Because snowpack rarely persists for more than two weeks in this region, Welty et al. [215] argued that deicers should be more frequently mobilized into local urban streams by precipitation events and less frequently by snow melt. The observation that nearly 80% of spikes in stream salinity align with model-predicted snow melt events in Flatlick Branch challenges that argument, although about 16% of the model-predicted snow melt events were associated with simultaneous rain events.

Occasional mismatches in the timing of stream salinity spikes and model-predicted snow melt events can arise for at least three reasons: (1) as noted above, deicers may occasionally be transported to the stream during precipitation events that follow periods of deicer or anti-icer application [215]; (2) HBV model predictions of snow melt are likely to be error prone when the local temperature fluctuates around freezing because, under such conditions, temperature and precipitation measurements at a single weather station may not represent the melting or freezing conditions everywhere in the catchment (Figure B.8); and (3) salt application guidelines rely on local forecasts of temperature and precipitation [140], and when

these forecasts are wrong deicers may be applied when snow accumulation does not occur (which could lead to spikes in stream salinity in the absence of model-predicted snow melt events) or no deicers may be applied when snow accumulation does occur (which could lead to model-predicted snow melt events in the absence of measured spikes in stream salinity).

T-TTD theory estimates for the mean age of water in the stream were calculated by flow-weighting the expected value of the time-varying age distributions of water in direct runoff, interflow and groundwater (see Section B.3 for details). The resulting estimates of mean water age in Flatlick Branch ranged from 2 days (e.g., during intense summer rains when the infiltration fraction is small and much of the stream flow is from direct runoff) to 13.7 years (5000 days) at the end of long antecedent dry periods (black curve, Figure 3.3d). When plotted against T-TTD predictions of mean stream age, hourly measurements of stream salinity over the six-year validation period separate into three well-defined end members: (1) young stream water containing high-salinity snow melt (upper left in Figure 3.5); (2) young stream water containing low-salinity rain water (lower left in the figure); and (3) older stream water with a specific conductance of between 490 and 550  $\mu\text{S cm}^{-1}$  (far right in the figure). The latter is very similar to the specific conductance measured previously in groundwater samples collected from the Mesozoic Lowland HGMR in Virginia (median 540  $\mu\text{S cm}^{-1}$ , violin plot in Figure 3.5, see also Section B.7 and Tables B.3-B.5), consistent with the idea that the end-member on the far right of Figure 3.5 is groundwater. The moderately high specific conductance associated with groundwater in the Mesozoic Lowland HGMR reflects the relative solubility of carbonate material in the region's Triassic deposits of sandstone and shale [72, 120, 214].

Not all of the hourly stream salinity measurements separate cleanly into the three age-dependent end-members noted above (e.g., in a few cases high stream salinity is associated with very old water, Figure 3.5). In these cases there is a short (sub-daily) phase lag between

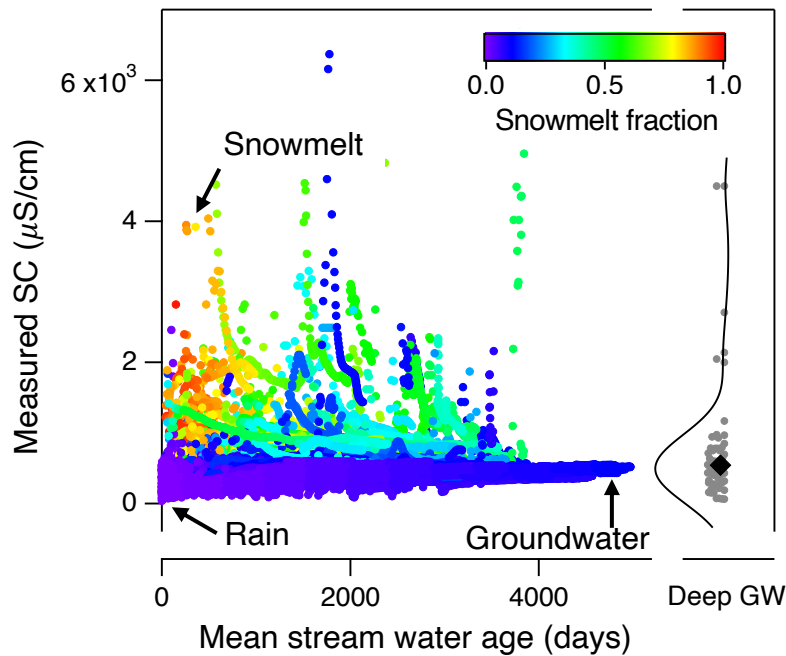


Figure 3.5: **Stream water age is a master variable for stream salinization.** When plotted against stream water age, measured stream specific conductance (SC) separates into snow melt, rain and groundwater end-members. The violin plot shows SC measurements of deep groundwater (GW) in the Mesozoic Lowland HGMR; the filled diamond is the median value.

the rise in stream salinity and the decrease in stream water age (or vice versa, see Figure B.11), presumably reflecting event-specific spatial and temporal variability in rainfall, snow melt, deicer application and subsurface flow path activation—variability that cannot be explicitly represented, at least not at an hourly time step, using the lumped transit time model framework employed here.

Individual snow melt or rain events have a reproducible pattern in which stream salinity starts out high (snow melt events) or low (rain events), and then relaxes back toward the background salinity with increasing stream water age (Figure 3.6). Generally speaking, the relaxation age-scales are shorter for snow melt events (median 270 days) and longer for rain events (median 580 days) ( $p < 0.1$ , non-parametric bootstrap comparison of medians [100]),

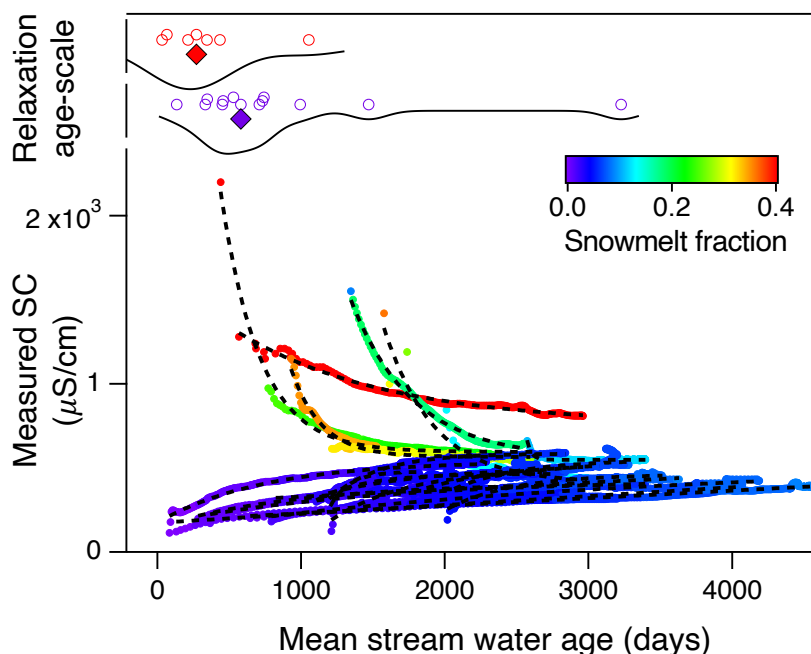


Figure 3.6: SC measurements associated with individual rain (N=14) or snow melt (N=6) events, all with postcedent dry periods of at least three days (there are fewer snow melt events because, in this region, snow melt events are frequently followed by rain events). Top set of violin plots represent relaxation age-scales estimated by fitting an exponential model (dashed curves) to the SC data for each rain (purple) or snow melt (red) event. Filled diamonds are median values. Note that, for rain events, the snow melt fraction (see color bar) increases with stream water age, signaling the presence of old snow melt in groundwater.

see violin plots at the top of Figure 3.6). This pattern can be explained by noting that the mean age of water in the stream generally starts out older for snow melt events and younger for rain events (Figure 3.6). Consequently, the net change in water age (i.e., the age-scale) is shorter and longer, respectively, for these two types of events. The ultimate cause is the seasonal variation in infiltration noted earlier. Most summer rainfall is routed directly to the stream with an age close to  $T = 0$  (low infiltration), while most snow melt travels along subsurface flow paths and is therefore older when it arrives at the stream (high infiltration).

The order-of-magnitude difference between rain or snow melt timescales (tens of days) and relaxation age-scales (hundreds of days) highlights the important distinction between wave

celerity and subsurface transit times. The much shorter rain or snowmelt event timescales reflect the duration of the events themselves and the fast propagation of pressure disturbances through groundwater (celerity). The much longer relaxation age-scales reflects the evolving mixture of young and old water in the stream over the storm hydrograph (transit times). During summer rain events, the model-predicted mean age of water in the stream declines dramatically because a large fraction of water in the stream consists of relatively young water from direct runoff (see direct flow path in Figure 3.2a). This behavior contrasts with the “old water paradox” in some natural [115] and urban [31] catchments, where the rapid release of water during storm events consists substantially of old water from catchment storage rather than new water from the event.

### 3.4 Conceptual Model of Salinity Sources and Physical and Geochemical Processes

A conceptual model of these results is presented in Figure 3.7. Water entering the catchment as snow melt or rainfall initially have either high or low salinity, respectively. This initial state is represented in the figure by a set of white circles entering the top of the catchment control volume. As water parcels transit along subsurface flow paths, they progressively lose memory of their initial condition through mixing with ambient groundwater and geochemical reactions that collectively drive salinity of the water parcel toward some geology-specific value (see inset, Figure 3.7) [200]. Relevant geochemical reactions might include cation exchange along shallow subsurface flowpaths [106, 109]) and, at our site, dissolution of rift basin deposits that tend to increase the specific conductance of groundwater and springs in the Mesozoic Lowland HGMR [72, 120, 133, 214]. The older water is when it exits the catchment and enters the stream, the closer its salinity approximates the geology-specific

value (represented in the figure by dark brown balls exiting the control volume along the longest flow paths).

The mean age and salinity of water in the stream depends on the relative contribution of young and old water (traveling along short and long flow paths, respectively) to stream flow, which varies from hour-to-hour and seasonally. During wet weather, stream flow consists mostly of young water transiting along short flow paths (e.g., direct runoff and interflow through the vadose zone). Consequently, stream salinity is biased toward the initial salinity of water parcels entering the catchment as either snow melt or rain (right diagram, Figure 3.7). The seasonal infiltration patterns noted earlier will tend to favor the delivery of younger low-salinity water to the stream by direct runoff during intense summer rains. During dry weather, stream flow consists mostly of older water transiting along longer flow paths (e.g., through groundwater) and thus stream salinity is biased toward the geology-specific value (left diagram, Figure 3.7).

Apart from the exchange of sodium ions in soils [106, 109], subsurface geochemical reactions should not dramatically alter the concentration of sodium and chloride ions, the major constituents of rock salt frequently used for deicer applications, as water transits along subsurface flow paths to the stream. Chloride is not a major component of silicate or carbonate mineralogy; in fact, it is often used to track the component of stream water chemistry derived from atmospheric input alone (i.e., it provides a “seawater correction”) [74, 175, 196]. Likewise, while sodium is often a major component of silicate mineralogy, this cation does not incorporate into the vast majority of common secondary clay phases and, consequently, is frequently used to track the extent to which other solutes have been lost to the formation of new minerals [38, 66, 76, 78]. Thus, if sodium and chloride ion concentrations increase or decrease substantially along subsurface flow paths, it is likely due to mixing and dilution with ambient groundwater, not geochemical reactions.

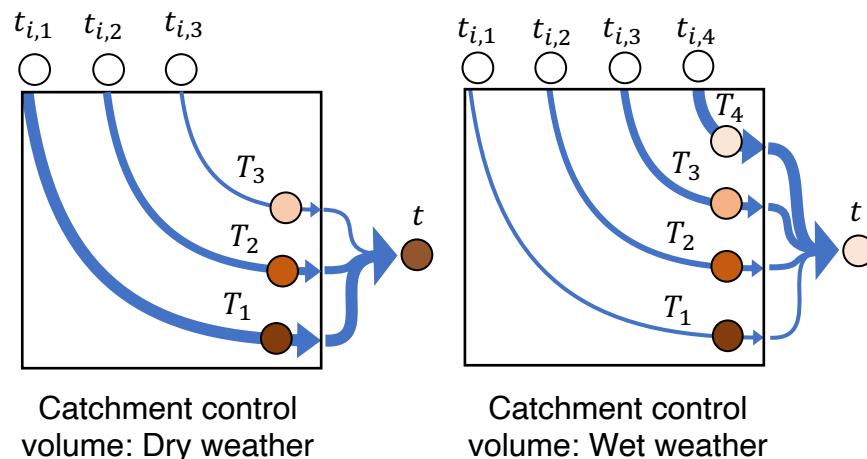


Figure 3.7: A conceptual model for how initial conditions (high or low salinity associated with snow melt or rain), geochemical reactions along sub-surface flow paths, and weather-dependent biasing of stream flow from either short or long flow paths influence salinization patterns. The symbols represent the catchment entry and exit times of individual water parcels ( $t_i$  and  $t$ ), and the age of water entering the stream along a particular streamline ( $T = t - t_i$ ).

The conceptual model presented in Figure 3.7 also highlights how deicers might lead to legacy salt pollution in streams. For our T-TTD simulations at Flatlick Branch, for example, the fraction of old snow melt in groundwater rarely drops below 15% (Figure B.10). As a result, between rain events, the predicted fraction of old snow melt in the stream rarely falls below 8% during snow-free periods of the year (Figure 3.3). To the extent that old snow melt retains a high-salinity signal associated with historical deicer use, baseflow salinity in the stream will likely exceed the geology-specific baseline values, and the timescale over which this legacy salt pollution responds to engineering or policy interventions in the watershed (e.g., designed to reduce the impacts of deicer use, see below) will likely be similar to the median subsurface flow age, which at this site is  $\approx 5.2$  years [13].

### 3.5 Deicer Application Rates and Stream Salinity

Our analysis also reveals a cause-and-effect relationship between peak stream salinity and rough estimates for the cumulative area-normalized mass of road salt deposited in the lead up to a snow melt event (Figure 3.8). The latter was estimated by first generating a daily time series of recommended salt application (in units of  $\text{kg m}^{-2}$ ) based on local deicer application guidelines [140] and historical weather data (see Section B.5). Over the eight year calibration and validation periods, we then summed the predicted daily mass of road salt (as sodium chloride) applied from the end of the penultimate storm to the snow melt event in question. Measurements of peak stream salinity at Flatlick Branch increase non-linearly with these predictions of cumulative deicer application, from at least two times the background level for 0.02 to 0.03  $\text{kg NaCl m}^{-2}$  to between three and fifteen times the background level for  $> 0.1 \text{ kg NaCl m}^{-2}$  (red symbols in Figure 3.8). These specific conductance values can be translated into equivalent chloride concentrations using the site-specific regression relationship described in Section B.6. At higher salt application rates the inferred peak stream chloride concentrations are nearly four times the U.S. Environmental Protection Agency’s acute aquatic life threshold of 860  $\text{mg L}^{-1}$  (blue symbols in Figure 3.8).

### 3.6 Extensibility of Model and Site Observations

In translating our results to other locations several points should be kept in mind. First, within the context of T-TTD theory, at present there is uncertainty about how best to represent the sampling of water in storage for outflow; i.e., the choice of the StorAgeSelection (SAS) function [112]. Following Benettin et al. [23], we chose uniform SAS functions for the vadose zone and groundwater storages. However, as noted earlier, the selection function for

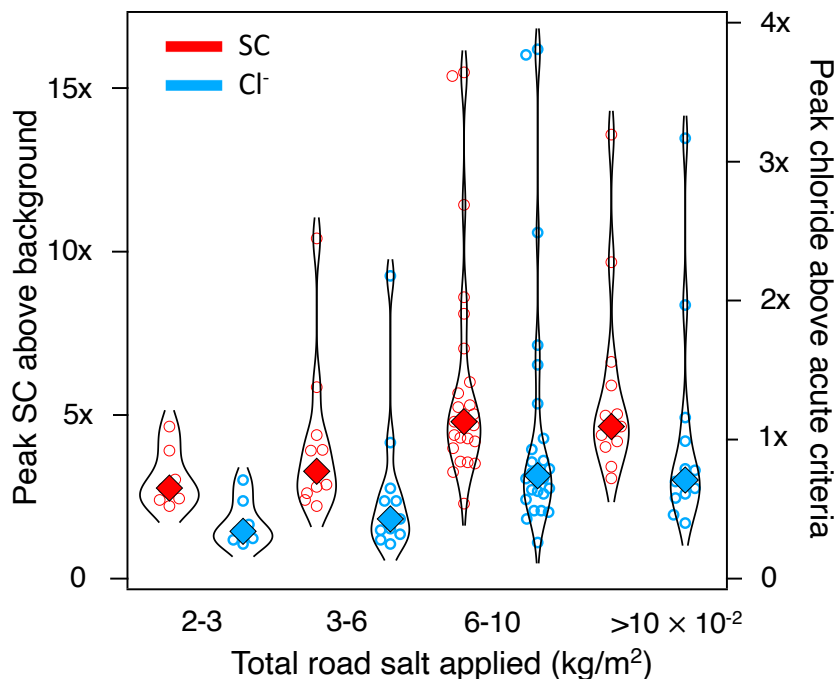


Figure 3.8: Cause-and-effect relationship at Flatlick Branch between the cumulative road salt applied in the lead-up to a storm, and the peak stream SC and inferred chloride concentrations during snow melt events. Filled diamonds are median values.

the overall system is neither uniform nor time-invariant. During storms, especially during the summer, a substantial fraction of the rainfall is routed directly to the stream (e.g., through community drainage systems) with an effective age of  $T = 0$  hours. The mean age of water in the stream is an instantaneous flow weighting of the mean age of water entering the stream from direct runoff, interflow, and groundwater discharge. Thus, the selection of water from storage is heavily biased toward younger water (i.e., direct runoff) during storm events—a pattern often observed in practice [96, 134] and known in the literature as the inverse storage effect [24, 88, 206]. Furthermore, because the division of rain and snow melt between infiltration and direct runoff varies seasonally (more infiltration in the winter, less in the summer), the overall system SAS also varies seasonally. Thus, the overall system SAS employed here is both non-uniform (biased toward younger water during storms) and time-varying (the bias toward younger water is more pronounced during the summer). While

other SAS functions could have been adopted for the vadose zone and groundwater boxes [25], the advantage of our approach is that the mean age of water leaving these two boxes can be calculated from simple analytical expressions, which are derived in Appendix B. While not the focus of this study, analytical expressions for various young water fractions can also be derived using a similar approach [117]. It remains to be seen if the overall SAS function adopted here is widely applicable to other urban catchments.

Second, unlike many previous implementations of T-TTD theory, including the one used as a template for our study [23], as presently formulated our model does not predict the stream concentration of the solute of interest. This is because the source function for the solute of interest in this case, salt ions from road deicing activities, is very poorly constrained. While some sense of the source term can be obtained by using weather forecasts to estimate the deicer mass applied per lane mile or unit area of impervious surface (e.g., using Salt Institute guidelines, as illustrated in Figure 3.8), the fact is that these guidelines are just that—actual deicer application rates could be much higher or lower than recommended, vary dramatically across the catchment landscape depending on local road and impervious density, and depend on the level of service required by individual clients and the professionalism and environmental sensitivity of the commercial or government deicer applicators [191]. Indeed, because deicer application rates are so difficult to determine *a priori*, one promising application of our modeling framework involves “doing water quality backwards” (analogous to “doing hydrology backwards” [116]), by estimating catchment-average deicer application rates from high frequency measurements of flow and specific conductance in a stream. As noted in the Appendix (Section B.8), this involves a remarkably simple “deconvolution” of measured salt mass loading in the stream using the time-varying age distribution of stream water provided by the T-TTD model. Deconvolution of the stream data into deicer application rates would not only yield greater insight into the human behavioral, hydrologic

and climate factors that collectively determine deicer use in a given catchment, but could also be used to monitor the effectiveness of experimental trials aimed at reducing the impact of deicers on stream health [67]. Examples of technological and behavioral best management practices along these lines are presented in the next section.

### 3.7 Conclusions

Our study links stream water salinity in an urban watershed to recharge provenance and water age through a combination of hydrologic models and high-frequency monitoring of stream flow and specific conductance. In particular, we report a reproducible association between “young” snow melt with high salinity; “young” rainwater with low salinity and “old” groundwater of moderate salinity. Stream water age is estimated by coupling three hydrologic modeling frameworks. The first (the HBV model’s snow routine) provides hourly rainfall and snow melt estimates; the second (a three-flow path model) provides estimates of stream flow as a dynamic water balance between runoff, interflow and groundwater; and the third (the T-TTD model) translates the outputs of the first two models into hourly estimates of mean stream age and the fraction of stream flow derived from snowmelt.

Applied to Flatlick Branch, a deicer impacted urban stream in Northern Virginia [163], we find that seasonal variations in storm intensity and ET likely influence the routing of water and salt to the stream. ET and the frequency of intense storms are higher (lower) in the summer (winter), resulting in lower (higher) infiltration, more (less) direct routing of runoff to the stream, increased (reduced) root interception of infiltrated water, and reduced (increased) groundwater storage. These seasonal patterns, together with the fact that deicers are applied during the winter, imply that salt pollution can manifest as both fast transient peaks in specific conductance (e.g., associated with the delivery of young snow melt to

streams through stormwater conveyance systems) and slow increases in specific conductance over time (e.g., associated with build-up of old deicer salts in the groundwater). At our field site, the latter legacy pollution adds to the already moderately high specific conductance of groundwater in contact with carbonate-rich Triassic sandstone and shale deposits in the Mesozoic Lowlands HGMR.

In addition to providing new insights into the physical and geochemical mechanisms that drive freshwater salinization, our results also open the door to monitoring deicer loading rates through the deconvolution of high frequency measurements of stream flow and salinity. This would allow evaluation of both the human behavioral aspects of this grand challenge (e.g., by exploring how closely actual deicer loading rates conform to industry standard guidelines) and the long-term monitoring of experimental interventions aimed at mitigating, and ideally reversing, inland freshwater salinization [186]. Because stream salinity at Flatlick Branch peaks very quickly after the onset of a snow melt event (Figure 3.3c), conventional stormwater drainage infrastructure in the watershed could be modified to capture and temporarily store young (i.e., “first-flush”) snow melt for subsequent treatment using grey or green treatment technologies. An example of the former is the dynamic blending of low-salinity runoff generated during rain events with higher-salinity snow melt in storage (e.g., using active control of storm water infrastructure [111]), with the goal of discharging water with a predefined reference salinity. An example of the latter is the planting of halophytes that concentrate salt in their above ground tissue for later harvesting and use, for example as feedstock, as an energy crop, or for biochar production [123].

Potential policy interventions include: (1) education, regulation, and enforcement efforts aimed at promoting conservative deicer use on roads and parking lots, ideally keeping the total cumulative salt application below  $0.01 \text{ kg NaCl m}^{-2}$  (Figure 3.8); (2) the development and testing of alternative deicers with fewer ecological impacts [93]; and (3) social marketing

efforts to lower public expectations of clean roads immediately following winter storms [84]. Such interventions could also be designed to evaluate the potential effects of climate change, which in the Mid-Atlantic United States could result in higher average temperatures, higher total precipitation, and a decrease in the fraction of precipitation that falls as snow [99].

Lastly, the inherent simplicity and low computational cost of transit time simulations opens the door to interactive participatory modeling exercises with stakeholders [85], for example aimed at elucidating the likely impacts of future population growth and climate change on inland freshwater salinization and catalyzing the formulation of management strategies to address this emerging environmental grand challenge [84].

# Chapter 4

## Transit Times Link Sodium Sources to Drinking Water Quality in a One Water System

### 4.1 Introduction

The One Water approach to water resource management aims to improve water equity, affordability and access through the co-management of all local water resources (drinking water, wastewater, stormwater, and groundwater), taking into account ecological conditions, geographic settings, regulatory constraints, governance structures, and human influences [162]. This approach has numerous engineering, economic, ecosystem, and community benefits, including improved water quality, increased water supply reliability, reduced freshwater withdrawal, reduced water age in distribution networks, and net energy savings despite the substantial energy costs associated with wastewater treatment and recycling [82, 127].

However, broad adoption of the One Water approach will challenge traditional institutional arrangements for water resource management. In the United States, it is often the case that different organizations separately manage drinking water, wastewater and stormwater systems according to different rules, norms, and shared strategies [162]. Such fragmen-

tation poses challenges for cross-sectoral coordination [57] and impedes technological and governance innovations [51, 113, 130, 197]. This is particularly true for water quality and quantity challenges that have no obvious regulatory solutions and thus require the voluntary “collective action” of local actors to solve [152].

Our project is using a convergence research approach [6, 18, 75] to tackle a canonical water quality challenge in One Water systems, salt management, using the Occoquan Reservoir, a drinking water resource for up to one million people in northern Virginia, as our testbed. The Occoquan Reservoir is the United State’s first large-scale experiment in deliberate indirect potable reuse for surface water augmentation, the practice of deliberately adding highly treated wastewater, or “reclaimed water”, to a reservoir used for drinking water supply [5]. This One Water system encompasses a minimum of eight different utilities and government agencies, including the local drinking water utility (Fairfax Water), the water reclamation facility (Upper Occoquan Service Authority, UOSA), the state transportation agency (Virginia Department of Transportation, VDOT), and separate city and county departments in six jurisdictions responsible for stormwater management (City of Manassas, City of Manassas Park, Prince William County, Fairfax County, Loudoun Country, Fauquier County).

For the past 50 years, these entities have successfully navigated a host of water quality and quantity challenges through a quasi-regulatory governance system called the Occoquan Policy (codified in the Virginia Administrative Code at 9 VAC 25-410), which predates the United States’ Federal Safe Drinking Water Act (SDWA) and Clean Water Act (CWA) [84]. The Occoquan Policy has jurisdiction only over regulated contaminants (such as nitrogen and phosphorous) in the reclaimed water. Thus, it cannot be used to control the input of non-point source pollution to the reservoir, nor the input of point and non-point source contaminants for which the State of Virginia has not adopted regulatory thresholds [84].

A case in point is sodium ions, the concentration of which has been steadily increasing in

the reservoir over the past four decades [32]. Sodium ion concentrations in the reservoir now routinely exceed drinking water health advisories issued by the United States Environmental Protection Agency (EPA) for individuals on a severely restricted sodium diet ( $20 \text{ Na}^+ \text{ mg L}^{-1}$ ) and the lower drinking water taste threshold ( $30 \text{ Na}^+ \text{ mg L}^{-1}$ ) [32]. Concerned that the upward trend might continue, Fairfax Water began exploring planning-level options, including a reverse osmosis treatment upgrade that would likely cost more than \$1 billion, not including brine disposal costs, energy and carbon footprint costs, and lost production capacity [60]. A more sustainable and cost-effective solution would be to reduce the upstream sources of sodium ions entering the reservoir (e.g., from road deicing activities, reclaimed water and treatment processes), but only a handful of states, not including Virginia, have adopted sodium-specific thresholds (criteria) for drinking water. Thus, regulatory frameworks like the Occoquan Policy cannot be used to coordinate a system-level response to this emerging water quality threat.

We hypothesize that polycentric co-management of unregulated contaminants, such as sodium ions in drinking water, can be catalyzed through the application of Nobel Laureate Elinor Ostrom’s social-ecological systems (SES) framework [152]. Preliminary application of this framework to sodium pollution in the Occoquan system revealed three key areas (formally termed “second-level variables” by Ostrom) where focused, stakeholder-engaged research might help set the stage for bottom-up collective action on this issue [84]. These three variables are: (1) Predictability of System Dynamics (second-level variable RS7), (2) Knowledge of the SES (A7); and (3) Collective Choice Rules (GS6).

Herein we present a mechanistic assessment of the upstream sources of sodium, their temporal dynamics, and how these sources, both individually and collectively, influence the sodium ion concentration in the Occoquan reservoir and in the final drinking water produced from this system. To accomplish this, we utilize a parsimonious modeling framework based on

unsteady transit time theory [90], with the goal of addressing the biophysical dimensions of Ostrom’s second-level variables mentioned above: RS7 (“if a particular source is reduced by a certain percentage, what is the likely impact on sodium ion concentrations in the reservoir and in the finished drinking water?”); A7 (“how do system-level processes and feedbacks influence options and outcomes?”); and GS6 (“who should be engaged, what rules should they follow, and why should they participate?”). In the context of Ostrom’s SES framework, we hypothesize that stakeholder-engaged transit time modeling can help catalyze bottom-up management of unregulated contaminants and, more generally, inform the practice of convergence as a research approach.

## 4.2 The Occoquan One Water System

The Occoquan Reservoir is one of two primary sources of raw water for Fairfax Water, a drinking water utility that provides drinking water for approximately 2 million customers in Fairfax County and surrounding communities in Northern Virginia. The utility operates two major water treatment plants (Figure 4.1a). Fairfax Water’s Corbalis water treatment plant sources its raw water from the Potomac River (Station 1 in Figure 4.1a). Finished drinking water from the Corbalis water treatment plant is pumped through local water retailers to homes and businesses (Station 2), and from there is flushed “down the drain” to one of several sewage collection systems that, in turn, flow by gravity and pressurized networks to the UOSA water reclamation facility (Station 3) or other regional wastewater treatment facilities. At UOSA, the wastewater undergoes primary, secondary and advanced treatment (Station 4). The reclaimed water is then discharged to Bull Run, where it blends with dry and wet weather runoff from the surrounding 390 km<sup>2</sup> Bull Run watershed (Station 6), which includes a mix of forested (39%), urban (47%) and agricultural (12%) land uses. Reclaimed water and

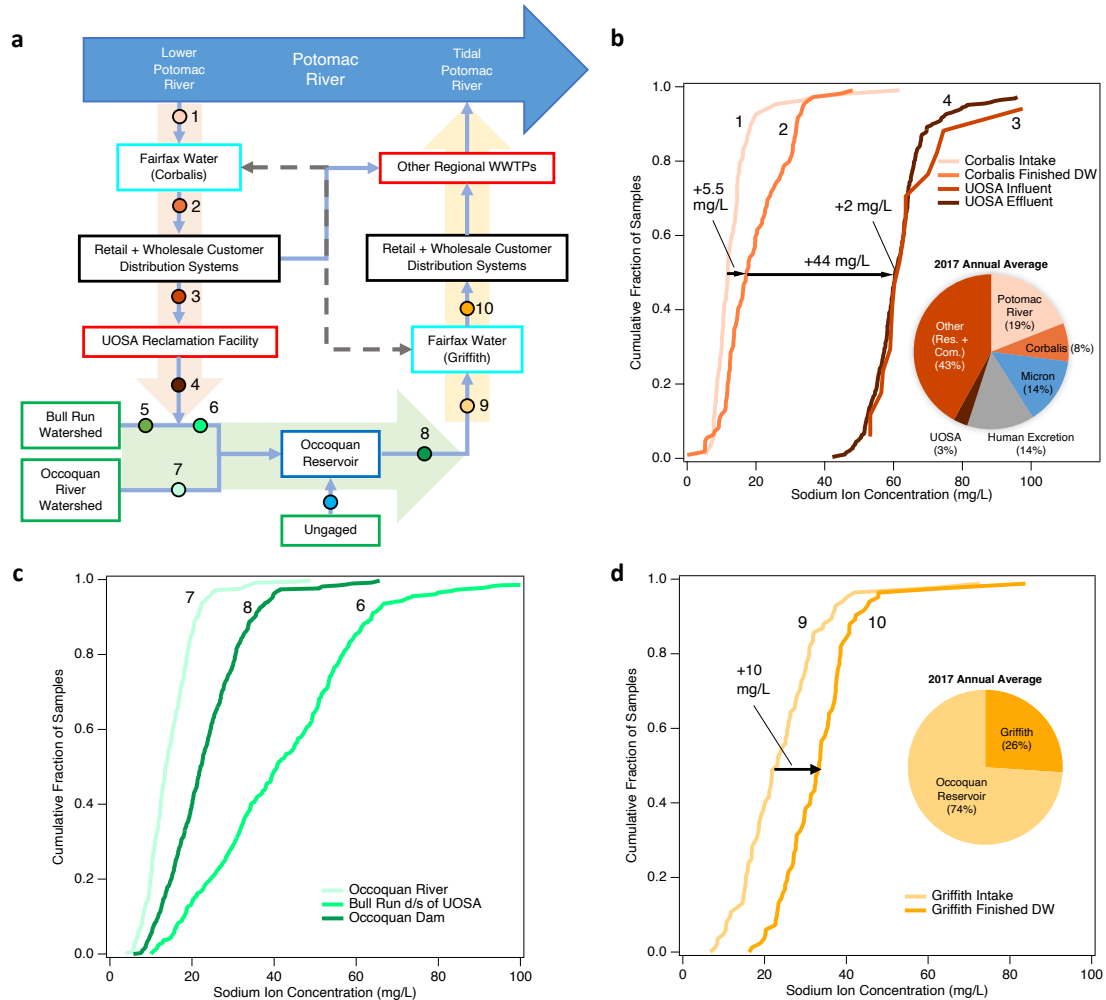


Figure 4.1: **Change in sodium ion concentrations along flow paths through the Occoquan “One Water” system.** (a) Schematic representation of flows entering and leaving the Occoquan Reservoir. (b),(c),(d) Empirical cumulative distributions of measured sodium ion concentration collected from 2015-2022 along (b) the reclaimed water flow path (Stations 1 to 4), (c) the watershed and reservoir flow path (Stations 6 to 8) and (d) the Griffith drinking water plant flow path (Stations 9 and 10). Empirical distributions of sodium ion concentrations at each station were constructed from measurements by Fairfax Water (Stations 1 (N=107) and 2 (N=107)), UOSA (Stations 3 (N=16) and 4 (N=287)), Virginia Tech’s Occoquan Watershed Monitoring Lab (Stations 6 (N=408), 7 (N=385) and 8 (N=385)), and Fairfax Water (Stations 9 (N=84) and 10 (N=83)). Sodium ion concentration at Station 5 were not measured, but inferred from mass balance (see Methods). Pie chart insets (panel b and d) illustrate, for the year 2017, annually averaged sodium mass load contributions from specific sodium sources in their respective flow paths.

runoff from the Bull Run watershed flow into the upstream end of the Occoquan Reservoir, along with dry and wet weather runoff from the 890 km<sup>2</sup> Occoquan River watershed (Station 7), which drains a mix of forested (48%), urban (19%) and agricultural (32%) land uses. The Occoquan River Watershed is currently less developed than the Bull Run Watershed (see Figure C.1). These two watersheds are expected to add around 60,000 and 80,000 people, respectively, by 2040 [10].

Fairfax Water’s Griffith water treatment plant draws its raw water from the far downstream end of the Occoquan Reservoir near the Occoquan Dam (Station 8). After treatment (Stations 9 and 10), the finished drinking water is pumped through water retailers to local homes and businesses. From there, it flows through sewage collection systems to a set of regional wastewater treatment plants that discharge to the tidal portion of the Potomac River.

Figure 4.1a vividly illustrates the complex network of urban infrastructure that makes up this One Water system, including drinking water treatment plants, wastewater treatment plants, water reclamation plants, road networks, along with city and county stormwater systems that impact both the quantity and quality of dry and wet weather runoff entering the reservoir from the Bull Run, Occoquan River and ungaged portions of the watershed. Here, “ungaged” refers to areas of the watershed that drain to the reservoir downstream of flow meters on Bull Run and Occoquan River (Stations 6 and 7). To a first approximation, the Occoquan Reservoir is a one-pass-through system in which water from the Potomac River (Station 1) cascades through various urban water systems (Stations 2-9), eventually returning to the downstream (tidal) portion of the Potomac River. In practice, a substantial portion of water leaving the Occoquan Reservoir flows through the dam’s spillway and directly into the tidal portion of the Potomac River (i.e., not all water leaving the Occoquan Reservoir enters the Griffith water treatment plant, as indicated in Figure (4.1a)). Further, Fairfax Water can transfer drinking water across different water distribution systems (e.g., from Griffith to

Corbalis, and vice versa, grey dashed double-sided arrow in Figure (4.1a)), and some of the finished drinking water from Corbalis is discharged to other (non-UOSA) regional wastewater treatment facilities (light blue arrow, Figure (4.1a)).

### 4.3 Sources of Sodium along One Water flow paths

From monitoring data provided by the local utilities along with water quality monitoring of the tributaries and reservoir by Virginia Tech's Occoquan Watershed Monitoring Laboratory, we can trace the evolution of the median sodium ion concentration along each of the flow paths described in the last section (Figure 4.1b-d). As water flows from the Potomac River to Bull Run (Stations 1-4, Figure 4.1b), approximately 6 mg/L of sodium is added by the Corbalis plant during water treatment, a remarkable 44 mg/L is added as the finished drinking water passes through homes and businesses and into the sanitary sewer system, and approximately 2 mg/L is added by UOSA during wastewater treatment (for the time period of analysis, 2015 to 2022, relatively few samples of UOSA's influent water were analyzed for sodium ion concentration (N=16) so the 2 mg/L reported here is based on an analysis of the wastewater treatment plant's chemical usage data (UOSA, personal communication)). For the year 2017, on an annual average, approximately 19% of the total sodium mass in UOSA's reclaimed water comes from the raw water in the Potomac River, 8% is added during water treatment at Corbalis, 14% is from Micron Technologies, a local micro-fabrication facility, 14% is from human excretion, and 3% comes from UOSA's wastewater treatment processes [32] (pie chart in Figure 4.1b). That leaves around 43% of the total sodium in UOSA's reclaimed water unaccounted for. A likely source of this "missing sodium" is down-drain disposal of sodium-rich products in homes and businesses in the sewershed draining to UOSA [32].

The median sodium concentration drops approximately 20 mg/L as UOSA's reclaimed water mixes with the generally less concentrated dry and wet weather runoff from the Bull Run watershed (see curves 4 and 6 in Figures 4.1b and c). This downward trend continues as water from Bull Run enters the reservoir and mixes with the generally less concentrated dry and wet weather runoff from the Occoquan River. At the far downstream end of the reservoir near the Griffith water treatment plant's intake, the sodium ion concentration (median 23 mg/L) generally falls between that of Bull Run downstream of UOSA (median 41 mg/L) and in the Occoquan River (median 13 mg/L) (compare curves 6-8, Figure 4.1c). On a median basis, the Griffith Water Treatment plant adds another 10 mg/L of sodium during the treatment process (see curves 9 and 10, Figure 4.1d). For the year 2017, on an annual basis, approximately 26% of the sodium mass load in Griffith's finished drinking water is added by water treatment processes at the Griffith plant, while 74% is contributed by raw water from the Occoquan reservoir (see pie chart in Figure 4.1d).

## 4.4 Transit time model of the reservoir

Based on the flow path analysis summarized in the last section, one might conclude that inputs of sodium to the reservoir decrease in the following order: UOSA's reclaimed water, runoff from the more developed Bull Run Watershed, and runoff from the less developed Occoquan River Watershed. As stakeholders in the region pointed out (personal communication), this ranking is based on median concentrations of water flowing into the reservoir, while a more management-relevant breakdown would focus on the relative contribution of each upstream source to sodium ion concentrations at Griffith's intake at the Occoquan Dam and in Griffith's finished drinking water. Furthermore, the sample-to-sample variability in these monitoring data can be substantial. For example, the median sodium concentration

measured in Griffith’s final drinking water is 31 mg/L, but on a sample-to-sample basis ranges from <20 to >80 mg/L (see curve 10, Figure 4.1d). Because the median concentration is nearly equal to the taste threshold recommended by EPA [61], drinking water produced by the Griffith treatment plant exceeds EPA’s recommended threshold roughly 50% of the time. Similar variability is evident at all points in the system (see Figures 4.1b-d). These observations beg the following questions: (1) what is the relative contribution of the upstream sources to sodium ion concentrations in Griffith’s finished drinking water? (2) over what timescales are these contributions varying and what processes are responsible? and (3) how might the answers to (1) and (2) be leveraged to reduce sodium ion concentrations in the reservoir and in Griffith’s final drinking water?

To address these questions, and more broadly, to contribute to the biophysical dimensions of the three Ostrom second-level variables described earlier, we developed a predictive model of daily average sodium concentrations at the intake to the Griffith water treatment plant (Station 8 in Figure 4.1a). Typically, such models start by first resolving the unsteady flow field in the reservoir and then “layering on” mass conservation laws in one-, two-, or three-dimensions (e.g., [33, 124]). Here we test a promising alternative approach, unsteady transit time theory, that tracks the flux and age distribution of water and solutes moving into and out of a control volume drawn around the system of interest [135]. By eliminating the need to resolve the movement of water and solutes within the reservoir, this framework vastly simplifies model development and deployment (e.g., at most three parameter values needed to be specified in the unsteady transit time model described below) and computational requirements are reduced to the point that simulations can be easily run in real-time. As we shall demonstrate shortly, unsteady transit time theory is also strongly data driven, and thus leverages the region’s multi-decadal investment in high frequency flow and water quality monitoring at key points in the system. Transit time theory is implemented in five steps as

described next (see Methods Section 4.10 for details) [83].

#### 4.4.1 Step 1: Define the Control Volume

Our control volume encloses all water in the Occoquan Reservoir. Inputs to the control volume include UOSA’s reclaimed water, runoff from the Bull Run and Occoquan River watersheds, runoff from the ungaged portions of the watershed, and direct precipitation onto the reservoir surface. Outputs from the control volume include abstractions by the Griffith water treatment plant, water discharged through the dam’s spillway, and evaporation off the reservoir’s surface. Groundwater may serve as either an input or output, depending on hydrologic conditions.

#### 4.4.2 Step 2: Perform Water Budget

A daily water budget over the control volume was performed for the most recent decade for which data are available, 2010–2021, including inflows (represented here by the variable  $J(t)$ ), outflows ( $Q(t)$ ), and the stored volume of water in the reservoir ( $S(t)$ ) as a function of time,  $t$  (Figure 4.2). Most terms in the water budget equation (top of the figure) were measured at least daily, including inflows from the Occoquan River ( $J_{\text{OR}}(t)$ , Station 7 in Figure 4.1a), inflows from Bull Run downstream of UOSA’s discharge ( $J_{\text{BR+UOSA}}(t)$ , Station 6), and inflows from UOSA ( $J_{\text{UOSA}}(t)$ , Station 4). Daily inflows from the Bull Run watershed ( $J_{\text{BR}}(t)$ , Station 5), were calculated by subtracting the last two terms. Outflows included daily measurements of abstraction and flow over the dam’s spillway ( $Q_{\text{OUT}}(t)$ , Stations 8 and 9) and daily estimates of evaporation from the reservoir ( $E(t)$ ) obtained from the NASA Land Surface Model [159]. Daily reservoir storage levels,  $S(t)$ , were calculated from daily measurements of reservoir pool elevation (see Table C.1). Finally, daily inflows from the

ungaged portion of the watershed ( $J_{UG}(t)$ ) were estimated from all other terms by rearranging the water balance equation. This last step neglects direct precipitation (which we know is a negligible component of the overall water balance,  $< 2\%$ ) and groundwater exchange. In the event that direct rainfall and groundwater exchange are not negligible, their influence on the water balance is included in the  $J_{UG}(t)$  term. By this approach, water balance over the reservoir was closed to a remarkable degree of precision (over the eleven year period of study, cumulative inflows equal cumulative outflows to within 0.003%, see Section C).

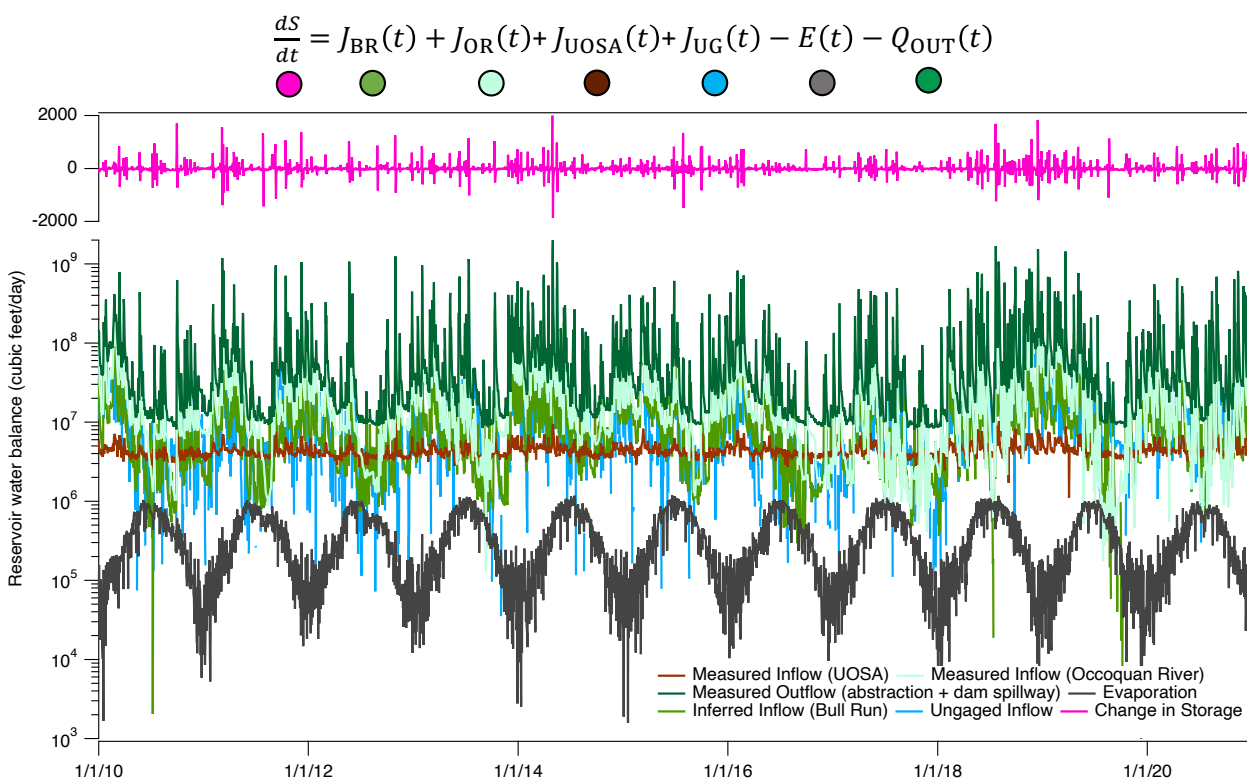


Figure 4.2: **Daily water balance for the Occoquan reservoir (N=4018)**. Daily inflows and outflow over the dam spillway are measured by Virginia Tech’s Occoquan Watershed Monitoring Lab (Stations 6,7 and 8). Daily outflow by abstraction is measured by Fairfax Water. Daily storage is estimated from the measured pool elevation and daily evaporation is obtained from NASA Land Surface Model.

Not surprisingly, outflow from the reservoir (from abstraction and discharge over the dam) is the largest term in the water balance (dark green curve) while outflow via evaporation is

generally the smallest term (black curve) (Figure 4.2). Generally speaking, daily inflows to the reservoir decrease in the order: Occoquan River > Bull Run > Ungaged > UOSA. On a day-to-day basis, however, inflow from the watersheds varies dramatically (in some cases by more than 100-fold), while inflow of reclaimed water from UOSA is remarkably steady (compare green, light green, light blue, and brown curves in the figure). Occasionally, during prolonged dry weather, inflows from the two main tributaries, Occoquan River and Bull Run, drop below the inflow from UOSA, underscoring the water supply benefits of water reclamation.

#### 4.4.3 Step 3: Select a StorAge Selection (SAS) function

In the context of unsteady transit time theory, processes that effect water and solute transport through the control volume are captured by a StorAge Selection (SAS) function, which represents how the selection of water and solute for outflow is biased by age [176]. The SAS function is an emergent property of the physics, biology and chemistry underpinning water and solute transport through a particular system, and is typically represented by one of several analytical probability distributions. In this study we evaluated three forms of the SAS function: a two parameter model (the Gamma distribution [88]), a one parameter model (the Shifted-Uniform distribution [83]), and a zero parameter model (the Uniform distribution [135]). The Gamma distribution's two parameters include the scale parameter  $\beta$  (units of storage) and the shape parameter  $\alpha$  (unitless). The scale parameter was set equal to the volume of water stored in the control volume, while the shape parameter is a measure of how outflow from storage is biased by age. Younger water is preferentially selected for outflow when  $\alpha < 1$  and older water is preferentially selected for outflow when  $\alpha > 1$ . The Shifted Uniform distribution's single parameter,  $p$ , reflects where a particular system is situated along a continuum from pure plug flow sampling (for which only the oldest water

in storage is selected for outflow,  $p = 1$ ) to pure uniform sampling (for which all water in storage has an equal probability of being selected regardless of age,  $p = 0$ ). Conceptually, these two limits represent solute transport by, respectively, advection (plug flow sampling) and dispersive mixing (uniform sampling) [83]. The Uniform SAS, which has no fitting parameters, uniformly selects water and solute for discharge regardless of age. It corresponds to the limit  $p = 0$  in the Shifted-Uniform distribution.

#### 4.4.4 Step 4: Solve the Age Conservation Equation

From the water balance presented in Step 2, and for a particular choice of the three SAS functions described in Step 3, the age conservation equation (ACE) is solved to yield time-varying age distributions of water in storage and outflow from the control volume. These age distributions vary with time because the inflows, outflows and storage in the control volume are all constantly changing. For example, during a storm event, runoff from the watersheds flushes large volumes of new water into the reservoir, skewing the age distributions in storage and outflow younger. The ACE can be solved analytically for the Shifted-Uniform and Uniform SAS functions [83, 158], while numerical solution approaches are required for the Gamma SAS function [89].

#### 4.4.5 Step 5: Predict Sodium Concentrations

In this last step, the sodium ion concentration in water exiting the control volume (i.e., at the Griffith intake; Station 8) is calculated by filtering (or in mathematical terms, convolving) the time-varying age distribution of outflow from Step 4 with the time-varying sodium ion concentration entering the reservoir in watershed runoff and UOSA's reclaimed water. This step requires estimating the daily sodium ion concentration entering the reservoir from all

inflows ( $J_{BR}(t)$ ,  $J_{OR}(t)$ ,  $J_{UOSA}(t)$ , and  $J_{UG}(t)$ ). Daily sodium ion concentrations for the first two inflows were estimated from sodium ion measurements on grab samples collected weekly to monthly at Stations 6 and 7 in Figure 4.1a over the period of interest, 2010 to 2021 (see Section 4.10). Sodium ion concentration in the reclaimed water was set equal to 66 mg/L, as recommended by UOSA (personal communication), which corresponds to the 80th percentile of the N=287 sodium ion concentration measurements on the reclaimed water from 2015 to 2022 (see Figure 4.1b). For obvious reasons, no sodium ion measurements are available for the ungaged inflow,  $J_{UG}(t)$ . Instead, we set the sodium ion concentration of ungaged inflow equal to the power-law function,  $aX^b$ , where  $a$  and  $b$  are unknown constants and  $X$  is the daily sodium ion concentration entering the reservoir from either  $J_{BR}(t)$  or  $J_{OR}(t)$ . Sodium mass loading to the reservoir from all inflows (calculated by multiplying the daily sodium ion concentration by the daily inflow volume) are presented in Appendix C Figure C.2 along with details of numerical implementation.

## 4.5 Transit time model calibration and performance

The transit time model predicts daily sodium ion concentrations at the Griffith intake (Station 8 in Figure 4.1a), based on time-varying inflows of water and sodium ions from the three watersheds ( $J_{BR}(t)$ ,  $J_{OR}(t)$ ,  $J_{UG}(t)$ ) and UOSA ( $J_{UOSA}(t)$ ), the time-varying volume of water in storage ( $S(t)$ ), and the time-varying loss of water from the reservoir by abstraction and flow over the dam spillway ( $Q_{OUT}(t)$ ) and evaporation ( $E(t)$ ). Depending on which SAS function is chosen, the model has between two and three unknown parameters. Two of these parameters are associated with estimating the daily sodium ion concentration entering the reservoir from ungaged flow (see Step 5 above). The Uniform SAS function has no additional parameters (for a total of two unknown parameters), while the Shifted-Uniform and Gamma

SAS functions each have one unknown parameter (for a total of three unknown parameters) (Step 3). In addition, there are two different ways to calculate the sodium ion concentration entering the reservoir from the ungaged portion of the watershed, depending on whether the daily sodium ion concentrations at the Occoquan River or Bull Run watersheds are substituted into the power-law expression (Step 5).

These various model forms were ranked by their ability to predict weekly sodium ion measurements at the far downstream end of the reservoir (at Station 8 in Figure 4.1a), using a model metric Akaike information criterion (AIC) that penalizes overly complicated models. The top ranked model (with the smallest AIC) has a uniform SAS and utilizes the Bull Run sodium ion timeseries in the power-law relationship for ungaged flow. Because the uniform SAS has no parameters, model calibration is simply a matter of inferring values for the two constants in the power-law expression:  $a = 0.4 \pm 0.2$  and  $b = 0.9 \pm 0.2$ . These inferred values for the power-law constants indicate that sodium ion concentrations in runoff from the ungaged portion of the watershed are, on average, about 60% lower than in runoff from the Bull Run watershed.

The calibrated transit time model closely reproduces weekly measurements of sodium ion concentrations at the Griffith intake (coefficient of determination = 64%, Pearson correlation coefficient = 0.8, Nash-Sutcliffe efficiency = 0.63, root mean squared error = 4.89 mg/L, bias = 1%, compare yellow points and black curve in the top panel of Figure 4.3). Model residuals (computed by subtracting model predictions from measurements) do not reveal seasonal patterns as might be expected, for example, if stratification of the reservoir during the summer or deicer wash-off during the winter influenced the age-biasing of solutes and water in the outflow (see Figure C.4).

One reasonable conceptualization of sodium ion transport through the reservoir is that sodium ions enter at the upstream end of the reservoir via Bull Run and the Occoquan

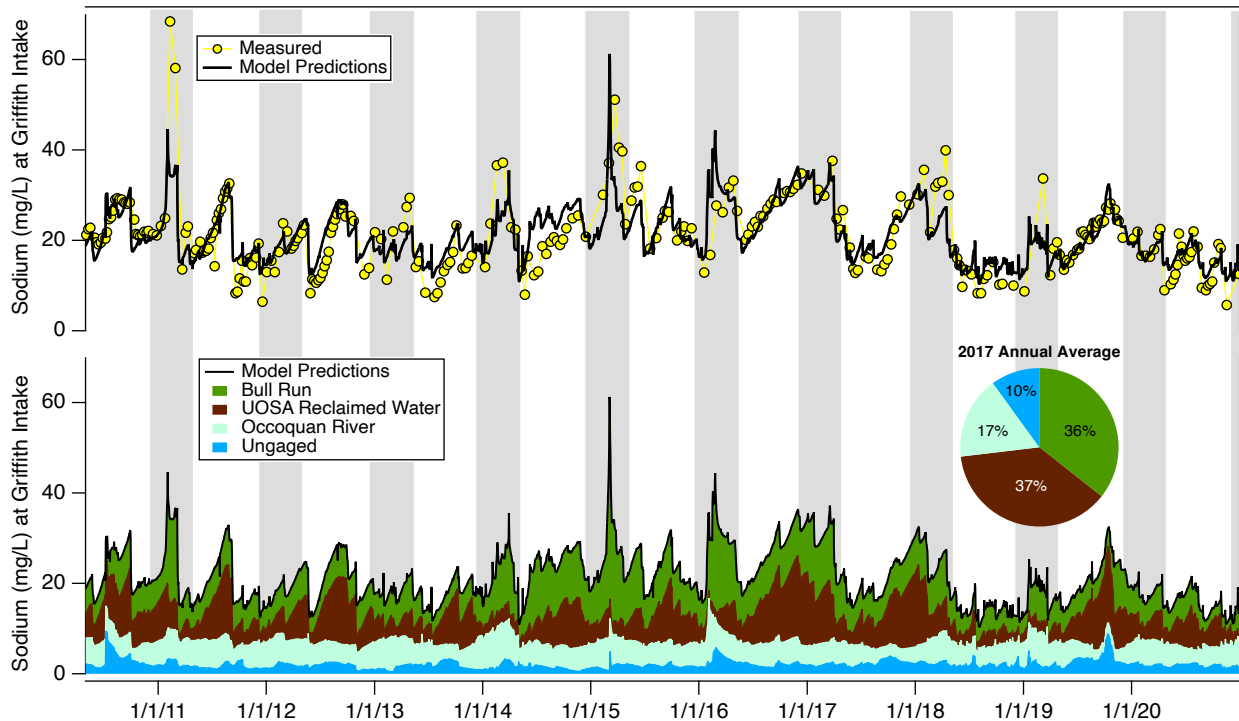


Figure 4.3: **Top panel:** measured and model-predicted sodium ion concentrations at the Griffith intake (Station 8 in Figure 1a). **Bottom panel:** contributions of the different sources shown to predicted sodium concentrations at the Griffith intake. Pie chart inset illustrates, for the year 2017, annually averaged sodium mass load contributions from individual watersheds and UOSA’s reclaimed water. Grey vertical bars denote winter months (December-April). Measurements of sodium ion concentration at station 8 were carried out by Virginia Tech’s Occoquan Watershed Monitoring Lab (N=303)

River, and then slowly transport and mix downstream until reaching the dam and Griffith’s intake. However, this conceptualization is inconsistent with a uniform SAS, for which water and solutes are selected uniformly from storage for outflow. This surprising result probably reflects what is known in the literature as “source dispersion” [23, 84]; i.e., sodium ions enter the reservoir all along its length, not just at the upstream end. Indeed, most of the sodium associated with ungaged flow probably enters the reservoir at the Occoquan dam via Hooes Run, which drains a developed region of Prince William County. In this interpretation, the uniform SAS is evenly sampling water and solute from storage across a wide range of solute travel times through the reservoir, from very short travel times (e.g., for water and solutes

entering the reservoir right at the dam from Hooes Run) to very long travel times (e.g., for water and solutes entering the reservoir at its most upstream end from Bull Run and the Occoquan River). In the next sections, we demonstrate how the transit time model can enhance the three Ostrom variables discussed earlier.

## 4.6 Second-Level Variable RS7: System Predictability

The transit time model enhances system predictability, second-level variable RS7, by quantifying the contribution of various sodium sources to sodium ion concentrations at the Griffith water intake and in the Griffith finished drinking water. Using the Principle of Linear Superposition, for example, the model-predicted sodium ion concentration at the Griffith intake can be expressed as the sum of contributions from watershed runoff (Bull Run, Occoquan River, and ungaged) and UOSA's reclaimed water (bottom panel, Figure 4.3). On average, the contribution of these sources to sodium ion concentrations at the Griffith intake decreases in order: UOSA's reclaimed water  $\approx$  Bull Run  $>$  Occoquan River  $>$  ungaged (pie chart in Figure 4.3). Perhaps even more interesting, however, is how the mix of sources varies seasonally. For example, some of the highest sodium ion concentrations occur during winter months (e.g., see concentration spikes in the winters of 2010, 2011 and 2015 in Figure 4.3), when the contribution of the three watersheds approaches 100%, a pattern consistent with the wash-off of road deicers. Indeed, these three spikes precisely align with likely periods of high deicer application rates, according to Salt Institute guidelines (which are based on temperature and precipitation forecasts) for how much rock salt should be applied per lane mile of road [140] (see Figure C.3). During most years, the contribution of UOSA's reclaimed water to sodium ion concentration at the Griffith intake increases progressively throughout the summer and then declines abruptly in early to late fall (e.g., see the summers of 2016,

2017 and 2019 in Figure 4.3). This seasonal pattern mirrors model predictions of the percent contribution of UOSA's reclaimed water to water behind the dam, which in most years peaks at around 20 to 30% in late summer (Figure C.7). The exception are extremely wet years, such as 2018, when UOSA's contribution to sodium ion concentrations at Griffith remained low year-round.

## 4.7 Second-Level Variable A7: Knowledge of the Social-Ecological System

One of the more surprising results from our flow path analysis is the relatively large fraction of sodium in Griffith's final drinking water that is added by the Griffith water treatment plant itself (around 26% annually, see inset in Figure 4.1d). The likely explanation illustrates the inherent complexity of One Water systems, such as the Occoquan, and specifically how changes in one part of the system can have unintended consequences in another part of the system. Much of the sodium added by the Griffith treatment plant is for pH adjustment, to optimize corrosion control treatment (CCT) and comply with federal regulations regarding lead and copper in drinking water distribution systems [21]. The water treatment operators are responding to a seasonal pattern in the pH and alkalinity of raw water drawn from the Occoquan Reservoir: in late summer the pH declines when the alkalinity (and buffering capacity) of the reservoir water is elevated (Figure 4.4, left panel). To slow the drop in pH and maintain CCT, plant operators add large quantities of the base sodium hydroxide (NaOH, see middle panel of Figure 4.4), which leads to a substantial increase in the concentration of sodium ions across the plant (adding up to 19 mg/L of Na<sup>+</sup> to the finished drinking water in late summer, see right panel of Figure 4.4).

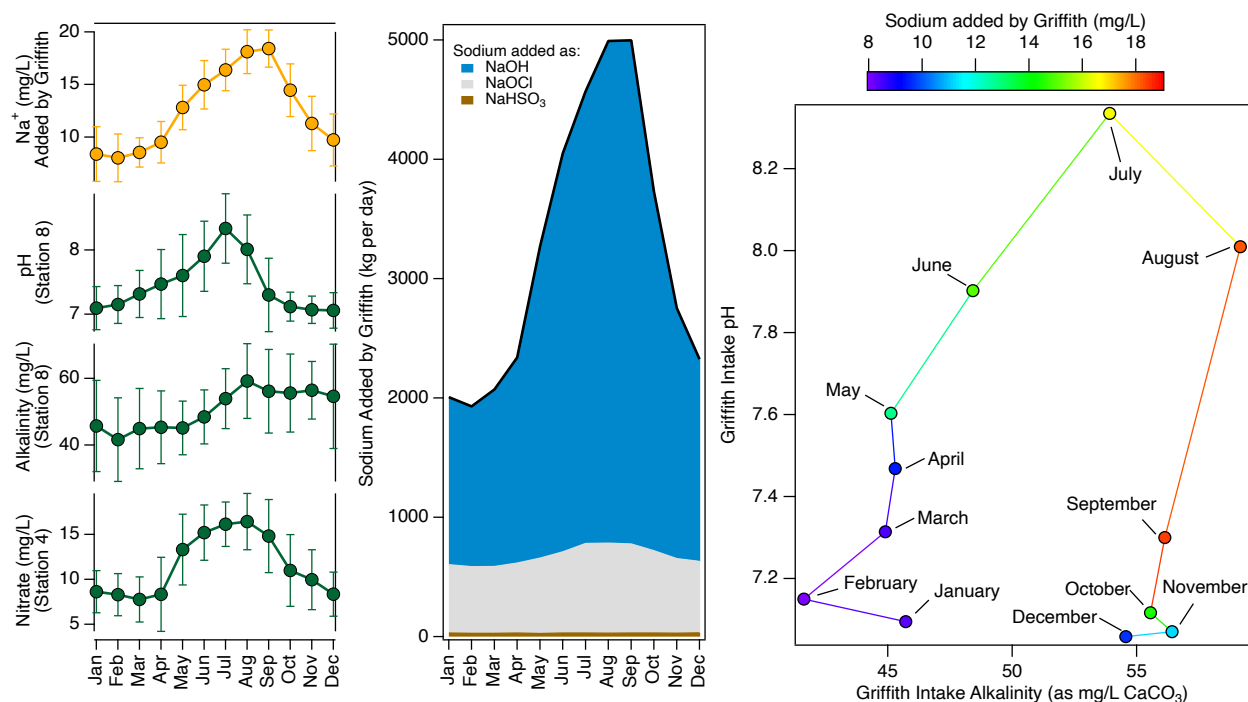


Figure 4.4: **Left panel:** seasonal patterns in sodium added by the Griffith water treatment plant (Stations 9 and 10), the concentration of nitrate in UOSA’s reclaimed water (Station 4), and the pH and alkalinity (as mg CaCO<sub>3</sub>) measured at the downstream end of the Occoquan Reservoir (Station 8 in Figure 1a). **Middle panel:** a seasonal breakdown in the sodium added to Griffith’s final drinking water, including from sodium bisulfite (NaHSO<sub>3</sub>), sodium hypochlorite (NaOCl), and sodium hydroxide (NaOH). **Right panel:** cross-plot of pH and alkalinity in the reservoir at Station 8. The color scale indicates the concentration increase of sodium across the Griffith treatment plant, based on the chemical usage data presented in the middle panel. Note that sodium addition peaks at around 19 mg/L during periods of high (and falling) pH and high alkalinity in the mid- to late-summer. These plots were based on measurements collected from 2010 to 2021 by UOSA (nitrate concentration at Station 4, N=3947), Virginia Tech’s Occoquan Watershed Monitoring Laboratory (pH and alkalinity at Station 8, N=344), and Fairfax Water’s Griffith Water Treatment Plant (chemical usage data, N=100).

In turn, the seasonal pattern in pH and alkalinity in the reservoir appears to be driven, at least in part, by UOSA’s practice of modifying their treatment processes during the summer so that the reclaimed water is rich in nitrate (Figure 4.4, left panel). As noted by Beutel et al. [30], this action has multiple benefits, including: (1) reducing the release of phosphorous from reservoir sediments during periods of hypolimnetic anoxia [52]; (2)

reducing the release of total organic carbon, which can serve as a precursor of cancer-causing disinfection byproducts during water treatment [30]; and (3) reducing the frequency of algal blooms in the reservoir and the quantities of copper sulfate needed for algal control [168]. Much of the nitrate released by UOSA during the summer is denitrified within the reservoir [30]. Because denitrification releases alkalinity and increases pH [180], and because reclaimed water constitutes a higher fraction of water behind the dam during the summer (based on the transit time model results presented earlier, see Figure C.7), UOSA's release of nitrate likely contributes to the need for base addition at the Griffith treatment plant during late summer. Sodium addition at the Griffith treatment plant is therefore linked, at a minimum, to UOSA's wastewater treatment processes, nitrogen and phosphorous cycles in the reservoir, algal bloom dynamics, transport and mixing processes in the reservoir, and the water treatment plant's imperative to comply with Federal rules regarding lead and copper in drinking water. Any strategy that focuses on reducing sodium added by the Griffith treatment plant would need to carefully consider the system-scale implications for the entire social-ecological system.

## 4.8 Second-Level Variable GS6: Collective Choice Rules

The results presented above support bottom-up collective management of sodium in the Occoquan Reservoir in at least three ways (Figure 4.5). First, by elucidating the relative contributions of specific sources to sodium pollution in the reservoir and Griffith's finished drinking water, our results indicate who should be involved in the formulation and rollout of potential changes in rules-in-use at the operational and collective-choice levels (the "who" in the bottom and middle levels, Figure 4.5). For example, the coupling of sodium pollution to the reservoir's nitrogen cycle implies that bilateral discussions between UOSA and Fairfax Water might lead to new operational strategies for the timing and magnitude of nitrate

released to the reservoir, with the triple goal of lowering the quantities of sodium added to Griffith's finished drinking water, maintaining CCT, and supporting the many benefits of nitrate addition to the reservoir noted earlier. Addressing the other sources of sodium will require a more diverse array of stakeholders, spanning residential, commercial, and industrial discharges to the sewage collection systems draining to UOSA, as well as the government agencies and private firms responsible for outdoor deicer application within the Bull Run, Occoquan River, and ungaged portions of the watershed. An example of such broad stakeholder engagement is the Virginia Department of Environmental Quality's collaborative development of best practices for winter deicer use, which resulted in a guidance document called the Salt Management Strategy (SaMS) for Northern Virginia [140].

Second, our analysis reveals a tight coupling between rules-in-use established for regulated contaminants and the emergence of unregulated pollution, here in the form of rising sodium ion concentration in the Occoquan Reservoir. Rules-in-use at the collective-choice level are clearly established for UOSA's point source discharge of nitrate to Bull Run (through the Occoquan Policy enforced by the Virginia Department of Environmental Quality) and Fairfax Water's CCT practices (through lead and copper rules enforced by the Virginia Department of Health) (right-hand side of bottom and middle tiers, Figure 4.5). By contrast, the collective-choice rules-in-use for sodium have evolved *de facto*, and can be summarized as, "do with sodium whatever is in service to other goals". However, as sodium ion concentrations rise in the reservoir, this norm may not be sufficient to sustain this critical water supply. Precisely because sodium is unregulated, operational actors can change the collective-choice institutions through voluntary collaboration (dashed arrow connecting left side of the middle and bottom tiers, Figure 4.5). Our analysis shows which actors have strong operational influence and which, therefore, might have strong collective choice influence, a potential leverage point Ostrom denoted as variable GS6 (Collective-Choice Rules) in her SES framework.

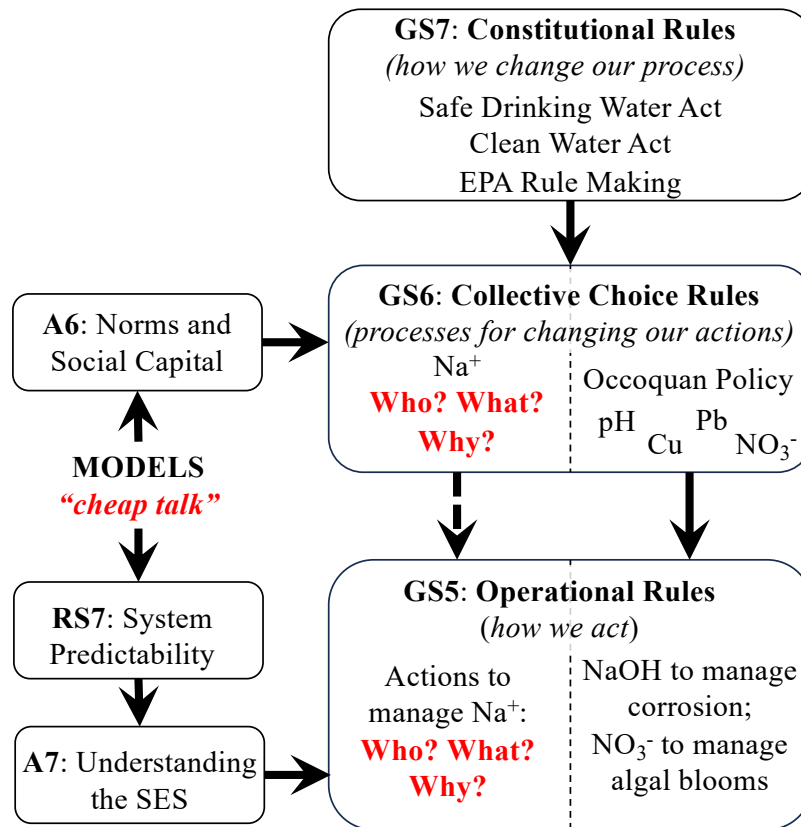


Figure 4.5: Ostrom [153] distinguished between rules-in-use at the operational, collective-choice, and constitutional levels (second-level variables GS5, GS6, and GS7, respectively). Operational rules-in-use determine actions with the natural resource itself, such as UOSA’s practice of increasing the nitrate concentration of their reclaimed water during the summer. Collective-choice rules-in-use set up processes by which actors change their operational practices. For example, the Occoquan Policy establishes the Occoquan Watershed Monitoring Subcommittee, which oversees UOSA’s operational practices. In turn, constitutional rules-in-use determine how to change collective-choice-level processes. The Occoquan Policy, while predating the Clean Water and Safe Drinking Water Acts, is now constrained by those laws and fulfills their mandates. Red lettering denotes leverage points where participatory modeling may help catalyze bottom-up action on the salt pollution problem through “cheap talk,” including “who” should be engaged, “what” rules they co-create, and “why” they are motivated to participate (after Gray et al. [85], see main text for details).

Third, through the 4Ps of participatory modeling [85], the model may support key stakeholders in developing new rules-in-use at both the operational and collective-choice levels (the “what” in the bottom and middle tiers, Figure 4.5) by fostering stronger norms, trust,

and social capital (the “why” in the bottom and middle tiers and second-level variable A6, Figure 4.5) and engendering collective learning through what Ostrom called “cheap talk”—communication with minimal transaction costs (a key part of the participatory modeling process) [154]. For example, the low computational demand of the transit time model enables live exercises in which stakeholders are invited to experiment with different sodium ion concentration thresholds, dial-up or down various sources in the system and witness the predicted effects of each choice in real-time. Informal, follow-up discussions can provide a low-commitment forum for stakeholders to explore, evaluate, and negotiate potential new system interventions and policy choices. As has been demonstrated in other participatory modeling efforts [73, 179, 210, 211], these real-time experiences with system predictability (second level variable RS7) aim to improve understanding of the SES (second level variable A7), facilitate trust, and ultimately enhance interest in, and capacity for, collaborative management around the sodium pollution issue (left side of Figure 4.5).

## 4.9 Conclusions and Future Directions

Decades of theoretical and empirical work suggest that collaborative environmental governance can address complex challenges in systems like the Occoquan [16, 36, 39, 50, 170]. Collaborative governance, central to the One Water approach [1], can be used as an alternative to, or in combination with, top-down governmental methods of water resource management, particularly when regulatory measures are lacking or existing policies and institutions do not have the capacity to handle multi-faceted, multi-scale challenges [98, 190]. By merging participatory modeling exercises with a transit time analysis of sodium sources in drinking water, we are exploring if convergence research in a One Water system can catalyze collaborative governance of an unregulated contaminant through various modes

of researcher-practitioner engagement. Our participatory convergence research approach is building capacity for a contextualized understanding of the system’s response to policy, action, and inaction [179], consistent with the goal of “moving beyond producing knowledge about the world to generating wisdom about how to act within it” [65].

## 4.10 Methods

### 4.10.1 Daily sodium mass loading to the reservoir

From the weekly grab samples collected by Virginia Tech’s Occoquan Watershed Monitoring Lab at Stations 6 and 7 (see Figure 4.1c), we constructed a synthetic daily time series of average sodium mass load using the method in Bhide et al. [32]. Briefly, a family of multiple linear regression (MLR) models of log-transformed sodium concentration (dependent variable) was generated (*glmulti* package in R Statistical Software, R Core Team) by adopting, on the basis of stakeholder recommendations, the following set of potential environmental covariates (independent variables): (1) hourly stream flow, (2) maximum daily rainfall in the preceding two weeks, (3) maximum daily snow depth in the preceding two weeks, (4) number of days below freezing in the preceding two weeks, (5) season (as represented by sine and cosine functions with annual periodicity), and (6) hourly in situ measurements of specific conductance (only at Station 6). The top-ranked MLR model (using Bayesian information criterion (BIC)) was then used to generate an eleven-year (2010–2021) synthetic time series of hourly sodium concentration at Stations 6 and 7 (see Table C.2), which was then combined with hourly flow measurements at each station and aggregated to daily sodium concentration and mass load using the USGS software package Loadflex [17].

The daily sodium mass load from Bull Run down stream of UOSA was further segregated

into mass load discharged from UOSA and mass load coming from the watershed upstream of UOSA using a mass balance approach (Equations 4.1a and 4.1b). Based on historical measurements, we set the sodium ion concentration in UOSA's effluent equal to,  $C_{\text{UOSA}} = 66$  mg/L, and then estimated the sodium concentration attributable to the Bull Run watershed upstream of UOSA,  $C_{\text{BR}}(t)$ , from daily estimates of sodium ion concentration on Bull Run downstream of UOSA's discharge ( $C_{\text{BR+UOSA}}(t)$ ), measurements of daily flow from UOSA ( $J_{\text{UOSA}}(t)$ ) and measurements of daily flow on Bull Run downstream of UOSA ( $J_{\text{BR+UOSA}}(t)$ ) (Equation 4.1b).

$$C_{\text{BR}}(t) = \frac{1}{J_{\text{BR}}(t)} (C_{\text{BR+UOSA}}(t)J_{\text{BR+UOSA}}(t) - C_{\text{UOSA}}J_{\text{UOSA}}(t)) \quad (4.1a)$$

$$J_{\text{BR}}(t) = J_{\text{BR+UOSA}}(t) - J_{\text{UOSA}}(t) \quad (4.1b)$$

Many sources of sodium also exist in the ungaged portion of the reservoir (e.g., surface runoff, groundwater, deicers, etc.). We assumed a power law equation for sodium ion concentration in ungaged flow,  $C_{\text{UG}}(t)$ , testing both  $C_{\text{BR}}(t)$  and  $C_{\text{OR}}(t)$  as independent variables (Equation 4.2a).

$$C_{\text{UG}}(t) = aX^b \quad (4.2a)$$

$$X = \begin{cases} C_{\text{BR}}(t) \\ C_{\text{OR}}(t) \end{cases} \quad (4.2b)$$

Thus, on a daily basis, the total sodium mass load entering the reservoir,  $M_{\text{in}}(t)$ , can be

estimated by the following equation:

$$M_{\text{in}}(t) = C_{\text{OR}}(t)J_{\text{OR}}(t) + C_{\text{UOSA}}J_{\text{UOSA}}(t) + C_{\text{BR}}(t)J_{\text{BR}}(t) + C_{\text{UG}}(t)J_{\text{UG}}(t) \quad (4.3)$$

### 4.10.2 TTD solution, model calibration and validation

Once the dynamic water balance is solved, transit time theory allows us to estimate the time-varying age distribution of water stored in the reservoir and water leaving the reservoir as outflow (i.e., at the Griffith Water Treatment plant intake on the Occoquan Dam). The physics of mass transport through the reservoir (e.g., by advection and dispersion) is captured by the storage selection (SAS) function [176]. We evaluated three SAS functions for the reservoir as follows: (a) the “shifted-uniform” distribution, (b) a “uniform” distribution, and (c) the Gamma distribution.

#### Shifted-uniform SAS

The Shifted-Uniform SAS splits the total reservoir storage in two storage zones (or tanks) arranged in series [83]. The first tank is assigned a Plug-Flow SAS and represents, conceptually, the unsteady advection of solutes along the fastest flow paths through the reservoir. The second tank is assigned a Uniform SAS and represents, conceptually, dispersive mixing and transport of solutes out of the control volume [83]. The fraction,  $0 \leq p \leq 1$ , indicates the partitioning of total reservoir storage at any time,  $S(t)$ , between the upstream ( $pS(t)$ ) and downstream ( $(1-p)S(t)$ ) tanks. Grant and Harman [83] derived an explicit formula for the solute breakthrough concentration under Shifted-Uniform selection, for a single pulse of mass,  $M_i$ , entering the control volume at time  $t = t_{\text{pulse},i}$ , where  $\bar{\tau}(t, t_{\text{BT},i})$  is the discharge-weighted time from  $t$  to  $t_{\text{BT},i}$ , and  $t_{\text{BT},i}$  represents the breakthrough time at which solute

begins to appear in outflow from the control volume:

$$C_Q(t, M_i, t_{BT,i}) = \begin{cases} 0, & t \leq t_{BT,i} \\ \frac{M_i e^{-\bar{\tau}(t, t_{BT,i})}}{(1-p)S(t)}, & t > t_{BT,i} \end{cases} \quad (4.4a)$$

$$\bar{\tau}(t, t_{BT,i}) = \bar{\tau}(t) - \bar{\tau}(t_{BT,i}) \quad (4.4b)$$

$$\bar{\tau}(t) = \int_0^t \frac{Q_{OUT}(x)}{(1-p)S(x)} dx \quad (4.4c)$$

Note that when a non-zero fraction of storage is assigned to the plug-flow tank,  $p > 0$ , the breakthrough time of the  $i^{th}$  pulse is delayed relative to its entrance time,  $t_{BT,i} > t_{pulse,i}$ . This is because, under shifted-uniform sampling, the solute must first transit through the upstream tank (plug-flow sampling in the upstream tank) before it can mix out of the control volume (uniform sampling in the downstream tank). The breakthrough time for the  $i^{th}$  pulse,  $t_{BT,i}$ , is calculated from a set of implicit algebraic equations that depend on the parameter  $p$  and the entire history of inflows and outflows up to and including the breakthrough time (see Grant and Harman [83] for details). Using linear superposition, the solution for  $N$  consecutive pulses can be written as follows, where  $M_i$  is the mass loading for the  $i^{th}$  pulse:

$$C_Q(t) = \sum_{i=1}^N C_Q(t, M_i, t_{BT,i}) \quad (4.5)$$

A daily timeseries of sodium concentration at the Griffith intake was calculated from Equation (4.5) based on the daily sodium mass load entering the reservoir at each daily timestep (Equation (4.3)).

### Uniform SAS

Sodium breakthrough under uniform selection can be estimated from the shifted-uniform solution just presented (Equations 4.4a and 4.5) by setting the volume associated with plug flow through the reservoir equal to zero,  $p = 0$ , and setting the breakthrough time of the  $i^{\text{th}}$  pulse equal to its inflow time:  $t_{BT,i} = t_i$

### Gamma distribution SAS

For the choice of a gamma distribution SAS, sodium concentrations at the the Griffith intake were numerically estimated using the *mesas.py* Python module [89]. See Section C.1.3 for details.

### Model Calibration and Validation

The TTD model was calibrated as follows. For every for choice of  $X$ ,  $a \in (0, 1)$ ,  $b \in (0, 2)$ ,  $p \in (0.01, 1)$  (for the shifted-uniform SAS), and  $\alpha \in (0.01, 5)$  (for the gamma distribution SAS), for all possible combinations of parameter sets we estimated the sodium concentration in reservoir outflow on days when measured sodium concentrations were available. All parameter sets were subsequently ranked based on the root mean squared error (RMSE) between predicted and measured sodium concentration and AIC. The parameter set for the top-ranked model with lowest RMSE and AIC (see Table C.3) was used to generate daily predictions of sodium concentration in reservoir outflow.

# Chapter 5

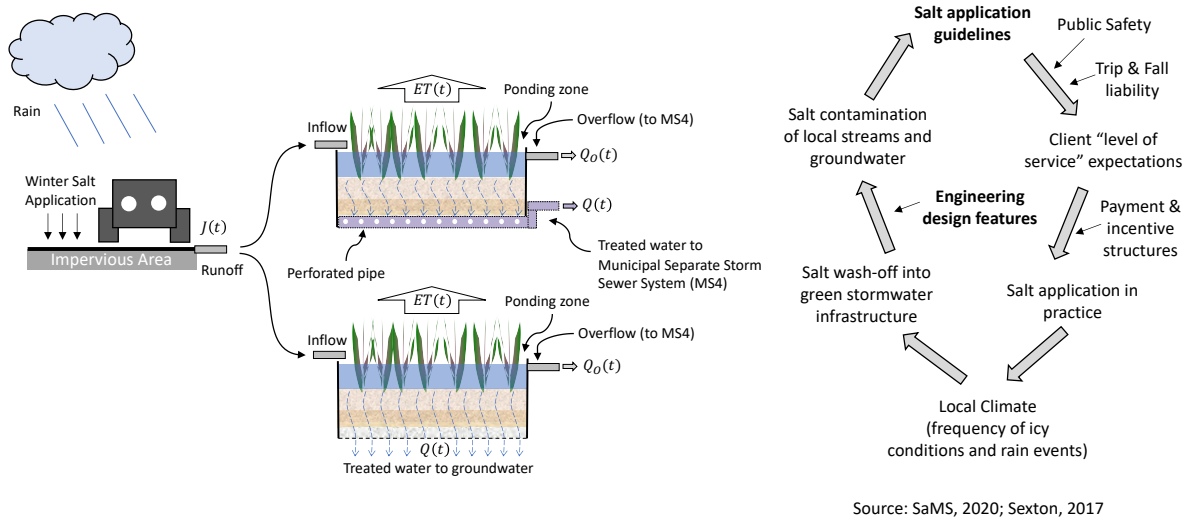
## Conclusions and Future Directions

The combination of studies presented in this dissertation leverage historical monitoring and climate data in the Occoquan Watershed for rigorous copula analyses and transit time modeling, demonstrate novel approaches for studying freshwater salinization and help set the stage for new solutions and possibilities to tackle salt-pollution. The source breakdown analysis for sodium mass loading into the Occoquan Reservoir (Chapter 2) helps in identifying a wide range of behavioural and technological interventions that could be applied at multiple scales in order to increase our salt productivity, i.e., the goods and services produced per unit of salt discharged to our inland freshwaters. The application of unsteady transit time distribution theory provides a novel modeling framework for understanding how salt ions transport through hydrologic systems like catchments (Chapter 3) and reservoirs (Chapter 4), and enables us to deploy a real-time predictive model for daily average sodium ion concentration at the Griffith water treatment plant's raw water intake location in the Occoquan Reservoir. This predictive model also aids in catalyzing stakeholder-led bottom-up management of sodium pollution in the Occoquan Reservoir by enabling participatory modeling exercises and providing an avenue to explore, evaluate and negotiate new system interventions and policy choices.

This dissertation also opens the door to future research possibilities. First, the coupled hydrologic + transit time modeling framework described in Chapter 3 can be extended to study road salt transport through urban stormwater systems. For example, green stormwa-

ter infrastructure (GSI), also known as Low Impact Development, captures and treats urban stormwater runoff before it reaches sensitive receiving waters by mimicking the natural hydrologic cycle and allowing opportunities for plant uptake and infiltration [19, 69, 82, 126]. Biofilters are a particular type of GSI where runoff first enters the ponding zone and is subsequently percolated by gravity into vegetated filter media. Based on the type of biofilter, treated stormwater runoff can either be infiltrated into the ground (infiltration type systems) or released into municipal separate stormwater systems (MS4s) (conveying type systems) (Figure 5.1). Recently, GSI has become popular in most urban stormwater management plans due to three main reasons: (a) they provide additional benefits like urban heat mitigation, habitat creation in support of urban biodiversity, carbon sequestration, recreational opportunities, and mental health [158]; (b) they are cost effective and hence ideal for cash-strapped municipalities that face demands to “green” and improve their existing stormwater infrastructure [138]; and (c) they allow for a range of hybrid design options [138, 202].

Road salts (e.g., NaCl) are applied on urban impervious surfaces (e.g., roads, parking lots, etc.) for deicing purposes during winter months. These salts can easily travel with stormwater runoff to underlying soils and receiving waters through biofilters as they are not designed to treat (i.e., remove) salts [40, 202]. Chloride, for example, is a relatively conservative ion in aqueous phase transport that neither interacts with other constituents nor is taken up by plants in the biofilter [40]. Sodium, on the other hand, behaves non-conservatively and undergoes ion exchange in soils, which can affect biofilter performance in numerous ways (e.g., by reducing the hydraulic conductivity of the filter media, releasing other cations, nutrients and metals, etc. [68, 101]). Thus, excess sodium and chloride can potentially impair biofilter vegetation and hamper the system’s nutrient and pollutant removal capabilities. Taguchi et al. [202], while pointing out shortcomings and limitations of GSI, noted that “Green is not



Source: SaMS, 2020; Sexton, 2017

Figure 5.1: Left panel: Conceptual sketch of biofilters and their role in transporting road salts from impervious surfaces to either groundwater or MS4s. Right panel: Illustration of how engineering design features of GSI, local road salt application guidelines and climate interact.

the same as infallible” and suggested “it may be productive to prevent meltwater on salted surfaces from reaching GSI, at least during periods of winter melting”. Burgis et al. [40] also noted “infiltration type GSI may not be the best choice for drainage areas with high deicing salt loading”. Therefore, it is necessary to understand how salts transport through GSI in order to predict salt mass load and concentration in GSI outflows.

In the context of freshwater salinization, studying this interaction can potentially provide crucial insights about existing salt application guidelines and human behavior (Figure 5.1) [191]. Every region has a standard set of salt application guidelines that are designed with respect to public safety and trip and fall liability concerns to achieve certain client “level of service” expectations (e.g., bare pavement regaining time of  $\approx 2$  hours after a snow event [191]). However due to payment incentive structures (e.g., pay-per-pound schemes), the

actual amount salt application can exceed that specified in the guidelines and the frequency of application depends the local climate (e.g., precipitation chances, icy conditions, etc.). Local climate (e.g., rainfall, snowmelt, etc.) influences runoff from impervious surfaces, that governs the amount of salt washed off into GSI where a combination of engineering design features determines the salt concentration discharged from GSI outflows leading to contamination of local streams and groundwater. This in turn could inform salt application guidelines and human behavior (e.g., rally public/organizational support for revising the current salt application guidelines, etc.).

Future work should combine (1) a transit time based framework (similar to the one described in Chapter 3) for predicting unsteady solute transport through GSI (described in Grant and Harman [83], Parker et al. [158]); (2) local salt application guidelines; and (3) local climate data to develop a reduced order hydrologic model for predicting salt concentrations and mass loads discharged from GSI. Specifically, the interaction between engineering design of GSI (e.g., biofilters), salt application guidelines and local climate may determine the concentration of salt pulses (e.g., sodium, chloride, etc.) entering MS4 systems and local groundwater from urban impervious surfaces (e.g., roads, parking lots, etc.). This would also allow a comparison of salt pulse concentrations under different salt application guidelines. For example, Sexton [191] described different sets of established salt application rates (e.g., those developed by University of Waterloo, Sustainable Salt Initiative, Snow and Ice Management Association, etc.) and found that the recommended application rates for similar weather conditions (pavement temperatures between of 15-20 °F) differed significantly (ranging from 130 lbs./acre to 775 lbs./acre).

Second, the transit time model that predicts the fate and transport of sodium ions through the Occoquan Reservoir (described in Chapter 4) can be extended to include other ions like chloride and nitrate that also affect salinity in the reservoir and in the final drinking water

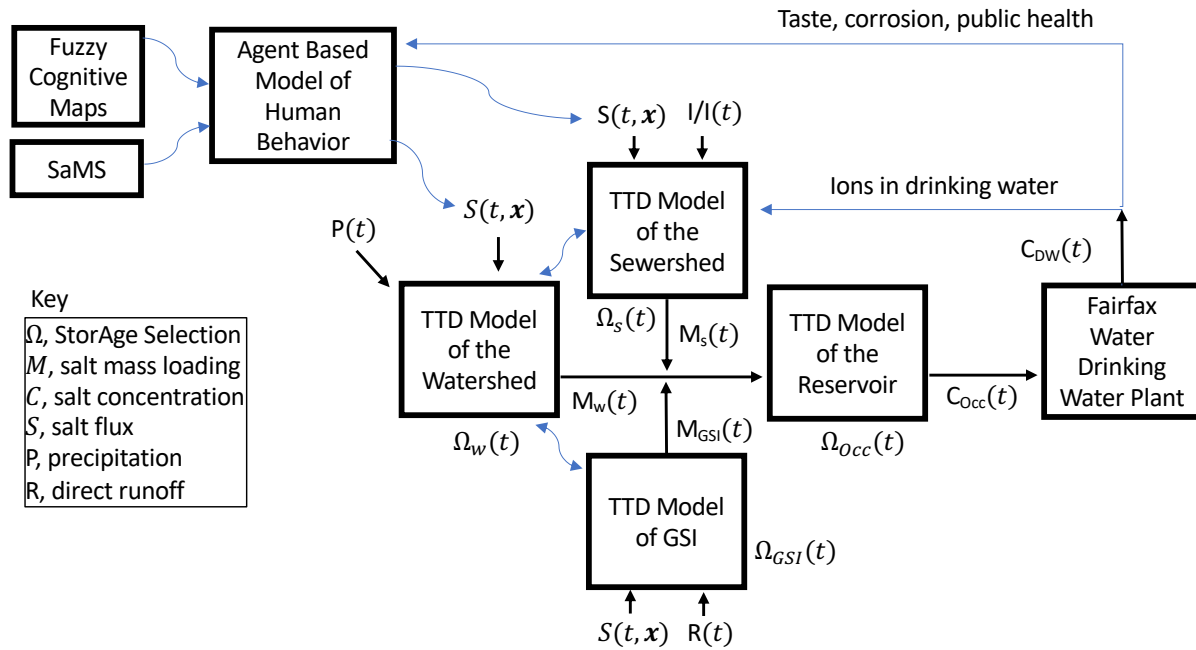


Figure 5.2: A grand vision for an integrated transit time model for salt transport in the Occoquan One Water system.

produced from the Occoquan system. This can potentially be integrated with the current model to investigate the effects of changing UOSA’s practice of releasing highly nitric effluent in summer (see Chapter 4). The transit time theory can also be applied to model the fate and transport of salt ions in UOSA’s sewershed, to better understand the effects of interventions at the household scale (e.g., switching to low sodium products) and those aimed at reducing industrial and commercial salt discharge into the sewershed.

A major advantage of the transit time approach is that all the individual transit time models for salt transport through the sewershed, watershed, green stormwater infrastructure and the reservoir can be linked together in series and/or parallel to account for interactions across multiple urban water systems. Figure 5.2 presents a grand vision for an integrated model of salt transport in the Occoquan system to predict salt concentration at Griffith’s water intake location in the Occoquan Reservoir. This integrated model can also potentially be paired

with agent-based models of human behavior that simulate salt inputs to the watershed in different real-world scenarios. These models can potentially capture the positive and negative feedbacks between engineered, ecological and social system components that might influence the emergence of new institutions for managing freshwater salinization [27, 132].

# Bibliography

- [1] One Water Roadmap: The Sustainable Management of Life’s Most Essential Resource | U.S. Climate Resilience Toolkit. URL <https://toolkit.climate.gov/reports/one-water-roadmap-sustainable-management-lifes-most-essential-resource>.
- [2] Guidelines for drinking-water quality. volume Vol. 2, Health criteria and other supporting information. World Health Organization, Geneva, 2nd edition edition, 1996. Section: Sodium in Drinking Water.
- [3] Ambient Water Quality Criteria for Chloride. Technical Report EPA 440/5-88-001, U.S. Environmental Protection Agency, Washington D.C., 1998.
- [4] Drinking Water Advisory: Consumer Acceptability Advice and Health Effects Analysis on Sodium. Technical Report EPA 822-R-03-006, U.S. Environmental Protection Agency, Washington D.C., February 2003.
- [5] *Water Reuse: Potential for Expanding the Nation’s Water Supply Through Reuse of Municipal Wastewater*. National Academies Press, Washington, D.C., July 2012. ISBN 978-0-309-25749-7. doi: 10.17226/13303. URL <http://www.nap.edu/catalog/13303>.
- [6] *Convergence: Facilitating Transdisciplinary Integration of Life Sciences, Physical Sciences, Engineering, and Beyond*. National Academies Press, Washington, D.C., June 2014. ISBN 978-0-309-30151-0. doi: 10.17226/18722. URL <http://www.nap.edu/catalog/18722>.
- [7] Freshwater: Supply concerns continue, and uncertainties complicate planning. Tech-

- nical Report GAO-14-43, U.S. Government Accountability Office, 2014. URL <https://www.gao.gov/assets/670/663343.pdf>.
- [8] 2017 Potable Reuse Compendium. Technical report, U.S. Environmental Protection Agency, 2017. URL [https://www.epa.gov/sites/production/files/2018-01/documents/potablereusecompendium\\_3.pdf](https://www.epa.gov/sites/production/files/2018-01/documents/potablereusecompendium_3.pdf).
- [9] Comprehensive Annual Financial Report. Technical report, Upper Occoquan Service Authority, 2017.
- [10] Cooperative Forecasts: Employment, Population, and Household Forecasts by Transportation Analysis Zone | Metropolitan Washington Council of Governments, 2018. URL <https://www.mwcog.org/documents/2021/12/02/cooperative-forecasts-employment-population-and-household-forecasts-by-transportat>
- [11] Micron Announces Investment in its Semiconductor Manufacturing Plant in Manassas, VA [Press Release], August 2018. URL <https://investors.micron.com/node/37386/pdf>. Published: Press Release.
- [12] Draft National Water Reuse Action Plan. Technical report, U.S. Environmental Protection Agency, 2019. URL <https://www.epa.gov/waterreuse/draft-national-water-reuse-action-plan>.
- [13] Chesapeake Assessment and Scenario Tool (CAST), 2020. URL [Retrievedfromhttps://cast.chesapeakebay.net/](https://cast.chesapeakebay.net/).
- [14] International Stormwater BMP Database: 2020 Summary Statistics. Technical Report Project No. 4968, The Water Research Foundation, 2020.
- [15] M. A. Ahmed, S. G. Abdel Samie, and H. A. Badawy. Factors controlling mechanisms of groundwater salinization and hydrogeochemical processes in the Quaternary aquifer of

- the Eastern Nile Delta, Egypt. *Environmental Earth Sciences*, 68(2):369–394, January 2013. ISSN 1866-6299. doi: 10.1007/s12665-012-1744-6. URL <https://doi.org/10.1007/s12665-012-1744-6>.
- [16] Chris Ansell and Alison Gash. Collaborative Governance in Theory and Practice. *Journal of Public Administration Research and Theory*, 18(4):543–571, October 2008. ISSN 1053-1858. doi: 10.1093/jopart/mum032. URL <https://doi.org/10.1093/jopart/mum032>.
- [17] Alison P. Appling, Miguel C. Leon, and William H. McDowell. Reducing bias and quantifying uncertainty in watershed flux estimates: the R package loadflex. *Ecosphere*, 6(12):1–25, 2015. ISSN 2150-8925. doi: 10.1890/ES14-00517.1. URL <https://onlinelibrary.wiley.com/doi/abs/10.1890/ES14-00517.1>.  
\_eprint: <https://onlinelibrary.wiley.com/doi/pdf/10.1890/ES14-00517.1>.
- [18] Amanda Arnold and Katherine Bowman, editors. *Fostering the Culture of Convergence in Research: Proceedings of a Workshop*. National Academies Press, Washington, D.C., June 2019. ISBN 978-0-309-48495-4. doi: 10.17226/25271. URL <https://www.nap.edu/catalog/25271>.
- [19] Asal Askarizadeh, Megan A. Rippy, Tim D. Fletcher, David L. Feldman, Jian Peng, Peter Bowler, Andrew S. Mehring, Brandon K. Winfrey, Jasper A. Vrugt, Amir AghaKouchak, Sunny C. Jiang, Brett F. Sanders, Lisa A. Levin, Scott Taylor, and Stanley B. Grant. From Rain Tanks to Catchments: Use of Low-Impact Development To Address Hydrologic Symptoms of the Urban Stream Syndrome. *Environmental Science & Technology*, 49(19):11264–11280, October 2015. ISSN 0013-936X. doi: 10.1021/acs.est.5b01635. URL <https://doi.org/10.1021/acs.est.5b01635>. Publisher: American Chemical Society.

- [20] American Water Works Association and American Society of Civil Engineers. *Water treatment plant design*. McGraw-Hill, New York, 1998. ISBN 0-07-001643-7.
- [21] AWWA. *Managing Change and Unintended Consequences: Lead and Copper Rule Corrosion Control Treatment*. Technical report, AWWA, Denver, 2005.
- [22] Giuliano Di Baldassarre, Murugesu Sivapalan, Maria Rusca, Christophe Cudennec, Margaret Garcia, Heidi Kreibich, Megan Konar, Elena Mondino, Johanna Mård, Saket Pande, Matthew R. Sanderson, Fuqiang Tian, Alberto Viglione, Jing Wei, Yongping Wei, David J. Yu, Veena Srinivasan, and Günter Blöschl. Sociohydrology: Scientific Challenges in Addressing the Sustainable Development Goals. *Water Resources Research*, 55(8):6327–6355, August 2019. doi: 10.1029/2018wr023901. Publisher: American Geophysical Union (AGU).
- [23] Paolo Benettin, James W. Kirchner, Andrea Rinaldo, and Gianluca Botter. Modeling chloride transport using travel time distributions at Plynlimon, Wales. *Water Resources Research*, 51(5):3259–3276, 2015. ISSN 1944-7973. doi: 10.1002/2014WR016600. URL <https://onlinelibrary.wiley.com/doi/abs/10.1002/2014WR016600>. \_\_eprint: <https://onlinelibrary.wiley.com/doi/pdf/10.1002/2014WR016600>.
- [24] Paolo Benettin, Chris Soulsby, Christian Birkel, Doerthe Tetzlaff, Gianluca Botter, and Andrea Rinaldo. Using SAS functions and high-resolution isotope data to unravel travel time distributions in headwater catchments. *Water Resources Research*, 53(3):1864–1878, 2017. ISSN 1944-7973. doi: 10.1002/2016WR020117. URL <https://onlinelibrary.wiley.com/doi/abs/10.1002/2016WR020117>. \_\_eprint: <https://onlinelibrary.wiley.com/doi/pdf/10.1002/2016WR020117>.
- [25] Paolo Benettin, Nicolas B. Rodriguez, Matthias Sprenger, Minseok Kim, Julian Klaus, Ciaran J. Harman, Ype van der Velde, Markus Hrachowitz, Gi-

- anluca Botter, Kevin J. McGuire, James W. Kirchner, Andrea Rinaldo, and Jeffrey J. McDonnell. Transit Time Estimation in Catchments: Recent Developments and Future Directions. *Water Resources Research*, 58(11): e2022WR033096, 2022. ISSN 1944-7973. doi: 10.1029/2022WR033096. URL <https://onlinelibrary.wiley.com/doi/abs/10.1029/2022WR033096>. \_eprint: <https://onlinelibrary.wiley.com/doi/pdf/10.1029/2022WR033096>.
- [26] Lawrence Benjamin, Ronald W. Green, Anita Smith, and Stephan Summerer. Pilot Testing a Limestone Contactor in British Columbia. *Journal - American Water Works Association*, 84(5):70–79, May 1992. doi: 10.1002/j.1551-8833.1992.tb07356.x. Publisher: Wiley.
- [27] Emily Zechman Berglund. Using Agent-Based Modeling for Water Resources Planning and Management. *Journal of Water Resources Planning and Management*, 141(11):04015025, November 2015. ISSN 1943-5452. doi: 10.1061/(ASCE)WR.1943-5452.0000544. URL <https://ascelibrary.org/doi/10.1061/%28ASCE%29WR.1943-5452.0000544>. Publisher: American Society of Civil Engineers.
- [28] Sten Bergström. The Development of a Snow Routine for the Hbv-2 Model. *Nordic Hydrology*, 6(2):73–92, April 1975. ISSN 00291277. URL <https://www.proquest.com/docview/1943669082/abstract/39539BED77E4EC4PQ/1>.
- [29] E. Bertuzzo, M. Thomet, G. Botter, and A. Rinaldo. Catchment-scale herbicides transport: Theory and application. *Advances in Water Resources*, 52:232–242, February 2013. ISSN 0309-1708. doi: 10.1016/j.advwatres.2012.11.007. URL <https://www.sciencedirect.com/science/article/pii/S0309170812002898>.
- [30] Marc W. Beutel, Ricardi Duvil, Francisco J. Cubas, David A. Matthews, Frank M. Wilhelm, Thomas J. Grizzard, David Austin, Alexander J. Horne, and Seyoum Ge-

- bremariam. A review of managed nitrate addition to enhance surface water quality. *Critical Reviews in Environmental Science and Technology*, 46(7):673–700, April 2016. ISSN 1064-3389. doi: 10.1080/10643389.2016.1151243. URL <https://doi.org/10.1080/10643389.2016.1151243>. Publisher: Taylor & Francis \_eprint: <https://doi.org/10.1080/10643389.2016.1151243>.
- [31] Aditi S. Bhaskar and Claire Welty. Analysis of subsurface storage and streamflow generation in urban watersheds. *Water Resources Research*, 51(3):1493–1513, 2015. ISSN 1944-7973. doi: 10.1002/2014WR015607. URL <https://onlinelibrary.wiley.com/doi/abs/10.1002/2014WR015607>. \_eprint: <https://onlinelibrary.wiley.com/doi/pdf/10.1002/2014WR015607>.
- [32] Shantanu V. Bhide, Stanley B. Grant, Emily A. Parker, Megan A. Rippy, Adil N. Godrej, Sujay Kaushal, Greg Prelewicz, Niffy Saji, Shannon Curtis, Peter Vikesland, Ayella Maile-Moskowitz, Marc Edwards, Kathryn G. Lopez, Thomas A. Birkland, and Todd Schenk. Addressing the contribution of indirect potable reuse to inland freshwater salinization. *Nature Sustainability*, 4(8):699–707, August 2021. ISSN 2398-9629. doi: 10.1038/s41893-021-00713-7. URL <https://www.nature.com/articles/s41893-021-00713-7>.
- [33] Shantanu Vidyadhar Bhide. *The Effects of Basin Slope and Boundary Friction on the Character and Plunge Location of Hyperpycnal Flows Entering a Laterally Unbounded Basin*. Thesis, Virginia Tech, June 2019. URL <https://vtechworks.lib.vt.edu/handle/10919/90380>. Accepted: 2019-06-20T08:02:14Z Artwork Medium: ETD Interview Medium: ETD.
- [34] Darcy L. Bird, Peter M. Groffman, Christopher J. Salice, and Joel Moore. Steady-State Land Cover but Non-Steady-State Major Ion Chemistry in Urban Streams. *Environ-*

- mental Science & Technology*, 52(22):13015–13026, November 2018. ISSN 0013-936X. doi: 10.1021/acs.est.8b03587. URL <https://doi.org/10.1021/acs.est.8b03587>.
- [35] Thomas P. Bonacquisti. The Fairfax County Water Authority response to the Colonial oil spill of March 28, 1993. April 1994. URL <https://vtechworks.lib.vt.edu/handle/10919/46368>. Accepted: 2014-03-14T21:52:14Z Artwork Medium: BTD Interview Medium: BTD Publisher: Virginia Tech.
- [36] David E. Booher and Judith E. Innes. Governance for Resilience: CALFED as a Complex Adaptive Network for Resource Management. *Ecology and Society*, 15(3), 2010. ISSN 1708-3087. URL <https://www.jstor.org/stable/26268176>. Publisher: Resilience Alliance Inc.
- [37] Gianluca Botter, Enrico Bertuzzo, and Andrea Rinaldo. Catchment residence and travel time distributions: The master equation. *Geophysical Research Letters*, 38(11), 2011. ISSN 1944-8007. doi: 10.1029/2011GL047666. URL <https://onlinelibrary.wiley.com/doi/abs/10.1029/2011GL047666>. \_eprint: <https://onlinelibrary.wiley.com/doi/pdf/10.1029/2011GL047666>.
- [38] Stéphanie Brichau, Uwe Ring, Andrew Carter, Robert Bolhar, Patrick Monié, Daniel Stockli, and Maurice Brunel. Timing, slip rate, displacement and cooling history of the Mykonos detachment footwall, Cyclades, Greece, and implications for the opening of the Aegean Sea basin. *Journal of the Geological Society*, 165(1):263–277, January 2008. doi: 10.1144/0016-76492006-145. URL <https://www.lyellcollection.org/doi/abs/10.1144/0016-76492006-145>. Publisher: The Geological Society of London.
- [39] Marie Claire Brisbois and Rob C. de Loë. State roles and motivations in collaborative approaches to water governance: A power theory-based analysis. *Geoforum*, 74:202–

- 212, August 2016. ISSN 0016-7185. doi: 10.1016/j.geoforum.2016.06.012. URL <https://www.sciencedirect.com/science/article/pii/S0016718515302086>.
- [40] Charles R. Burgis, Gail M. Hayes, Derek A. Henderson, Wuhuan Zhang, and James A. Smith. Green stormwater infrastructure redirects deicing salt from surface water to groundwater. *Science of The Total Environment*, 729:138736, August 2020. ISSN 0048-9697. doi: 10.1016/j.scitotenv.2020.138736. URL <https://www.sciencedirect.com/science/article/pii/S0048969720322531>.
- [41] Vincent Calcagno and Claire de Mazancourt. glmulti: An R Package for Easy Automated Model Selection with (Generalized) Linear Models. *Journal of Statistical Software*, 34:1–29, May 2010. ISSN 1548-7660. doi: 10.18637/jss.v034.i12. URL <https://doi.org/10.18637/jss.v034.i12>.
- [42] Miguel Cañedo-Argüelles, Ben Kefford, and Ralf Schäfer. Salt in freshwaters: causes, effects and prospects - introduction to the theme issue. *Philosophical Transactions of the Royal Society B: Biological Sciences*, 374(1764):20180002, December 2018. doi: 10.1098/rstb.2018.0002. Publisher: The Royal Society.
- [43] Martyn P. Clark, Richard M. Vogel, Jonathan R. Lamontagne, Naoki Mizukami, Wouter J. M. Knoben, Guoqiang Tang, Shervan Gharari, Jim E. Freer, Paul H. Whitfield, Kevin R. Shook, and Simon Michael Papalexiou. The Abuse of Popular Performance Metrics in Hydrologic Modeling. *Water Resources Research*, 57(9):e2020WR029001, 2021. ISSN 1944-7973. doi: 10.1029/2020WR029001. URL <https://onlinelibrary.wiley.com/doi/abs/10.1029/2020WR029001>.
- [44] Mary E. Cogswell, Catherine M. Loria, Ana L. Terry, Lixia Zhao, Chia-Yih Wang, Te-Ching Chen, Jacqueline D. Wright, Christine M. Pfeiffer, Robert Merritt, Claudia S. Moy, and Lawrence J. Appel. Estimated 24-Hour Urinary Sodium and Potassium

- Excretion in US Adults. *JAMA*, 319(12):1209–1220, March 2018. ISSN 0098-7484. doi: 10.1001/jama.2018.1156. URL <https://doi.org/10.1001/jama.2018.1156>.
- [45] Maria Collivignarelli, Alessandro Abbà, Ilaria Benigna, Sabrina Sorlini, and Vincenzo Torretta. Overview of the Main Disinfection Processes for Wastewater and Drinking Water Treatment Plants. *Sustainability*, 10(2):86, December 2017. doi: 10.3390/su10010086. Publisher: MDPI AG.
- [46] Viviana Consonni, Davide Ballabio, and Roberto Todeschini. Evaluation of model predictive ability by external validation techniques. *Journal of Chemometrics*, 24(3-4):194–201, February 2010. doi: 10.1002/cem.1290. Publisher: Wiley.
- [47] Curtis A. Cooper, Paul M. Mayer, and Barton R. Faulkner. Effects of road salts on groundwater and surface water dynamics of sodium and chloride in an urban restored stream. *Biogeochemistry*, 121(1):149–166, October 2014. ISSN 1573-515X. doi: 10.1007/s10533-014-9968-z. URL <https://doi.org/10.1007/s10533-014-9968-z>.
- [48] Steven R. Corsi, Steven W. Geis, Jorge E. Loyo-Rosales, Clifford P. Rice, Rebecca J. Sheesley, Greg G. Failey, and Devon A. Cancilla. Characterization of Aircraft Deicer and Anti-Icer Components and Toxicity in Airport Snowbanks and Snowmelt Runoff. *Environmental Science & Technology*, 40(10):3195–3202, May 2006. ISSN 0013-936X. doi: 10.1021/es052028m. URL <https://doi.org/10.1021/es052028m>. Publisher: American Chemical Society.
- [49] Steven R. Corsi, Laura A. De Cicco, Michelle A. Lutz, and Robert M. Hirsch. River chloride trends in snow-affected urban watersheds: increasing concentrations outpace urban growth rate and are common among all seasons. *Science of The Total Environment*, 508:488–497, March 2015. doi: 10.1016/j.scitotenv.2014.12.012. Publisher: Elsevier BV.

- [50] Barbara Cosens, J. B. Ruhl, Niko Soininen, Lance Gunderson, Antti Belinskij, Thorsten Blenckner, Alejandro E. Camacho, Brian C. Chaffin, Robin Kundis Craig, Holly Doremus, Robert Glicksman, Anna-Stiina Heiskanen, Rhett Larson, and Jukka Similä. Governing complexity: Integrating science, governance, and law to manage accelerating change in the globalized commons. *Proceedings of the National Academy of Sciences*, 118(36):e2102798118, September 2021. doi: 10.1073/pnas.2102798118. URL <https://www.pnas.org/doi/abs/10.1073/pnas.2102798118>. Publisher: Proceedings of the National Academy of Sciences.
- [51] Beatrice I. Crona and John N. Parker. Learning in Support of Governance: Theories, Methods, and a Framework to Assess How Bridging Organizations Contribute to Adaptive Resource Governance. *Ecology and Society*, 17(1), 2012. ISSN 1708-3087. URL <https://www.jstor.org/stable/26269019>. Publisher: Resilience Alliance Inc.
- [52] Francisco J. Cubas, John T. Novak, Adil N. Godrej, and Thomas J. Grizzard. Effects of Nitrate Input from a Water Reclamation Facility on the Occoquan Reservoir Water Quality. *Water Environment Research*, 86(2):123–133, 2014. ISSN 1554-7531. doi: 10.2175/106143013X13596524517067.
- [53] Michelle L. Daley, Jody D. Potter, and William H. McDowell. Salinization of urbanizing New Hampshire streams and groundwater: effects of road salt and hydrologic variability. *Journal of the North American Benthological Society*, 28(4): 929–940, December 2009. ISSN 0887-3593. doi: 10.1899/09-052.1. URL <https://www.journals.uchicago.edu/doi/10.1899/09-052.1>.
- [54] P. J. Davies, I. A. Wright, O. J. Jonasson, and S. J. Findlay. Impact of concrete and PVC pipes on urban water chemistry. *Urban Water Journal*, 7(4):233–241, August 2010. doi: 10.1080/1573062x.2010.484502. Publisher: Informa UK Limited.

- [55] Mackenzie L. Davis. *Water and wastewater engineering : design principles and practice*. McGraw-Hill, New York, 2010. ISBN 978-0-07-171384-9.
- [56] Andrea M. Dietrich and Gary A. Burlingame. Critical Review and Rethinking of USEPA Secondary Standards for Maintaining Organoleptic Quality of Drinking Water. *Environmental Science & Technology*, 49(2):708–720, January 2015. ISSN 0013-936X. doi: 10.1021/es504403t. URL <https://doi.org/10.1021/es504403t>.
- [57] Ines Dombrowsky, Andrea Lenschow, Franziska Meergans, Nora Schütze, Evelyn Lukat, Ulf Stein, and Ali Yousefi. Effects of policy and functional (in)coherence on coordination – A comparative analysis of cross-sectoral water management problems. *Environmental Science & Policy*, 131:118–127, May 2022. ISSN 1462-9011. doi: 10.1016/j.envsci.2022.01.019. URL <https://www.sciencedirect.com/science/article/pii/S1462901122000302>.
- [58] Aaron D. Dotson, Caitlin E. Rodriguez, and Karl G. Linden. UV disinfection implementation status in US water treatment plants. *Journal - American Water Works Association*, 104(5):E318–E324, May 2012. doi: 10.5942/jawwa.2012.104.0075. Publisher: Wiley.
- [59] Hilary A. Dugan, Sarah L. Bartlett, Samantha M. Burke, Jonathan P. Doubek, Flora E. Krivak-Tetley, Nicholas K. Skaff, Jamie C. Summers, Kaitlin J. Farrell, Ian M. McCullough, Ana M. Morales-Williams, Derek C. Roberts, Zutao Ouyang, Facundo Scordo, Paul C. Hanson, and Kathleen C. Weathers. Salting our freshwater lakes. *Proceedings of the National Academy of Sciences*, 114(17):4453–4458, April 2017. doi: 10.1073/pnas.1620211114. Publisher: Proceedings of the National Academy of Sciences.

- [60] Steve Edgemon. Letter from the General Manager of Fairfax Water to Stan Grant, January 2020.
- [61] EPA. Drinking Water Advisory: Consumer Acceptability Advice and Health Effects Analysis on Sodium. Technical Report EPA 822-R-03-006, EPA, 2003.
- [62] Lennart Eriksson, Joanna Jaworska, Andrew P. Worth, Mark T. D. Cronin, Robert M. McDowell, and Paola Gramatica. Methods for reliability and uncertainty assessment and for applicability evaluations of classification- and regression-based QSARs. *Environmental Health Perspectives*, 111(10):1361–1375, August 2003. doi: 10.1289/ehp.5758. Publisher: Environmental Health Perspectives.
- [63] Marlene Evans and Cherie Frick. The effects of road salts on aquatic ecosystems. Technical Report 02-308, Environment Canada, August 2001. URL <https://vegvesen.brage.unit.no/vegvesen-xmlui/handle/11250/193946>. Accepted: 2014-04-07T07:16:30Z Publisher: Environment Canada.
- [64] Ian R. Falconer, Heather F. Chapman, Michael R. Moore, and Geetha Ranmuthugala. Endocrine-disrupting compounds: A review of their challenge to sustainable and safe water supply and water reuse. *Environmental Toxicology*, 21(2):181–191, 2006. doi: 10.1002/tox.20172. Publisher: Wiley.
- [65] Ioan Fazey, Niko Schöpke, Guido Caniglia, Anthony Hodgson, Ian Kendrick, Christopher Lyon, Glenn Page, James Patterson, Chris Riedy, Tim Strasser, Stephan Verveen, David Adams, Bruce Goldstein, Matthias Klaes, Graham Leicester, Alison Linyard, Adrienne McCurdy, Paul Ryan, Bill Sharpe, Giorgia Silvestri, Ali Yansyah Abdurrahim, David Abson, Olufemi Samson Adetunji, Paulina Aldunce, Carlos Alvarez-Pereira, Jennifer Marie Amparo, Helene Amundsen, Lakin Anderson, Lotta Andersson, Michael Asquith, Karoline Augenstein, Jack Barrie, David Bent, Julia Bentz,

Arvid Bergsten, Carol Berzonsky, Olivia Bina, Kirsty Blackstock, Joanna Boehnert, Hilary Bradbury, Christine Brand, Jessica Böhme (born Sangmeister), Marianne Mille Bøjer, Esther Carmen, Lakshmi Charli-Joseph, Sarah Choudhury, Supot Chunchoti-ananta, Jessica Cockburn, John Colvin, Irena L. C. Connon, Rosalind Cornforth, Robin S. Cox, Nicholas Cradock-Henry, Laura Cramer, Almendra Cremaschi, Halvor Dannevig, Catherine T. Day, Cathel de Lima Hutchison, Anke de Vrieze, Vikas Desai, Jonathan Dolley, Dominic Duckett, Rachael Amy Durrant, Markus Egermann, Emily Elsner (Adams), Chris Fremantle, Jessica Fullwood-Thomas, Diego Galafassi, Jen Gobby, Ami Golland, Shiara Kirana González-Padrón, Irmelin Gram-Hanssen, Jakob Grandin, Sara Grenni, Jade Lauren Gunnell, Felipe Gusmao, Maike Hamann, Brian Harding, Gavin Harper, Mia Hesselgren, Dina Hestad, Cheryl Anne Heykoop, Johan Holmén, Kirsty Holstead, Claire Hoolohan, Andra-Ioana Horcea-Milcu, Lumina Geertruida Horlings, Stuart Mark Howden, Rachel Angharad Howell, Sarah Insia Huque, Mirna Liz Inturias Canedo, Chidinma Yvonne Iro, Christopher D. Ives, Beatrice John, Rajiv Joshi, Sadhbh Juarez-Bourke, Dauglas Wafula Juma, Bea Cecilie Karlsen, Lea Kliem, Andreas Kläy, Petra Kuenkel, Iris Kunze, David Patrick Michael Lam, Daniel J. Lang, Alice Larkin, Ann Light, Christopher Luederitz, Tobias Luthe, Cathy Maguire, Ana-Maria Mahecha-Groot, Jackie Malcolm, Fiona Marshall, Yihyeis Maru, Carly McLachlan, Peter Mmbando, Subhakanta Mohapatra, Michele-Lee Moore, Angela Moriggi, Mark Morley-Fletcher, Susanne Moser, Konstanze Marion Mueller, Mutizwa Mukute, Susan Mühlemeier, Lars Otto Naess, Marta Nieto-Romero, Paula Novo, Karen O'Brien, Deborah Anne O'Connell, Kathleen O'Donnell, Per Olsson, Kelli Rose Pearson, Laura Pereira, Panos Petridis, Daniela Peukert, Nicky Phear, Siri Renée Pisters, Matt Polsky, Diana Pound, Rika Preiser, Md. Sajidur Rahman, Mark S. Reed, Philip Revell, Iokiñe Rodriguez, Briony Cathryn Rogers, Jascha Rohr, Milda Nordbø Rosenberg, Helen Ross, Shona Russell, Melanie Ryan, Probal

- Saha, Katharina Schleicher, Flurina Schneider, Morgan Scoville-Simonds, Beverley Searle, Samuel Petros Sebhatu, Elena Sesana, Howard Silverman, Chandni Singh, Eleanor Sterling, Sarah-Jane Stewart, J. David Tabara, Douglas Taylor, Philip Thornton, Theresa Margarete Tribaldos, Petra Tschakert, Natalia Uribe-Calvo, Steve Waddell, Sandra Waddock, Liza van der Merwe, Barbara van Mierlo, Patrick van Zwanenberg, Sandra Judith Velarde, Carla-Leanne Washbourne, Kerry Waylen, Annika Weiser, Ian Wight, Stephen Williams, Mel Woods, Ruth Wolstenholme, Ness Wright, Stefanie Wunder, Alastair Wyllie, and Hannah R. Young. Transforming knowledge systems for life on Earth: Visions of future systems and how to get there. *Energy Research & Social Science*, 70:101724, December 2020. ISSN 2214-6296. doi: 10.1016/j.erss.2020.101724. URL <https://www.sciencedirect.com/science/article/pii/S2214629620302991>.
- [66] N. M. Fernandez, J. Bouchez, L. A. Derry, J. Chorover, J. Gaillardet, I. Giesbrecht, D. Fries, and J. L. Druhan. Resiliency of Silica Export Signatures When Low Order Streams Are Subject to Storm Events. *Journal of Geophysical Research: Biogeosciences*, 127(5):e2021JG006660, 2022. ISSN 2169-8961. doi: 10.1029/2021JG006660. URL <https://onlinelibrary.wiley.com/doi/abs/10.1029/2021JG006660>.  
\_eprint: <https://onlinelibrary.wiley.com/doi/pdf/10.1029/2021JG006660>.
- [67] Paul J. Ferraro, Todd L. Cherry, Jason F. Shogren, Christian A. Vossler, Timothy N. Cason, Hilary Byerly Flint, Jacob P. Hochard, Olof Johansson-Stenman, Peter Martinsson, James J. Murphy, Stephen C. Newbold, Linda Thunström, Daan van Soest, Klaas van 't Veld, Astrid Dannenberg, George F. Loewenstein, and Leaf van Boven. Create a culture of experiments in environmental programs. *Science*, 381(6659):735–737, August 2023. doi: 10.1126/science.adf7774. URL <https://www.science.org/>

- [doi/abs/10.1126/science.adf7774](https://doi.org/10.1126/science.adf7774). Publisher: American Association for the Advancement of Science.
- [68] Stuart E.G. Findlay and Victoria R. Kelly. Emerging indirect and long-term road salt effects on ecosystems. *Annals of the New York Academy of Sciences*, 1223(1): 58–68, 2011. ISSN 1749-6632. doi: 10.1111/j.1749-6632.2010.05942.x. URL <https://onlinelibrary.wiley.com/doi/abs/10.1111/j.1749-6632.2010.05942.x>.
- [69] Tim D. Fletcher, Ana Deletic, V. Grace Mitchell, and Belinda E. Hatt. Reuse of Urban Runoff in Australia: A Review of Recent Advances and Remaining Challenges. *Journal of Environmental Quality*, 37(S5): S-116–S-127, 2008. ISSN 1537-2537. doi: 10.2134/jeq2007.0411. URL <https://onlinelibrary.wiley.com/doi/abs/10.2134/jeq2007.0411>. \_eprint: <https://onlinelibrary.wiley.com/doi/pdf/10.2134/jeq2007.0411>.
- [70] Megan L. Fork, Jerker B. Fick, Alexander J. Reisinger, and Emma J. Rosi. Dosing the Coast: Leaking Sewage Infrastructure Delivers Large Annual Doses and Dynamic Mixtures of Pharmaceuticals to Urban Rivers. *Environmental Science & Technology*, 55(17):11637–11645, September 2021. ISSN 0013-936X. doi: 10.1021/acs.est.1c00379. URL <https://doi.org/10.1021/acs.est.1c00379>.
- [71] A. J. Froelich and Chester Zenone. Maps showing geologic terrane, drainage basins, overburden, and low flow of streams in Fairfax County and vicinity, Virginia. *IMAP*, 1985. doi: 10.3133/i1534. URL <https://pubs.er.usgs.gov/publication/i1534>. Number: 1534.
- [72] A. J. Froelich and Chester Zenone. The relation of water quality to geology and land use changes in Fairfax County and vicinity, Virginia. *IMAP*, 1985. doi: 10.3133/i1561. URL <https://pubs.er.usgs.gov/publication/i1561>. Number: 1561.

- [73] Erica J. Brown Gaddis, Hilary Harp Falk, Clare Ginger, and Alexey Voinov. Effectiveness of a participatory modeling effort to identify and advance community water resource goals in St. Albans, Vermont. *Environmental Modelling & Software*, 25(11): 1428–1438, November 2010. ISSN 1364-8152. doi: 10.1016/j.envsoft.2009.06.004. URL <https://www.sciencedirect.com/science/article/pii/S136481520900142X>.
- [74] J. Gaillardet, B. Dupré, P. Louvat, and C. J. Allègre. Global silicate weathering and CO<sub>2</sub> consumption rates deduced from the chemistry of large rivers. *Chemical Geology*, 159(1):3–30, July 1999. ISSN 0009-2541. doi: 10.1016/S0009-2541(99)00031-5. URL <https://www.sciencedirect.com/science/article/pii/S0009254199000315>.
- [75] L.C Gajary, Shalini Misra, A Desai, D.M Evasius, J Frechtling, D.A Pendelebury, J.D Schnell, G Silverstein, and J Wells. Convergence Research as a ‘System-Of-Systems’: A Framework and Research Agenda. *Minerva*.
- [76] R. B. Georg, B. C. Reynolds, M. Frank, and A. N. Halliday. New sample preparation techniques for the determination of Si isotopic compositions using MC-ICPMS. *Chemical Geology*, 235(1):95–104, November 2006. ISSN 0009-2541. doi: 10.1016/j.chemgeo.2006.06.006. URL <https://www.sciencedirect.com/science/article/pii/S000925410600307X>.
- [77] Marc Girons Lopez, Marc J. P. Vis, Michal Jenicek, Nena Griessinger, and Jan Seibert. Assessing the degree of detail of temperature-based snow routines for runoff modelling in mountainous areas in central Europe. *Hydrology and Earth System Sciences*, 24(9): 4441–4461, September 2020. ISSN 1027-5606. doi: 10.5194/hess-24-4441-2020. URL <https://hess.copernicus.org/articles/24/4441/2020/>.
- [78] Sigurdur Reynir Gislason, Stefan Arnorsson, and Halldor Armannsson. Chemical weathering of basalt in Southwest Iceland; effects of runoff, age of rocks and veg-

- etative/glacial cover. *American Journal of Science*, 296(8):837–907, October 1996. doi: 10.2475/ajs.296.8.837. URL <https://ajs.scholasticahq.com/article/60737>. Publisher: American Journal of Science.
- [79] P. H. Gleick. Global Freshwater Resources: Soft-Path Solutions for the 21st Century. *Science*, 302(5650):1524–1528, November 2003. doi: 10.1126/science.1089967. Publisher: American Association for the Advancement of Science (AAAS).
- [80] Stephanie Glen. Unit Root: Simple Definition, Unit Root Tests, December 2016. URL <https://www.statisticshowto.com/unit-root/>. Published: Blog post.
- [81] K. S. Godwin, S. D. Hafner, and M. F. Buff. Long-term trends in sodium and chloride in the Mohawk River, New York: the effect of fifty years of road-salt application. *Environmental Pollution*, 124(2):273–281, July 2003. doi: 10.1016/s0269-7491(02)00481-5. Publisher: Elsevier BV.
- [82] S. B. Grant, J.-D. Saphores, D. L. Feldman, A. J. Hamilton, T. D. Fletcher, P. L. M. Cook, M. Stewardson, B. F. Sanders, L. A. Levin, R. F. Ambrose, A. Deletic, R. Brown, S. C. Jiang, D. Rosso, W. J. Cooper, and I. Marusic. Taking the "Waste" Out of "Wastewater" for Human Water Security and Ecosystem Sustainability. *Science*, 337(6095):681–686, August 2012. doi: 10.1126/science.1216852. Publisher: American Association for the Advancement of Science (AAAS).
- [83] Stanley B. Grant and Ciaran J. Harman. Solute Transport Through Unsteady Hydrologic Systems Along a Plug Flow-To-Uniform Sampling Continuum. *Water Resources Research*, 58(8):e2022WR032038, 2022. ISSN 1944-7973. doi: 10.1029/2022WR032038. URL <https://onlinelibrary.wiley.com/doi/abs/10.1029/2022WR032038>.
- [84] Stanley B. Grant, Megan A. Rippey, Thomas A. Birkland, Todd Schenk, Kristin Rowles, Shalini Misra, Payam Aminpour, Sujay Kaushal, Peter Vikesland, Emily Berglund, Je-

- sus D. Gomez-Velez, Erin R. Hotchkiss, Gabriel Perez, Harry X. Zhang, Kingston Armstrong, Shantanu V. Bhide, Lauren Krauss, Carly Maas, Kent Mendoza, Caitlin Shipman, Yadong Zhang, and Yinman Zhong. Can Common Pool Resource Theory Catalyze Stakeholder-Driven Solutions to the Freshwater Salinization Syndrome? *Environmental Science & Technology*, 56(19):13517–13527, October 2022. ISSN 0013-936X. doi: 10.1021/acs.est.2c01555. URL <https://doi.org/10.1021/acs.est.2c01555>.
- [85] Steven Gray, Alexey Voinov, Michael Paolisso, Rebecca Jordan, Todd BenDor, Pierre Bommel, Pierre Glynn, Beatrice Hedelin, Klaus Hubacek, Josh Introne, Nagesh Kolagani, Bethany Laursen, Christina Prell, Laura Schmitt Olabisi, Alison Singer, Eleanor Sterling, and Moira Zellner. Purpose, processes, partnerships, and products: four Ps to advance participatory socio-environmental modeling. *Ecological Applications*, 28(1):46–61, 2017. ISSN 1939-5582. doi: 10.1002/eap.1627. URL <https://onlinelibrary.wiley.com/doi/abs/10.1002/eap.1627>. \_eprint: <https://onlinelibrary.wiley.com/doi/pdf/10.1002/eap.1627>.
- [86] Stephen K. Hamilton. Biogeochemical time lags may delay responses of streams to ecological restoration. *Freshwater Biology*, 57(s1):43–57, 2012. ISSN 1365-2427. doi: 10.1111/j.1365-2427.2011.02685.x. URL <https://onlinelibrary.wiley.com/doi/abs/10.1111/j.1365-2427.2011.02685.x>.
- [87] Shahan Haq, Sujay S. Kaushal, and Shuiwang Duan. Episodic salinization and freshwater salinization syndrome mobilize base cations, carbon, and nutrients to streams across urban regions. *Biogeochemistry*, 141(3):463–486, December 2018. ISSN 1573-515X. doi: 10.1007/s10533-018-0514-2. URL <https://doi.org/10.1007/s10533-018-0514-2>.
- [88] C. J. Harman. Age-Ranked Storage-Discharge Relations: A Unified Description of Spatially Lumped Flow and Water Age in Hydrologic Systems. *Water Resources Re-*

- search*, 55(8):7143–7165, 2019. ISSN 1944-7973. doi: 10.1029/2017WR022304. URL <https://onlinelibrary.wiley.com/doi/abs/10.1029/2017WR022304>.
- [89] Ciaran Harman and Esther Xu Fei. mesas.py v1.0: A flexible Python package for modeling solute transport and transit times using StorAge Selection functions. *EGU-sphere*, pages 1–32, December 2022. doi: 10.5194/egusphere-2022-1262. URL <https://egusphere.copernicus.org/preprints/2022/egusphere-2022-1262/>. Publisher: Copernicus GmbH.
- [90] Ciaran J. Harman. Time-variable transit time distributions and transport: Theory and application to storage-dependent transport of chloride in a watershed. *Water Resources Research*, 51(1):1–30, 2015. ISSN 1944-7973. doi: 10.1002/2014WR015707. URL <https://onlinelibrary.wiley.com/doi/abs/10.1002/2014WR015707>.
- [91] Sasha Harris-Lovett and David Sedlak. Protecting the sewershed. *Science*, 369(6510): 1429–1430, September 2020. doi: 10.1126/science.abd0700. Publisher: American Association for the Advancement of Science (AAAS).
- [92] J. D. Helvey and J. H. Patric. Canopy and litter interception of rainfall by hardwoods of eastern United States. *Water Resources Research*, 1(2):193–206, 1965. ISSN 1944-7973. doi: 10.1029/WR001i002p00193. URL <https://onlinelibrary.wiley.com/doi/abs/10.1029/WR001i002p00193>.
- [93] William D. Hintz and Rick A. Relyea. A review of the species, community, and ecosystem impacts of road salt salinisation in fresh waters. *Freshwater Biology*, 64(6):1081–1097, 2019. ISSN 1365-2427. doi: 10.1111/fwb.13286. URL <https://onlinelibrary.wiley.com/doi/abs/10.1111/fwb.13286>.
- [94] William D Hintz, Laura Fay, and Rick A Relyea. Road salts, human safety, and the rising salinity of our fresh waters. *Frontiers in Ecology and the Environment*, 20(1):

- 22–30, 2022. ISSN 1540-9309. doi: 10.1002/fee.2433. URL <https://onlinelibrary.wiley.com/doi/abs/10.1002/fee.2433>.
- [95] P. K. Andrew Hong and Ying-Ying Macauley. Corrosion and Leaching of Copper Tubing Exposed to Chlorinated Drinking Water. *Water, Air, and Soil Pollution*, 108 (3/4):457–471, 1998. doi: 10.1023/a:1005060206953. Publisher: Springer Science and Business Media LLC.
- [96] George M. Hornberger, Peter F. Germann, and Keith J. Beven. Throughflow and solute transport in an isolated sloping soil block in a forested catchment. *Journal of Hydrology*, 124(1):81–99, April 1991. ISSN 0022-1694. doi: 10.1016/0022-1694(91)90007-5. URL <https://www.sciencedirect.com/science/article/pii/0022169491900075>.
- [97] Markus Hrachowitz, Paolo Benettin, Boris M. van Breukelen, Ophelie Fovet, Nicholas J.K. Howden, Laurent Ruiz, Ype van der Velde, and Andrew J. Wade. Transit times—the link between hydrology and water quality at the catchment scale. *WIREs Water*, 3(5):629–657, 2016. ISSN 2049-1948. doi: 10.1002/wat2.1155. URL <https://onlinelibrary.wiley.com/doi/abs/10.1002/wat2.1155>.
- [98] Frank Hüesker and Timothy Moss. The politics of multi-scalar action in river basin management: Implementing the EU Water Framework Directive (WFD). *Land Use Policy*, 42:38–47, January 2015. ISSN 0264-8377. doi: 10.1016/j.landusepol.2014.07.003. URL <https://www.sciencedirect.com/science/article/pii/S0264837714001495>.
- [99] IPCC. *Climate Change 2021: The Physical Science Basis. Contribution of Working Group I to the Sixth Assessment Report of the Intergovernmental Panel on Climate Change*, volume In Press. Cambridge University Press, Cambridge, United Kingdom and New York, NY, USA, 2021. doi: 10.1017/9781009157896. Type: Book.

- [100] Matthew G. Johnston and Christine Faulkner. A bootstrap approach is a superior statistical method for the comparison of non-normal data with differing variances. *New Phytologist*, 230(1):23–26, 2021. ISSN 1469-8137. doi: 10.1111/nph.17159. URL <https://onlinelibrary.wiley.com/doi/abs/10.1111/nph.17159>.
- [101] Sai P. Kakuturu and Shirley E. Clark. Clogging Mechanism of Stormwater Filter Media by NaCl as a Deicing Salt. *Environmental Engineering Science*, 32(2):141–152, February 2015. doi: 10.1089/ees.2014.0337. URL <https://www.liebertpub.com/doi/10.1089/ees.2014.0337>. Publisher: Mary Ann Liebert, Inc., publishers.
- [102] Brian G. Katz, Sandra M. Eberts, and Leon J. Kauffman. Using Cl/Br ratios and other indicators to assess potential impacts on groundwater quality from septic systems: A review and examples from principal aquifers in the United States. *Journal of Hydrology*, 397(3):151–166, February 2011. ISSN 0022-1694. doi: 10.1016/j.jhydrol.2010.11.017. URL <https://www.sciencedirect.com/science/article/pii/S0022169410007134>.
- [103] Sujay S. Kaushal, Peter M. Groffman, Gene E. Likens, Kenneth T. Belt, William P. Stack, Victoria R. Kelly, Lawrence E. Band, and Gary T. Fisher. Increased salinization of fresh water in the northeastern United States. *Proceedings of the National Academy of Sciences*, 102(38):13517–13520, September 2005. doi: 10.1073/pnas.0506414102. URL <https://www.pnas.org/doi/full/10.1073/pnas.0506414102>.
- [104] Sujay S. Kaushal, Katie Delaney-Newcomb, Stuart E. G. Findlay, Tamara A. Newcomer, Shuiwang Duan, Michael J. Pennino, Gwendolyn M. Sivorichi, Ashley M. Sides-Raley, Mark R. Walbridge, and Kenneth T. Belt. Longitudinal patterns in carbon and nitrogen fluxes and stream metabolism along an urban watershed continuum. *Bio-*

- geochemistry*, 121(1):23–44, April 2014. doi: 10.1007/s10533-014-9979-9. Publisher: Springer Science and Business Media LLC.
- [105] Sujay S. Kaushal, Gene E. Likens, Michael L. Pace, Ryan M. Utz, Shahan Haq, Julia Gorman, and Melissa Grese. Freshwater salinization syndrome on a continental scale. *Proceedings of the National Academy of Sciences*, 115(4):E574–E583, January 2018. doi: 10.1073/pnas.1711234115. URL <https://www.pnas.org/doi/abs/10.1073/pnas.1711234115>.
- [106] Sujay S. Kaushal, Gene E. Likens, Michael L. Pace, Shahan Haq, Kelsey L. Wood, Joseph G. Galella, Carol Morel, Thomas R. Doody, Barret Wessel, Pirkko Kortelainen, Antti Räike, Valerie Skinner, Ryan Utz, and Norbert Jaworski. Novel ‘chemical cocktails’ in inland waters are a consequence of the freshwater salinization syndrome. *Philosophical Transactions of the Royal Society B*, January 2019. doi: 10.1098/rstb.2018.0017. URL <https://royalsocietypublishing.org/doi/10.1098/rstb.2018.0017>. Publisher: The Royal Society.
- [107] Sujay S. Kaushal, Gene E. Likens, Michael L. Pace, Jenna E. Reimer, Carly M. Maas, Joseph G. Galella, Ryan M. Utz, Shuiwang Duan, Julia R. Kryger, Alexis M. Yaculak, Walter L. Boger, Nathan W. Bailey, Shahan Haq, Kelsey L. Wood, Barret M. Wessel, Cedric Evan Park, Daniel C. Collison, Belie Y.’aaqob I. Aisin, Taylor M. Gedeon, Sona K. Chaudhary, Jacob Widmer, Charles R. Blackwood, Claire M. Bolster, Matthew L. Devilbiss, Diego L. Garrison, Sharon Halevi, Gannon Q. Kese, Emily K. Quach, Christina M. P. Rogelio, Maggie L. Tan, Henry J. S. Wald, and Seyram A. Woglo. Freshwater salinization syndrome: from emerging global problem to managing risks. *Biogeochemistry*, 154(2):255–292, June 2021. ISSN 1573-515X. doi: 10.1007/s10533-021-00784-w. URL <https://doi.org/10.1007/s10533-021-00784-w>.

- [108] Sujay S. Kaushal, Paul M. Mayer, Gene E. Likens, Jenna E. Reimer, Carly M. Maas, Megan A. Rippey, Stanley B. Grant, Ian Hart, Ryan M. Utz, Ruth R. Shatkay, Barrett M. Wessel, Christine E. Maietta, Michael L. Pace, Shuiwang Duan, Walter L. Boger, Alexis M. Yaculak, Joseph G. Galella, Kelsey L. Wood, Carol J. Morel, William Nguyen, Shane Elizabeth C. Querubin, Rebecca A. Sukert, Anna Lowien, Alyssa Wellman Houde, Anaïs Roussel, Andrew J. Houston, Ari Cacopardo, Cristy Ho, Haley Talbot-Wendlandt, Jacob M. Widmer, Jairus Slagle, James A. Bader, Jeng Hann Chong, Jenna Wollney, Jordan Kim, Lauren Shepherd, Matthew T. Wilfong, Megan Houlihan, Nathan Sedghi, Rebecca Butcher, Sona Chaudhary, and William D. Becker. Five state factors control progressive stages of freshwater salinization syndrome. *Limnology and Oceanography Letters*, n/a(n/a), 2022. ISSN 2378-2242. doi: 10.1002/lol2.10248. URL <https://onlinelibrary.wiley.com/doi/abs/10.1002/lol2.10248>.
- [109] Sujay S. Kaushal, Jenna E. Reimer, Paul M. Mayer, Ruth R. Shatkay, Carly M. Maas, William D. Nguyen, Walter L. Boger, Alexis M. Yaculak, Thomas R. Doody, Michael J. Pennino, Nathan W. Bailey, Joseph G. Galella, Aaron Weingrad, Daniel C. Collison, Kelsey L. Wood, Shahan Haq, Tamara A. Newcomer-Johnson, Shuiwang Duan, and Kenneth T. Belt. Freshwater salinization syndrome alters retention and release of chemical cocktails along flowpaths: From stormwater management to urban streams. *Freshwater Science*, 41(3):420–441, September 2022. ISSN 2161-9549. doi: 10.1086/721469. URL <https://www.journals.uchicago.edu/doi/full/10.1086/721469>.
- [110] Victoria R. Kelly, Gary M. Lovett, Kathleen C. Weathers, Stuart E. G. Findlay, David L. Strayer, David J. Burns, and Gene E. Likens. Long-Term Sodium Chloride Retention in a Rural Watershed: Legacy Effects of Road Salt on Streamwater Concentration. *Environmental Science & Technology*, 42(2):410–415, January 2008. doi: 10.1021/es071391l. Publisher: American Chemical Society (ACS).

- [111] Branko Kerkez, Cyndee Gruden, Matthew Lewis, Luis Montestruque, Marcus Quigley, Brandon Wong, Alex Bedig, Ruben Kertesz, Tim Braun, Owen Cadwalader, Aaron Poresky, and Carrie Pak. Smarter Stormwater Systems. *Environmental Science & Technology*, 50(14):7267–7273, July 2016. ISSN 0013-936X. doi: 10.1021/acs.est.5b05870. URL <https://doi.org/10.1021/acs.est.5b05870>.
- [112] Minseok Kim, Luke A. Pangle, Charléne Cardoso, Marco Lora, Till H. M. Volkmann, Yadi Wang, Ciaran J. Harman, and Peter A. Troch. Transit time distributions and StorAge Selection functions in a sloping soil lysimeter with time-varying flow paths: Direct observation of internal and external transport variability. *Water Resources Research*, 52(9):7105–7129, 2016. ISSN 1944-7973. doi: 10.1002/2016WR018620. URL <https://onlinelibrary.wiley.com/doi/abs/10.1002/2016WR018620>. \_eprint: <https://onlinelibrary.wiley.com/doi/pdf/10.1002/2016WR018620>.
- [113] Michael Kiparsky, Barton H. Thompson, Christian Binz, David L. Sedlak, Lars Tummers, and Bernhard Truffer. Barriers to Innovation in Urban Wastewater Utilities: Attitudes of Managers in California. *Environmental Management*, 57(6):1204–1216, June 2016. ISSN 1432-1009. doi: 10.1007/s00267-016-0685-3. URL <https://doi.org/10.1007/s00267-016-0685-3>.
- [114] Rudolf Kiralj and Márcia M. C. Ferreira. Basic validation procedures for regression models in QSAR and QSPR studies: theory and application. *Journal of the Brazilian Chemical Society*, 20(4):770–787, 2009. doi: 10.1590/s0103-50532009000400021. Publisher: FapUNIFESP (SciELO).
- [115] James W. Kirchner. A double paradox in catchment hydrology and geochemistry. *Hydrological Processes*, 17(4):871–874, 2003. ISSN 1099-1085. doi: 10.1002/hyp.5108.

- URL <https://onlinelibrary.wiley.com/doi/abs/10.1002/hyp.5108>. \_eprint:  
<https://onlinelibrary.wiley.com/doi/pdf/10.1002/hyp.5108>.
- [116] James W. Kirchner. Catchments as simple dynamical systems: Catchment characterization, rainfall-runoff modeling, and doing hydrology backward. *Water Resources Research*, 45(2), 2009. ISSN 1944-7973. doi: 10.1029/2008WR006912. URL <https://onlinelibrary.wiley.com/doi/abs/10.1029/2008WR006912>.
- [117] James W. Kirchner. Quantifying new water fractions and transit time distributions using ensemble hydrograph separation: theory and benchmark tests. *Hydrology and Earth System Sciences*, 23(1):303–349, January 2019. ISSN 1027-5606. doi: 10.5194/hess-23-303-2019. URL <https://hess.copernicus.org/articles/23/303/2019/>. Publisher: Copernicus GmbH.
- [118] James W. Kirchner, Xiaohong Feng, and Colin Neal. Fractal stream chemistry and its implications for contaminant transport in catchments. *Nature*, 403(6769):524–527, February 2000. ISSN 1476-4687. doi: 10.1038/35000537. URL <https://www.nature.com/articles/35000537>.
- [119] Denis Kwiatkowski, Peter C. B. Phillips, Peter Schmidt, and Yongcheol Shin. Testing the null hypothesis of stationarity against the alternative of a unit root. *Journal of Econometrics*, 54(1-3):159–178, October 1992. doi: 10.1016/0304-4076(92)90104-y. Publisher: Elsevier BV.
- [120] J. D. Larson. Chemical composition of streams during low flow; Fairfax County, Virginia. Technical Report 78-719, U.S. Geological Survey, 1978. URL <https://pubs.usgs.gov/publication/ofr78719>. ISSN: 2331-1258 Publication Title: Open-File Report.

- [121] V. Lazarova, P. Savoye, M. L. Janex, E. R. Blatchley, and M. Pommepey. Advanced Wastewater Disinfection Technologies: State of the Art and Perspectives. *Water Science and Technology*, 40(4-5), 1999. doi: 10.1016/s0273-1223(99)00502-8. Publisher: IWA Publishing.
- [122] Raymond Letterman. *Water quality and treatment : a handbook of community water supplies*. McGraw-Hill, New York, 1999. ISBN 978-0-07-001659-0.
- [123] Lichen Liang, Weitao Liu, Yuebing Sun, Xiaohui Huo, Song Li, and Qixing Zhou. Phytoremediation of heavy metal contaminated saline soils using halophytes: current progress and future perspectives. *Environmental Reviews*, 25(3):269–281, September 2017. ISSN 1181-8700. doi: 10.1139/er-2016-0063. URL <https://cdnsiencepub.com/doi/full/10.1139/er-2016-0063>.
- [124] Karl-Erich Lindenschmidt, Meghan K. Carr, Amir Sadeghian, and Luis Morales-Marin. CE-QUAL-W2 model of dam outflow elevation impact on temperature, dissolved oxygen and nutrients in a reservoir. *Scientific Data*, 6(1):312, December 2019. ISSN 2052-4463. doi: 10.1038/s41597-019-0316-y. URL <https://www.nature.com/articles/s41597-019-0316-y>.
- [125] Cong Liu, Yunlai Li, Chenguang Lu, Ying Liu, Shile Feng, and Yahua Liu. Robust Slippery Liquid-Infused Porous Network Surfaces for Enhanced Anti-icing/Deicing Performance. *ACS Applied Materials & Interfaces*, 12:25471–25477, 2020. doi: 10.1021/acsami.0c05954. URL <https://pubs.acs.org/doi/epdf/10.1021/acsami.0c05954>.
- [126] Jia Liu, David J. Sample, Cameron Bell, and Yuntao Guan. Review and Research Needs of Bioretention Used for the Treatment of Urban Stormwater. *Water*, 6(4): 1069–1099, April 2014. ISSN 2073-4441. doi: 10.3390/w6041069. URL <https://>

- [www.mdpi.com/2073-4441/6/4/1069](http://www.mdpi.com/2073-4441/6/4/1069). Number: 4 Publisher: Multidisciplinary Digital Publishing Institute.
- [127] Lu Liu, Evan Lopez, Leonardo Dueñas-Osorio, Lauren Stadler, Yuefeng Xie, Pedro J. J. Alvarez, and Qilin Li. The importance of system configuration for distributed direct potable water reuse. *Nature Sustainability*, 3(7):548–555, July 2020. ISSN 2398-9629. doi: 10.1038/s41893-020-0518-5. URL <https://www.nature.com/articles/s41893-020-0518-5>. Number: 7 Publisher: Nature Publishing Group.
- [128] Stefan Löfgren. The Chemical Effects of Deicing Salt on Soil and Stream Water of Five Catchments in Southeast Sweden. *Water, Air, and Soil Pollution*, 130(1):863–868, August 2001. ISSN 1573-2932. doi: 10.1023/A:1013895215558. URL <https://doi.org/10.1023/A:1013895215558>.
- [129] Shahrbanou Madadgar, Amir AghaKouchak, Alireza Farahmand, and Steven J. Davis. Probabilistic estimates of drought impacts on agricultural production. *Geophysical Research Letters*, 44(15):7799–7807, August 2017. doi: 10.1002/2017gl073606. Publisher: American Geophysical Union (AGU).
- [130] Richard D. Margerum. *Beyond Consensus: Improving Collaborative Planning and Management*. MIT Press, August 2011. ISBN 978-0-262-29772-1. Google-Books-ID: gNLxCwAAQBAJ.
- [131] Barbara Martin and Steve Via. Integrating Water Reuse Into the US Water Supply Portfolio. *Journal - American Water Works Association*, 112(1):8–14, January 2020. doi: 10.1002/awwa.1426. Publisher: Wiley.
- [132] Alireza Mashhadi Ali, M. Ehsan Shafiee, and Emily Zechman Berglund. Agent-based modeling to simulate the dynamics of urban water supply: Climate, population growth,

- and water shortages. *Sustainable Cities and Society*, 28:420–434, January 2017. ISSN 2210-6707. doi: 10.1016/j.scs.2016.10.001. URL <https://www.sciencedirect.com/science/article/pii/S221067071630453X>.
- [133] Joel P. Maynard. Springs of Virginia. Groundwater Characterization Program Open File Report 23-01, Virginia Department of Environmental Quality. URL <https://www.deq.virginia.gov/our-programs/water/water-quantity/groundwater-characterization-program>.
- [134] Jeffrey J. McDonnell and Keith Beven. Debates—The future of hydrological sciences: A (common) path forward? A call to action aimed at understanding velocities, celerities and residence time distributions of the headwater hydrograph. *Water Resources Research*, 50(6):5342–5350, 2014. ISSN 1944-7973. doi: 10.1002/2013WR015141. URL <https://onlinelibrary.wiley.com/doi/abs/10.1002/2013WR015141>. \_eprint: <https://onlinelibrary.wiley.com/doi/pdf/10.1002/2013WR015141>.
- [135] Kevin J. McGuire and Jeffrey J. McDonnell. A review and evaluation of catchment transit time modeling. *Journal of Hydrology*, 330(3):543–563, November 2006. ISSN 0022-1694. doi: 10.1016/j.jhydrol.2006.04.020. URL <https://www.sciencedirect.com/science/article/pii/S0022169406002150>.
- [136] Doug McKenzie-Mohr, Nancy R. Lee, and P. Wesley Schultz. *Social Marketing to Protect the Environment: What Works*. SAGE PUBLN, May 2011. ISBN 1-4129-9129-3. URL [https://www.ebook.de/de/product/14534710/doug\\_mckenzie\\_mohr\\_nancy\\_r\\_lee\\_p\\_wesley\\_schultz\\_social\\_marketing\\_to\\_protect\\_the\\_environment\\_what\\_works.html](https://www.ebook.de/de/product/14534710/doug_mckenzie_mohr_nancy_r_lee_p_wesley_schultz_social_marketing_to_protect_the_environment_what_works.html).
- [137] Scott M. McLennan. Weathering and Global Denudation. *The Journal of Geology*,

- 101(2):295–303, March 1993. doi: 10.1086/648222. Publisher: University of Chicago Press.
- [138] Lauren E. McPhillips and A. Marissa Matsler. Temporal Evolution of Green Stormwater Infrastructure Strategies in Three US Cities. *Frontiers in Built Environment*, 4, 2018. ISSN 2297-3362. URL <https://www.frontiersin.org/articles/10.3389/fbuil.2018.00026>.
- [139] Ralf Merz, Juraj Parajka, and Günter Blöschl. Time stability of catchment model parameters: Implications for climate impact analyses. *Water Resources Research*, 47(2), 2011. ISSN 1944-7973. doi: 10.1029/2010WR009505. URL <https://onlinelibrary.wiley.com/doi/abs/10.1029/2010WR009505>.
- [140] Heidi Moltz, Renee Bourassa, Erfaneh Sharifi, Andrea Nagel, Sarah Sivers, Will Isenberg, and David Evans. Virginia Salt Management Strategy: A toolkit to reduce the environmental impacts of winter maintenance practices. Technical report, Interstate Commission on the Potomac River Basin, 2020. URL [https://www.accotink.org/2021/SaMS\\_Toolkit\\_011521.pdf](https://www.accotink.org/2021/SaMS_Toolkit_011521.pdf).
- [141] Joel Moore, Darcy L. Bird, Seth K. Dobbis, and Gregory Woodward. Nonpoint Source Contributions Drive Elevated Major Ion and Dissolved Inorganic Carbon Concentrations in Urban Watersheds. *Environmental Science & Technology Letters*, 4(6):198–204, May 2017. doi: 10.1021/acs.estlett.7b00096. Publisher: American Chemical Society (ACS).
- [142] Joel Moore, Rosemary M. Fanelli, and Andrew J. Sekellick. High-Frequency Data Reveal Deicing Salts Drive Elevated Specific Conductance and Chloride along with Pervasive and Frequent Exceedances of the U.S. Environmental Protection Agency

- Aquatic Life Criteria for Chloride in Urban Streams. *Environmental Science & Technology*, 54(2):778–789, January 2020. ISSN 0013-936X. doi: 10.1021/acs.est.9b04316. URL <https://doi.org/10.1021/acs.est.9b04316>.
- [143] Maitreyee Mukherjee and Olivia Jensen. Making water reuse safe: A comparative analysis of the development of regulation and technology uptake in the US and Australia. *Safety Science*, 121:5–14, January 2020. doi: 10.1016/j.ssci.2019.08.039. Publisher: Elsevier BV.
- [144] Charles M Murray. A Message from the General Manager - A Close Call, 2016. URL [https://www.fairfaxwater.org/sites/default/files/retirees/connections/connections\\_2016\\_Q4.pdf](https://www.fairfaxwater.org/sites/default/files/retirees/connections/connections_2016_Q4.pdf).
- [145] Roger B. Nelsen. *An Introduction to Copulas*. Springer-Verlag GmbH, June 2007. ISBN 978-0-387-28678-5. URL [https://www.ebook.de/de/product/11428705/roger\\_b\\_nelsen\\_an\\_introduction\\_to\\_copulas.html](https://www.ebook.de/de/product/11428705/roger_b_nelsen_an_introduction_to_copulas.html).
- [146] C. K. Nguyen, K. R. Stone, B. Clark, G. Gagnon, A. Knowles, and M. A. Edwards. Impact of Chloride:Sulfate Mass Ratio (CSMR) Changes on Lead Leaching in Potable Water. Technical report, Water Research Foundation and U. S. Environmental Protection Agency, 2010.
- [147] Caroline K. Nguyen, Kendall R. Stone, and Marc A. Edwards. Chloride-to-sulfate mass ratio: Practical studies in galvanic corrosion of lead solder. *Journal - American Water Works Association*, 103(1):81–92, January 2011. doi: 10.1002/j.1551-8833.2011.tb11384.x. Publisher: Wiley.
- [148] Georg H. Niedrist, Miguel Cañedo-Argüelles, and Sophie Cauvy-Fraunié. Salinization of Alpine rivers during winter months. *Environmental Science and Pollution Research*,

- 28(6):7295–7306, February 2021. ISSN 1614-7499. doi: 10.1007/s11356-020-11077-4. URL <https://doi.org/10.1007/s11356-020-11077-4>.
- [149] Antti J. Niemi. Residence time distributions of variable flow processes. *The International Journal of Applied Radiation and Isotopes*, 28(10):855–860, October 1977. ISSN 0020-708X. doi: 10.1016/0020-708X(77)90026-6. URL <https://www.sciencedirect.com/science/article/pii/0020708X77900266>.
- [150] Eric V. Novotny, Andrew R. Sander, Omid Mohseni, and Heinz G. Stefan. Chloride ion transport and mass balance in a metropolitan area using road salt. *Water Resources Research*, 45(12), 2009. ISSN 1944-7973. doi: 10.1029/2009WR008141. URL <https://onlinelibrary.wiley.com/doi/abs/10.1029/2009WR008141>.
- [151] John R. Olson. Predicting combined effects of land use and climate change on river and stream salinity. *Philosophical Transactions of the Royal Society B: Biological Sciences*, 374(1764):20180005, December 2018. doi: 10.1098/rstb.2018.0005. Publisher: The Royal Society.
- [152] Elinor Ostrom. A General Framework for Analyzing Sustainability of Social-Ecological Systems. *Science*, 325(5939):419–422, 2009. doi: 10.1126/science.1172133. URL [https://www.science.org/doi/full/10.1126/science.1172133?casa\\_token=ycTEhnj56QIAAAAA%3AVw05Fbj\\_aBHRHki3emzWpuBzzHt1GJnRI\\_s2k8VUIeF7fBUsyDouWzlr47KfYBAraEKesbivcXml](https://www.science.org/doi/full/10.1126/science.1172133?casa_token=ycTEhnj56QIAAAAA%3AVw05Fbj_aBHRHki3emzWpuBzzHt1GJnRI_s2k8VUIeF7fBUsyDouWzlr47KfYBAraEKesbivcXml).
- [153] Elinor Ostrom. *Understanding Institutional Diversity*. Princeton University Press, November 2009. ISBN 978-1-4008-3173-9. Google-Books-ID: LbeJaji\_AfEC.
- [154] Elinor Ostrom. Beyond Markets and States: Polycentric Governance of Complex Economic Systems. *American Economic Review*, 100(3):641–672, June 2010. ISSN

- 0002-8282. doi: 10.1257/aer.100.3.641. URL <https://www.aeaweb.org/articles?id=10.1257/aer.100.3.641>.
- [155] Alycia Overbo, Sara Heger, and John Gulliver. Evaluation of chloride contributions from major point and nonpoint sources in a northern U.S. state. *Science of The Total Environment*, 764:144179, April 2021. ISSN 0048-9697. doi: 10.1016/j.scitotenv.2020.144179. URL <https://www.sciencedirect.com/science/article/pii/S004896972037710X>.
- [156] Shay Palachy. Detecting stationarity in time series data, July 2019. URL <https://towardsdatascience.com/detecting-stationarity-in-time-series-data-d29e0a21e638>. Published: Blog post.
- [157] Shay Palachy. Stationarity in time series analysis, April 2019. URL <https://towardsdatascience.com/stationarity-in-time-series-analysis-90c94f27322>. Published: Blog post.
- [158] E. A. Parker, S. B. Grant, Y. Cao, M. A. Rippey, K. J. McGuire, P. A. Holden, M. Feraud, S. Avasarala, H. Liu, W. C. Hung, M. Rugh, J. Jay, J. Peng, S. Shao, and D. Li. Predicting Solute Transport Through Green Stormwater Infrastructure With Unsteady Transit Time Distribution Theory. *Water Resources Research*, 57(2):e2020WR028579, 2021. ISSN 1944-7973. doi: 10.1029/2020WR028579. URL <https://onlinelibrary.wiley.com/doi/abs/10.1029/2020WR028579>.
- [159] Emily A. Parker, Stanley B. Grant, Abdullah Sahin, Jasper A. Vrugt, and Matthew W. Brand. Can Smart Stormwater Systems Outsmart the Weather? Stormwater Capture with Real-Time Control in Southern California. *ACS ES&T Water*, 2(1):10–21,

- January 2022. doi: 10.1021/acsestwater.1c00173. URL <https://doi.org/10.1021/acsestwater.1c00173>.
- [160] Peter C. B. Phillips and Pierre Perron. Testing for a unit root in time series regression. *Biometrika*, 75(2):335–346, 1988. doi: 10.1093/biomet/75.2.335. Publisher: Oxford University Press (OUP).
- [161] Kelsey J. Pieper, Min Tang, C. Nathan Jones, Stephanie Weiss, Andrew Greene, Hisyam Mohsin, Jeffrey Parks, and Marc A. Edwards. Impact of Road Salt on Drinking Water Quality and Infrastructure Corrosion in Private Wells. *Environmental Science & Technology*, 52(24):14078–14087, December 2018. ISSN 0013-936X. doi: 10.1021/acs.est.8b04709. URL <https://doi.org/10.1021/acs.est.8b04709>.
- [162] Sarin Raj Pokhrel, Gyan Chhipi-Shrestha, Kasun Hewage, and Rehan Sadiq. Sustainable, resilient, and reliable urban water systems: making the case for a “one water” approach. *Environmental Reviews*, 30(1):10–29, March 2022. ISSN 1181-8700. doi: 10.1139/er-2020-0090. URL <https://cdnsiencepub.com/doi/full/10.1139/er-2020-0090>. Publisher: NRC Research Press.
- [163] Aaron J. Porter, James S. Webber, Jonathan W. Witt, and John D. Jastram. Spatial and temporal patterns in streamflow, water chemistry, and aquatic macroinvertebrates of selected streams in Fairfax County, Virginia, 2007–18. Technical Report 2020-5061, U.S. Geological Survey, 2020. URL <https://pubs.er.usgs.gov/publication/sir20205061>. ISSN: 2328-0328 Publication Title: Scientific Investigations Report.
- [164] Alex Posner and Chester Zenone. Chemical quality of ground water in the Culpeper Basin, Virginia and Maryland. *IMAP*, 1983. doi: 10.3133/i1313D. URL <https://pubs.er.usgs.gov/publication/i1313D>. Number: 1313-D.

- [165] J. D. Potter, W. H. McDowell, A. M. Helton, and M. L. Daley. Incorporating urban infrastructure into biogeochemical assessment of urban tropical streams in Puerto Rico. *Biogeochemistry*, 121(1):271–286, October 2014. ISSN 1573-515X. doi: 10.1007/s10533-013-9914-5. URL <https://doi.org/10.1007/s10533-013-9914-5>.
- [166] Jason Potts. The innovation deficit in public services: The curious problem of too much efficiency and not enough waste and failure. *Innovation*, 11(1):34–43, April 2009. doi: 10.5172/impp.453.11.1.34. Publisher: Informa UK Limited.
- [167] Jeff Racine and Rob Hyndman. Using R to teach econometrics. *Journal of Applied Econometrics*, 17(2):175–189, 2002. ISSN 1099-1255. doi: 10.1002/jae.657. URL <https://onlinelibrary.wiley.com/doi/abs/10.1002/jae.657>. \_eprint: <https://onlinelibrary.wiley.com/doi/pdf/10.1002/jae.657>.
- [168] C. W. Randall and T. J. Grizzard. Management of the occoquan river basin: A 20-year case history. *Water Science and Technology*, 32(5):235–243, January 1995. ISSN 0273-1223. doi: 10.1016/0273-1223(95)00668-0. URL <https://www.sciencedirect.com/science/article/pii/0273122395006680>.
- [169] W. Rauch and M. Kleidorfer. Replace contamination, not the pipes. *Science*, 345(6198):734–735, August 2014. doi: 10.1126/science.1257988. Publisher: American Association for the Advancement of Science (AAAS).
- [170] Mark S. Reed. Stakeholder participation for environmental management: A literature review. *Biological Conservation*, 141(10):2417–2431, October 2008. ISSN 0006-3207. doi: 10.1016/j.biocon.2008.07.014. URL <https://www.sciencedirect.com/science/article/pii/S0006320708002693>.
- [171] D. Regúes and F. Gallart. Seasonal patterns of runoff and erosion responses to simulated rainfall in a badland area in Mediterranean mountain conditions (Vallcebre,

- southeastern Pyrenees). *Earth Surface Processes and Landforms*, 29(6):755–767, 2004. ISSN 1096-9837. doi: 10.1002/esp.1067. URL <https://onlinelibrary.wiley.com/doi/abs/10.1002/esp.1067>.
- [172] J. P. Rehring and M. Edwards. Copper Corrosion in Potable Water Systems: Impacts of Natural Organic Matter and Water Treatment Processes. *CORROSION*, 52(4): 307–317, April 1996. doi: 10.5006/1.3293642. Publisher: NACE International.
- [173] Jacelyn Rice and Paul Westerhoff. High levels of endocrine pollutants in US streams during low flow due to insufficient wastewater dilution. *Nature Geoscience*, 10(8): 587–591, August 2017. ISSN 1752-0908. doi: 10.1038/ngeo2984. URL <https://www.nature.com/articles/ngeo2984>. Number: 8 Publisher: Nature Publishing Group.
- [174] Colin S. Richards, Fei Wang, William C. Becker, and Marc A. Edwards. A 21st-Century Perspective on Calcium Carbonate Formation in Potable Water Systems. *Environmental Engineering Science*, 35(3):143–158, March 2018. doi: 10.1089/ees.2017.0115. Publisher: Mary Ann Liebert Inc.
- [175] J. P. Riley and M. Tongudai. The major cation/chlorinity ratios in sea water. *Chemical Geology*, 2:263–269, January 1967. ISSN 0009-2541. doi: 10.1016/0009-2541(67)90026-5. URL <https://www.sciencedirect.com/science/article/pii/0009254167900265>.
- [176] Andrea Rinaldo, Paolo Benettin, Ciaran J. Harman, Markus Hrachowitz, Kevin J. McGuire, Ype van der Velde, Enrico Bertuzzo, and Gianluca Botter. Storage selection functions: A coherent framework for quantifying how catchments store and release water and solutes. *Water Resources Research*, 51(6):4840–4847, 2015. ISSN 1944-7973. doi: 10.1002/2015WR017273. URL <https://onlinelibrary.wiley.com/doi/abs/10.1002/2015WR017273>.

- [177] José Rivera-Utrilla, Manuel Sánchez-Polo, María Ángeles Ferro-García, Gonzalo Prados-Joya, and Raúl Ocampo-Pérez. Pharmaceuticals as emerging contaminants and their removal from water. A review. *Chemosphere*, 93(7):1268–1287, October 2013. doi: 10.1016/j.chemosphere.2013.07.059. Publisher: Elsevier BV.
- [178] Michael O. Rivett, Mark O. Cuthbert, Richard Gamble, Lucy E. Connon, Andrew Pearson, Martin G. Shepley, and John Davis. Highway deicing salt dynamic runoff to surface water and subsequent infiltration to groundwater during severe UK winters. *Science of The Total Environment*, 565:324–338, September 2016. ISSN 0048-9697. doi: 10.1016/j.scitotenv.2016.04.095. URL <https://www.sciencedirect.com/science/article/pii/S0048969716307768>.
- [179] Anais Roque, Amber Wutich, Barbara Quimby, Sarah Porter, Madeleine Zheng, Mohammed Jobayer Hossain, and Alexandra Brewis. Participatory approaches in water research: A review. *WIREs Water*, 9(2):e1577, 2022. ISSN 2049-1948. doi: 10.1002/wat2.1577. URL <https://onlinelibrary.wiley.com/doi/abs/10.1002/wat2.1577>. \_eprint: <https://onlinelibrary.wiley.com/doi/pdf/10.1002/wat2.1577>.
- [180] Christine M. Rust, C. Marjorie Aelion, and Joseph R. V. Flora. Control of pH during denitrification in subsurface sediment microcosms using encapsulated phosphate buffer. *Water Research*, 34(5):1447–1454, April 2000. ISSN 0043-1354. doi: 10.1016/S0043-1354(99)00287-0. URL <https://www.sciencedirect.com/science/article/pii/S0043135499002870>.
- [181] Mojtaba Sadegh, Elisa Ragno, and Amir AghaKouchak. Multivariate Copula Analysis Toolbox (MvCAT): Describing dependence and underlying uncertainty using a Bayesian framework. *Water Resources Research*, 53(6):5166–5183, June 2017. doi: 10.1002/2016wr020242. Publisher: American Geophysical Union (AGU).

- [182] Mohammad Safeeq, Gordon E. Grant, Sarah L. Lewis, and Christina L. Tague. Coupling snowpack and groundwater dynamics to interpret historical streamflow trends in the western United States. *Hydrological Processes*, 27(5):655–668, 2013. ISSN 1099-1085. doi: 10.1002/hyp.9628. URL <https://onlinelibrary.wiley.com/doi/abs/10.1002/hyp.9628>. \_eprint: <https://onlinelibrary.wiley.com/doi/pdf/10.1002/hyp.9628>.
- [183] O. P. Sahu and P. K. Chaudhari. Review on Chemical treatment of Industrial Waste Water. *Journal of Applied Sciences and Environmental Management*, 17(2), August 2013. doi: 10.4314/jasem.v17i2.8. Publisher: African Journals Online (AJOL).
- [184] Said E. Said and David A. Dickey. Testing for unit roots in autoregressive-moving average models of unknown order. *Biometrika*, 71(3):599–607, 1984. doi: 10.1093/biomet/71.3.599. Publisher: Oxford University Press (OUP).
- [185] Brett F. Sanders and Stanley B. Grant. Re-envisioning stormwater infrastructure for ultrahazardous flooding. *WIREs Water*, 7(2):e1414, 2020. ISSN 2049-1948. doi: 10.1002/wat2.1414. URL <https://onlinelibrary.wiley.com/doi/abs/10.1002/wat2.1414>. \_eprint: <https://onlinelibrary.wiley.com/doi/pdf/10.1002/wat2.1414>.
- [186] Matthew S. Schuler, Miguel Cañedo-Argüelles, William D. Hintz, Brenda Dyack, Sebastian Birk, and Rick A. Relyea. Regulations are needed to protect freshwater ecosystems from salinization. *Philosophical Transactions of the Royal Society B: Biological Sciences*, 374(1764):20180019, January 2019. doi: 10.1098/rstb.2018.0019. URL <https://royalsocietypublishing.org/doi/10.1098/rstb.2018.0019>.
- [187] Kurt Schwabe, Mehdi Nemati, Refat Amin, Quynh Tran, and David Jassby. Unintended consequences of water conservation on the use of treated municipal wastewater.

- ter. *Nature Sustainability*, 3(8):628–635, August 2020. ISSN 2398-9629. doi: 10.1038/s41893-020-0529-2. URL <https://www.nature.com/articles/s41893-020-0529-2>.
- [188] Gideon Schwarz. Estimating the Dimension of a Model. *The Annals of Statistics*, 6(2):461–464, March 1978. doi: 10.1214/aos/1176344136. Publisher: Institute of Mathematical Statistics.
- [189] Gerrit Schüürmann, Ralf-Uwe Ebert, Jingwen Chen, Bin Wang, and Ralph Kühne. External Validation and Prediction Employing the Predictive Squared Correlation Coefficient — Test Set Activity Mean vs Training Set Activity Mean. *Journal of Chemical Information and Modeling*, 48(11):2140–2145, October 2008. doi: 10.1021/ci800253u. Publisher: American Chemical Society (ACS).
- [190] Tyler Scott. Does Collaboration Make Any Difference? Linking Collaborative Governance to Environmental Outcomes. *Journal of Policy Analysis and Management*, 34(3):537–566, 2015. ISSN 1520-6688. doi: 10.1002/pam.21836. URL <https://onlinelibrary.wiley.com/doi/abs/10.1002/pam.21836>. \_eprint: <https://onlinelibrary.wiley.com/doi/pdf/10.1002/pam.21836>.
- [191] Phil Sexton. *Sustainability Analysis of the Commercial Winter Management Industry’s Use of Salt*. PhD thesis, Harvard Extension School, 2017. URL <https://dash.harvard.edu/handle/1/33826971>.
- [192] Nazih K. Shamma and Lawrence K. Wang. *Water Engineering: Hydraulics, Distribution and Treatment*. John Wiley & Sons, May 2015. ISBN 0-470-39098-0. URL [https://www.ebook.de/de/product/22142211/wang\\_shamma\\_okun\\_water\\_engineering.html](https://www.ebook.de/de/product/22142211/wang_shamma_okun_water_engineering.html).
- [193] James B. Shanley. Effects of Ion Exchange on Stream Solute Fluxes in a Basin Receiving Highway Deicing Salts. *Journal of Environmental Quality*, 23(5):977–986,

1994. ISSN 1537-2537. doi: 10.2134/jeq1994.00472425002300050019x. URL <https://onlinelibrary.wiley.com/doi/abs/10.2134/jeq1994.00472425002300050019x>.
- [194] M. Shrestha, L. Wang, T. Koike, H. Tsutsui, Y. Xue, and Y. Hirabayashi. Correcting basin-scale snowfall in a mountainous basin using a distributed snowmelt model and remote-sensing data. *Hydrology and Earth System Sciences*, 18(2):747–761, February 2014. ISSN 1027-5606. doi: 10.5194/hess-18-747-2014. URL <https://hess.copernicus.org/articles/18/747/2014/>.
- [195] Joel W. Snodgrass, Joel Moore, Steven M. Lev, Ryan E. Casey, David R. Ownby, Robert F. Flora, and Grant Izzo. Influence of Modern Stormwater Management Practices on Transport of Road Salt to Surface Waters. *Environmental Science & Technology*, 51(8):4165–4172, April 2017. ISSN 0013-936X. doi: 10.1021/acs.est.6b03107. URL <https://doi.org/10.1021/acs.est.6b03107>.
- [196] R. F. Stallard and J. M. Edmond. Geochemistry of the Amazon: 1. Precipitation chemistry and the marine contribution to the dissolved load at the time of peak discharge. *Journal of Geophysical Research: Oceans*, 86(C10):9844–9858, 1981. ISSN 2156-2202. doi: 10.1029/JC086iC10p09844. URL <https://onlinelibrary.wiley.com/doi/abs/10.1029/JC086iC10p09844>. `_eprint:` <https://onlinelibrary.wiley.com/doi/pdf/10.1029/JC086iC10p09844>.
- [197] Brent S. Steel, Denise Lach, and Edward P. Weber. *New Strategies for Wicked Problems: Science and Solutions in the 21st Century*. Oregon State University Press, Corvallis, 2017. ISBN 978-0-87071-894-6. doi: 10.1353/book56396. URL [https://muse.jhu.edu/pub/205/edited\\_volume/book/56396](https://muse.jhu.edu/pub/205/edited_volume/book/56396).
- [198] M. K. Steele and J. A. Aitkenhead-Peterson. Long-term sodium and chloride surface water exports from the Dallas/Fort Worth region. *Science of The To-*

- tal Environment*, 409(16):3021–3032, July 2011. ISSN 0048-9697. doi: 10.1016/j.scitotenv.2011.04.015. URL <https://www.sciencedirect.com/science/article/pii/S004896971100372X>.
- [199] E. G. Stets, C. J. Lee, D. A. Lytle, and M. R. Schock. Increasing chloride in rivers of the conterminous U.S. and linkages to potential corrosivity and lead action level exceedances in drinking water. *Science of The Total Environment*, 613-614:1498–1509, February 2018. doi: 10.1016/j.scitotenv.2017.07.119. Publisher: Elsevier BV.
- [200] Werner Stumm and James J. Morgan. *Aquatic chemistry: chemical equilibria and rates in natural waters*. Environmental science and technology. Wiley, New York, 3rd ed edition, 1996. ISBN 978-0-471-51184-7 978-0-471-51185-4.
- [201] Jason G. Su, Michael Jerrett, Rob McConnell, Kiros Berhane, Genevieve Dunton, Ketan Shankardass, Kim Reynolds, Roger Chang, and Jennifer Wolch. Factors influencing whether children walk to school. *Health & Place*, 22:153–161, July 2013. doi: 10.1016/j.healthplace.2013.03.011. Publisher: Elsevier BV.
- [202] Vinicius J. Taguchi, Peter T. Weiss, John S. Gulliver, Mira R. Klein, Raymond M. Hozalski, Lawrence A. Baker, Jacques C. Finlay, Bonnie L. Keeler, and John L. Nieber. It Is Not Easy Being Green: Recognizing Unintended Consequences of Green Stormwater Infrastructure. *Water*, 12(2):522, February 2020. ISSN 2073-4441. doi: 10.3390/w12020522. URL <https://www.mdpi.com/2073-4441/12/2/522>. Number: 2 Publisher: Multidisciplinary Digital Publishing Institute.
- [203] Min Tang, Victoria Nystrom, Kelsey Pieper, Jeffrey Parks, Bob Little, Russell Williams, Thomas Esqueda, and Marc Edwards. The Relationship Between Discolored Water from Corrosion of Old Iron Pipe and Source Water Conditions. *Environmen-*

- tal Engineering Science*, 35(9):943–952, September 2018. doi: 10.1089/ees.2017.0435. Publisher: Mary Ann Liebert Inc.
- [204] Carl Tippler, Ian A. Wright, Peter J. Davies, and Alison Hanlon. The influence of concrete on the geochemical qualities of urban streams. *Marine and Freshwater Research*, 65(11):1009, 2014. doi: 10.1071/mf13164. Publisher: CSIRO Publishing.
- [205] Grace Tjandraatmadja, Clare Diaper, Yesim Gozukara, Lauren Burch, Chris Sheedy, and Guy Price. Sources of priority contaminants in domestic wastewater: Contaminant contribution from household products. *CSIRO: Water for a Healthy Country National Research Flagship*, 2008.
- [206] Y. van der Velde, P. J. J. F. Torfs, S. E. a. T. M. van der Zee, and R. Uijlenhoet. Quantifying catchment-scale mixing and its effect on time-varying travel time distributions. *Water Resources Research*, 48(6), 2012. ISSN 1944-7973. doi: 10.1029/2011WR011310. URL <https://onlinelibrary.wiley.com/doi/abs/10.1029/2011WR011310>. \_eprint: <https://onlinelibrary.wiley.com/doi/pdf/10.1029/2011WR011310>.
- [207] K. J. Van Meter, P. Van Cappellen, and N. B. Basu. Legacy nitrogen may prevent achievement of water quality goals in the Gulf of Mexico. *Science*, 360(6387):427–430, April 2018. doi: 10.1126/science.aar4462. URL <https://www.science.org/doi/10.1126/science.aar4462>.
- [208] Arjun K. Venkatesan, Sajjad Ahmad, Walter Johnson, and Jacimaria R. Batista. Systems dynamic model to forecast salinity load to the Colorado River due to urbanization within the Las Vegas Valley. *Science of The Total Environment*, 409(13):2616–2625, June 2011. doi: 10.1016/j.scitotenv.2011.03.018. Publisher: Elsevier BV.
- [209] Andrej Vidmar, Mitja Brilly, Klaudija Sapač, and Andrej Kryžanowski. Efficient Calibration of a Conceptual Hydrological Model Based on the Enhanced Gauss–Levenberg–

- Marquardt Procedure. *Applied Sciences*, 10(11):3841, January 2020. ISSN 2076-3417. doi: 10.3390/app10113841. URL <https://www.mdpi.com/2076-3417/10/11/3841>.
- [210] Alexey Voinov and Erica J. Brown Gaddis. Lessons for successful participatory watershed modeling: A perspective from modeling practitioners. *Ecological Modelling*, 216(2):197–207, August 2008. ISSN 0304-3800. doi: 10.1016/j.ecolmodel.2008.03.010. URL <https://www.sciencedirect.com/science/article/pii/S0304380008001403>.
- [211] Yorck von Korf, Katherine A. Daniell, Sabine Moellenkamp, Pieter Bots, and Rianne M. Bijlsma. Implementing Participatory Water Management: Recent Advances in Theory, Practice, and Evaluation. *Ecology and Society*, 17(1), 2012. ISSN 1708-3087. URL <https://www.jstor.org/stable/26268987>. Publisher: Resilience Alliance Inc.
- [212] Christopher J. Walsh, Tim D. Fletcher, and Matthew J. Burns. Urban Stormwater Runoff: A New Class of Environmental Flow Problem. *PLOS ONE*, 7(9):e45814, September 2012. ISSN 1932-6203. doi: 10.1371/journal.pone.0045814. URL <https://journals.plos.org/plosone/article?id=10.1371/journal.pone.0045814>.
- [213] Fei Wang, Christina L. Devine, and Marc A. Edwards. Effect of Corrosion Inhibitors on In Situ Leak Repair by Precipitation of Calcium Carbonate in Potable Water Pipelines. *Environmental Science & Technology*, 51(15):8561–8568, July 2017. doi: 10.1021/acs.est.7b01380. Publisher: American Chemical Society (ACS).
- [214] James S. Webber, Jeffrey G. Chanat, Aaron J. Porter, and John D. Jastram. Evaluating drivers of hydrology, water quality, and benthic macroinvertebrates in streams of Fairfax County, Virginia, 2007–18. Technical Report 2023-5027, U.S. Geological Survey, 2023. URL <https://pubs.usgs.gov/publication/sir20235027>. ISBN: 9781411345164 ISSN: 2328-0328 Publication Title: Scientific Investigations Report.

- [215] Claire Welty, Joel Moore, Daniel J. Bain, Mahdad Talebpour, John T. Kemper, Peter M. Groffman, and Jonathan M. Duncan. Spatial Heterogeneity and Temporal Stability of Baseflow Stream Chemistry in an Urban Watershed. *Water Resources Research*, 59(1):e2021WR031804, 2023. ISSN 1944-7973. doi: 10.1029/2021WR031804. URL <https://onlinelibrary.wiley.com/doi/abs/10.1029/2021WR031804>. \_eprint: <https://onlinelibrary.wiley.com/doi/pdf/10.1029/2021WR031804>.
- [216] M. Julia Wiener, Sebastián Moreno, Chad T. Jafvert, and Loring F. Nies. Time series analysis of water use and indirect reuse within a HUC-4 basin (Wabash) over a nine year period. *Science of The Total Environment*, 738:140221, October 2020. ISSN 0048-9697. doi: 10.1016/j.scitotenv.2020.140221. URL <https://www.sciencedirect.com/science/article/pii/S0048969720337426>.
- [217] Mara Wiest, Peter Fox, Timothy M. Thomure, and Wontae Lee. Evaluation of Alternatives to Domestic Ion Exchange Water Softeners. Technical report, Water Reuse Research Foundation, 2011.
- [218] Bruce H. Wilkinson. Humans as geologic agents: A deep-time perspective. *Geology*, 33(3):161, 2005. doi: 10.1130/g21108.1. Publisher: Geological Society of America.
- [219] W. D. Williams. Anthropogenic salinisation of inland waters. In *Saline Lakes*, pages 329–337. Springer Netherlands, 2001. doi: 10.1007/978-94-017-2934-5\_30.
- [220] I. A. Wright, P. J. Davies, S. J. Findlay, and O. J. Jonasson. A new type of water pollution: concrete drainage infrastructure and geochemical contamination of urban waters. *Marine and Freshwater Research*, 62(12):1355, 2011. doi: 10.1071/mf10296. Publisher: CSIRO Publishing.

# Appendices

# Appendix A

## Supplementary Information for Chapter 2

### A.1 MLR Model Validation and Stationarity Analysis

At stations ST10 and ST45 we validated the MLR model using the hold-out method [46, 189]. The entire dataset at these two stations (including timeseries of all relevant dependent and independent variables) were split into two groups: (a) calibration set (75%, used to train the MLR model) and (b) external validation (hold-out) set (25%, independent of the calibration set). The top-ranked MLR models (trained with the calibration set) were then used to generate instantaneous predictions (and associated errors) for sodium mass load and concentration for the external validation period using USGS-Loadflex (Figures A.2 and A.3). The following statistical parameters were evaluated as part of the external validation at ST10 and ST45: (a) root mean squared error of prediction (RMSEP)

$$RMSEP = \sqrt{\frac{\sum_{i=1}^{n_{EXT}} (y_{i,p} - y_i)^2}{n_{EXT}}} \quad (\text{A.1})$$

where  $n_{EXT}$  is the total number of data points in the external set,  $y_{i,p}$  is the  $i$ th predicted value and  $y_i$  is the corresponding observed value of log transformed sodium concentration; (b) prediction squared correlation coefficient ( $Q^2$ ), which is a measure of the model's predictive

power [46, 189]

$$Q^2 = 1 - \frac{\sum_{i=1}^{n_{EXT}} (y_{i,p} - y_i)^2 / n_{EXT}}{\sum_{i=1}^{n_C} (y_i - \bar{y}_C)^2 / n_C} \quad (\text{A.2})$$

where  $n_C$  is the total number of data points in the calibration set and  $\bar{y}_C$  is the mean of observed values in the calibration set.

Equation A.2 satisfies the mathematical properties of ergodicity and is corrected for the underlying assumption that the external dataset is not uniformly distributed over the entire range of the calibration dataset [46]. The metric used to gauge external validation is the difference between hold-out  $R^2$  and calculated  $Q^2$  (equation A.2). A large difference between the two values ( $R^2 - Q^2 > 0.3$ ) indicates that the model might: (a) suffer from overfitting, (b) contain a large number of outliers or (c) include irrelevant covariates [62, 114]. Both models at ST10 and ST45 performed satisfactorily ( $R^2 - Q^2 < 0.3$ ). Metrics for external validation are reported in Table A.4.

Because of the limited number of sodium measurements on UOSA's daily composite samples ( $N=68$ ), to evaluate the MLR model for this dataset we used leave-one-out cross validation coefficient of determination (LOOCV- $R^2$ ), which was evaluated as follows: (Step 1) omit one data point, fit the MLR model to the remaining dataset and use the model to predict the omitted data value; (Step 2) repeat Step 1 for all data points in the dataset; (Step 3) estimate LOOCV- $R^2$  by computing the  $R^2$  statistic from the predicted and measured point values from Step 2. The LOOCV- $R^2$  for UOSA is 51.6%.

**Stationarity:** Both the MLR and copula analysis described in the main text assume that the time series are stationary [157]. While we know that sodium concentration in the reservoir is not stationary over the past 40 years (see rising trend in Figure 2.1b, main text), the relevant datasets may be stationary over the subset of this time period encompassed by the MLR and copula analyses (2010 to 2018). To test for stationarity over the latter

timeframe, we conducted the following unit root tests [156]: (a) Augmented Dickey-Fuller (ADF) test [184], (b) Phillips-Perron (PP) test [160], and (c) Kwiatkowski-Phillips-Schmidt-Shin (KPSS) test [119]. A time series process, when mathematically expressed by a series of monomials each corresponding to a root, may contain a root equal to 1, called a unit root [80]. ADF and PP test the null hypothesis that a unit root is present in the time-series sample (and hence the process is not stationary); the alternate hypothesis is that the time-series is stationary. A negative test statistic and a p-value  $<0.05$  indicates rejection of the null hypothesis. For the KPSS test, the null hypothesis is that the timeseries is stationary and the alternate hypothesis is that the timeseries contains a unit root. In this case, a p-value  $>0.05$  indicates lower evidence of rejecting the null hypothesis. The results presented in Table A.5 confirm that the time-series data used for the copula analysis and MLR model generation is stationary. We did not perform these tests for UOSA's sodium concentration measurements as the sampling frequency at this station was too sporadic and infrequent.

## A.2 Supplementary Tables and Figures

Table A.1: Top-ranked MLR models of Sodium Concentration at ST10, ST45, and UOSA.

	ST10	ST45	UOSA
<b>Model Information</b>			
No. of observations	284	254	68
F statistic	43.63*** (df = 3; 280)	429.6*** (df = 4; 249)	78.98*** (df = 1; 66)
<b>Coefficients</b>			
Intercept	3.26***	2.99***	3.3***
lnQ	-0.1518***	-0.0657***	–
Specific Conductance ( $\mu\text{S}/\text{cm}$ )	–	0.0018***	0.0011***
Rainfall, maximum in the previous two weeks (inches)	–	–	–
Snow depth, maximum in the previous two weeks (inches)	0.0477***	0.0238***	–
Season	–	0.0311**	–
No. of days below freezing in the previous two weeks	0.011**	–	–
<b>Model performance metrics</b>			
Adjusted R <sup>2</sup>	0.31	0.87	0.54
RMSE	0.24	0.10	0.053
PBIAS	-2.9%	0.6%	0.7%
BIC	30.37	-398.14	-192.39
LOOCV prediction error	0.195	0.086	0.041

\*P&lt;0.05 \*\*P&lt;0.01 \*\*\*P&lt;0.001

Table A.2: Characteristics of the two watersheds.

	Occoquan River Watershed	Bull Run Watershed
Station	ST10	ST45
Drainage Area (square km)	890	390
Impervious Surface Cover (%)	4	11

Source: 2010 land use data for the Occoquan Watershed from Occoquan Watershed Monitoring Laboratory's Hydrologic Simulation Program FORTRAN (HSPF) model.

Table A.3: Steps during the drinking water treatment process that introduce sodium and alternative low-sodium or sodium-free methods or compounds.

Treatment Process	Sodium Introducing Compound(s)	Sodium-free Alternatives	Reference
Softening	Soda ash (sodium carbonate) or by ion-exchange processes	Electrically induced precipitation, template assisted crystallization, magnetic water treatment, and electrically induced precipitation or capacitive deionization, polyphosphate, or lower water heater temperature set points	refs: [122, 174, 192, 213, 217]
Increasing pH for corrosion control, or to counter any acid producing reactions	Soda Ash ( $\text{Na}_2\text{CO}_3$ ), Sodium bicarbonate ( $\text{NaHCO}_3$ ) or sodium hydroxide ( $\text{NaOH}$ )	Use potassium or calcium hydroxide (lime) to increase pH, or reduce/eliminate the acid producing reactions (i.e., coagulation) by using alternative such as membranes	refs: [172, 192]
Chlorine gas generation	$\text{NaCl}$ brine can leak into potable water if $\text{Cl}_2$ gas is generated onsite	Stop brine leaks	ref: [146]
Anion Exchange	$\text{NaCl}$ regeneration of columns used for nitrate, arsenic, uranium removal	Adsorption, biological treatment, coagulation as appropriate.	ref: [146]
Disinfection	Sodium hypochlorite or sodium chlorite or chloramine	$\text{Cl}_2$ gas. UV, ozone, membrane filtration, reverse osmosis can reduce doses	refs: [45, 58]
Fluoridation	Sodium fluoride, sodium fluorosilicate	Hexafluorosilicic acid	ref: [122]
Corrosion inhibitor	Sodium silicates, sodium phosphates	Replace the antiquated infrastructure at risk of corrosion, or use lime columns to adjust pH-alkalinity	refs: [26, 203]
Coagulation	Sodium aluminate, sodium alginate (coagulant aid)	Aluminum sulfate, ferric sulfate, ferrous sulfate	refs: [20, 183]

Table A.4: External (hold-out) validation metrics.

Model performance metrics	ST10	ST45
RMSEP	0.315	0.148
Hold-out $R^2$	0.15	0.81
$Q^2$	0.05	0.73
$R^2-Q^2$	0.1	0.08

Table A.5: ADF, PP and KPSS test results.

Variable		ADF statistic	PP statistic	KPSS statistic
ln (Na)	ST10	-4.25**	-129.83**	0.33
	ST45	-5.73**	-157.83**	0.09
ln ( $Q_{Total}$ )	ST10	-4.99**	-113.27**	0.21
	ST45	-5.43**	-167.81**	0.23
	UOSA	-8.53**	-632.71**	0.85
SC ( $\mu\text{S}/\text{cm}$ )	ST45	-6.19**	-207.09**	0.2
	UOSA	-8.08**	-321.24**	0.12
Max. antec. rainfall (in.)		-5.55**	-310.31**	0.25
Max. antec. snow (in.)		-7.22**	-311.15**	0.07
Antec. freezing days		-7.10**	-82.37**	0.01

\* $P < 0.05$  \*\* $P < 0.01$  \*\*\* $P < 0.001$

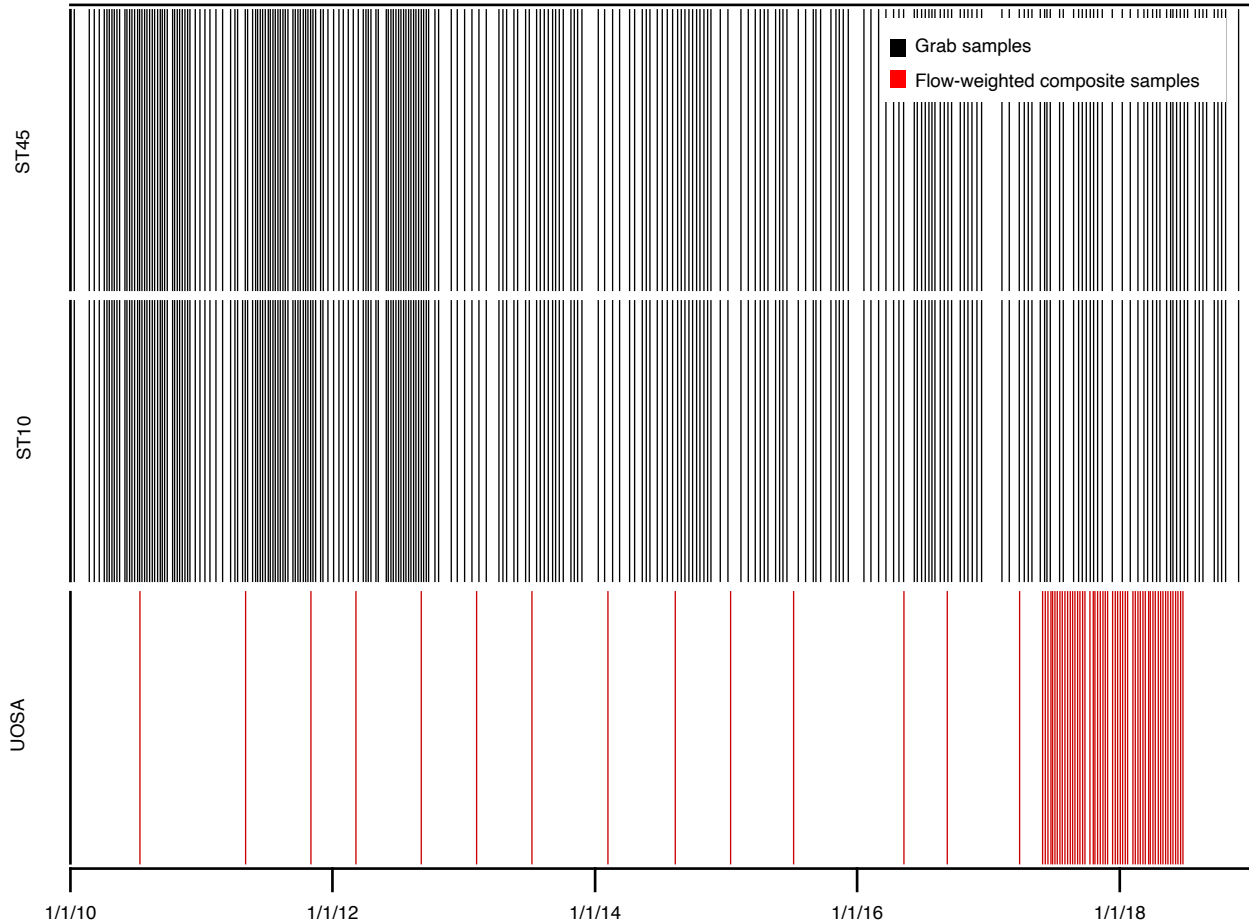


Figure A.1: **Schedule of sodium concentration measurements (vertical lines) available at ST10, ST45 and UOSA, respectively for the period 2010–2018.** White spaces indicate days with no sodium concentration measurements. Black lines represent measurements collected on grab samples (ST10 and ST45) and red lines represent measurements on daily flow-weighted composite samples (UOSA).

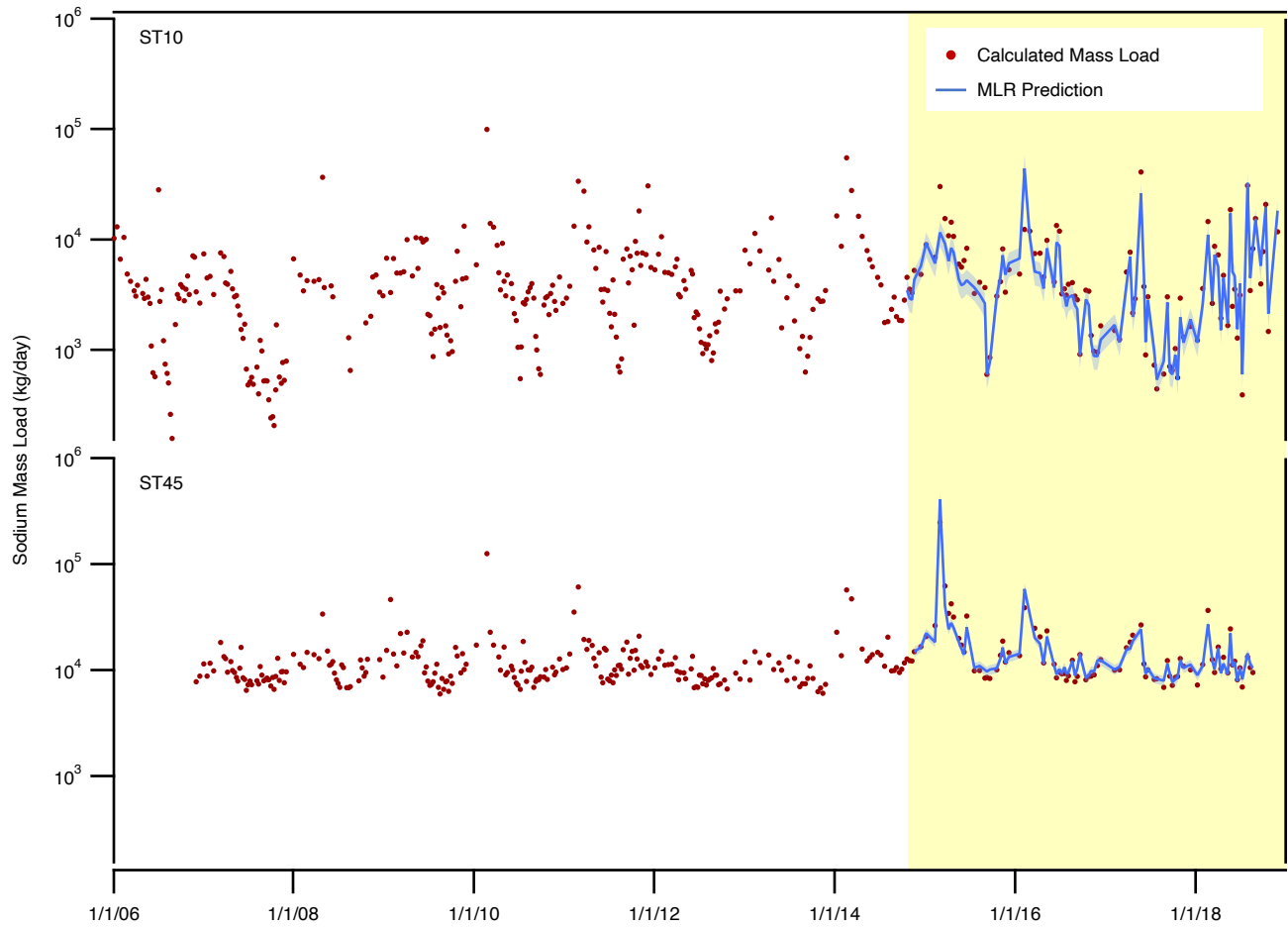


Figure A.2: Calculated sodium mass loads (from flow and sodium concentration measurements at ST10 and ST45) and MLR model predictions from USGS-Loadflex for the validation period (tinted portion). Ribbons indicate 95% confidence intervals.

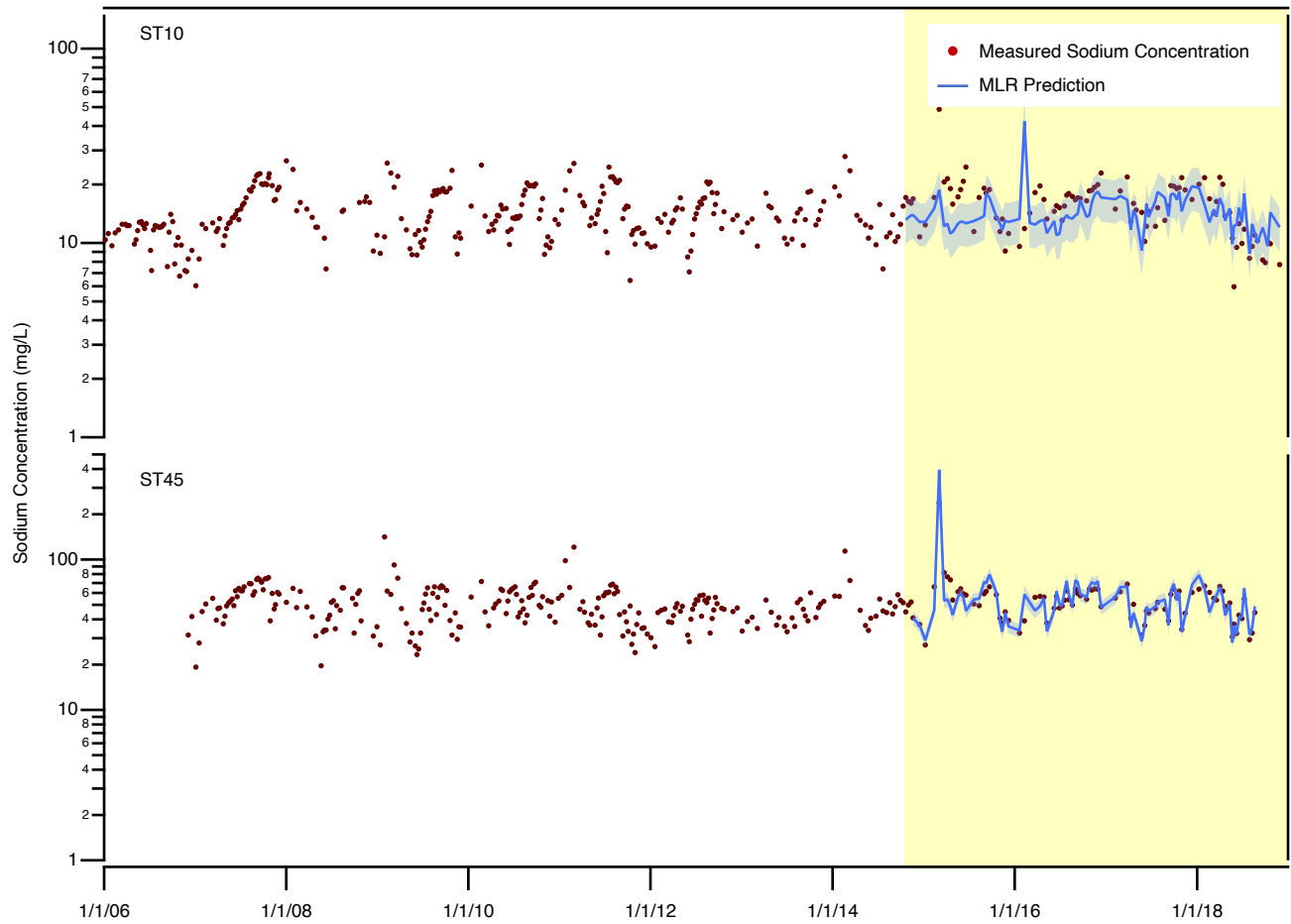


Figure A.3: Observed values of sodium concentration (ST10 and ST45) and MLR model predictions from USGS-Loadflex for the validation period (tinted portion), along with standard error of prediction. Ribbons indicate 95% confidence intervals.

# Appendix B

## Supplementary Information for Chapter 3

### B.1 HBV Model

The HBV model is a commonly used rainfall-runoff model with routines for different components of the water cycle (e.g., snow routine, soil routine, groundwater routine for response and routing, etc.) [77, 139, 209]. The snow routine of the HBV model was used to capture (1) the partitioning of precipitation,  $P(t)$  [L T<sup>-1</sup>], between rainfall,  $r(t)$  [L T<sup>-1</sup>], and snowfall, and (2) the accumulation of snowpack and generation of snowmelt,  $s(t)$  [L T<sup>-1</sup>]. Model parameters include (1) the threshold temperature,  $T_T$  [K], below which all precipitation is considered to fall as snow, (2) the snowfall correction factor,  $SF_{cf}$  [-], which accounts for snowfall undercatch due to wind turbulence, catchment vegetation, etc. [77, 194], (3) the degree-day factor,  $D_F$  [L T<sup>-1</sup> K<sup>-1</sup>], which is a proportionality constant for estimating snow melt, (4) the water holding capacity of the snowpack,  $W_H$  [-], and (5) the refreezing coefficient,  $F$  [-], which allows for refreezing of the melted water when air temperature,  $T_{air}(t)$  [K], falls below  $T_T$ . Model parameters for snow accumulation were chosen to mimic weather conditions in the Mid-Atlantic U.S. (Table B.1). To validate the HBV model results, we used data on daily accumulated snow depth at the nearby Dulles Airport (Figure 3.1), downloaded from the National Oceanic and Atmospheric Administration website ([www.ncei.noaa.gov](http://www.ncei.noaa.gov)),

to verify that the timing of predicted snow melt aligns with the date of zero accumulated snow depth reported at Dulles Airport after snow events. From these comparisons we estimated that the HBV model accurately predicts snow melt at Dulles roughly 83% of the time.

Table B.1: HBV model parameter values.

Parameter	Value
$T_T$	0° C
$SF_{cf}$	1.1
$D_F$	$7.29 \times 10^{-5} \text{ m } ^\circ\text{C}^{-1} \text{ h}^{-1}$
$W_H$	0.1
$F$	0.05

## B.2 Hydrologic Model

Streamflow was assumed to be the sum of direct runoff to the stream (e.g., through storm drain networks and overland flow), interflow through the vadose zone, and groundwater discharge:  $Q_{\text{stream}}(t) = Q_{\text{run}}(t) + Q_{\text{int}}(t) + Q_{\text{gw}}(t)$  [ $\text{L T}^{-1}$ ] (Figure B.1a). The three terms on the right hand side of this equation were calculated as follows. A fraction,  $\gamma_1(t)$  [-], of rain and snow melt (output from the HBV model) infiltrates to the vadose zone,  $J_{\text{vz}}(t) = \gamma_1(t)(r(t) + s(t))$  [ $\text{L T}^{-1}$ ], while the rest flows directly to the stream through storm drain networks and overland flow,  $Q_{\text{run}}(t) = (1 - \gamma_1(t))(r(t) + s(t))$  [ $\text{L T}^{-1}$ ] (Vadose Zone box, Figure 3.2a). Preliminary evaluation of the model indicated that infiltration into the vadose zone varies seasonally, presumably due to seasonal variations in vegetation cover and rainfall intensity (discussed further below) [171]. Accordingly, the infiltration fraction,  $\gamma_1(t)$ , was allowed to vary non-linearly with day,  $d$ , of the water year:  $\log_{10} \gamma_1(t) = x + i \sin \frac{2\pi(d+p)}{365}$ . In this expression,  $d = 0$  corresponds to the beginning of the water year, October 1st, and the

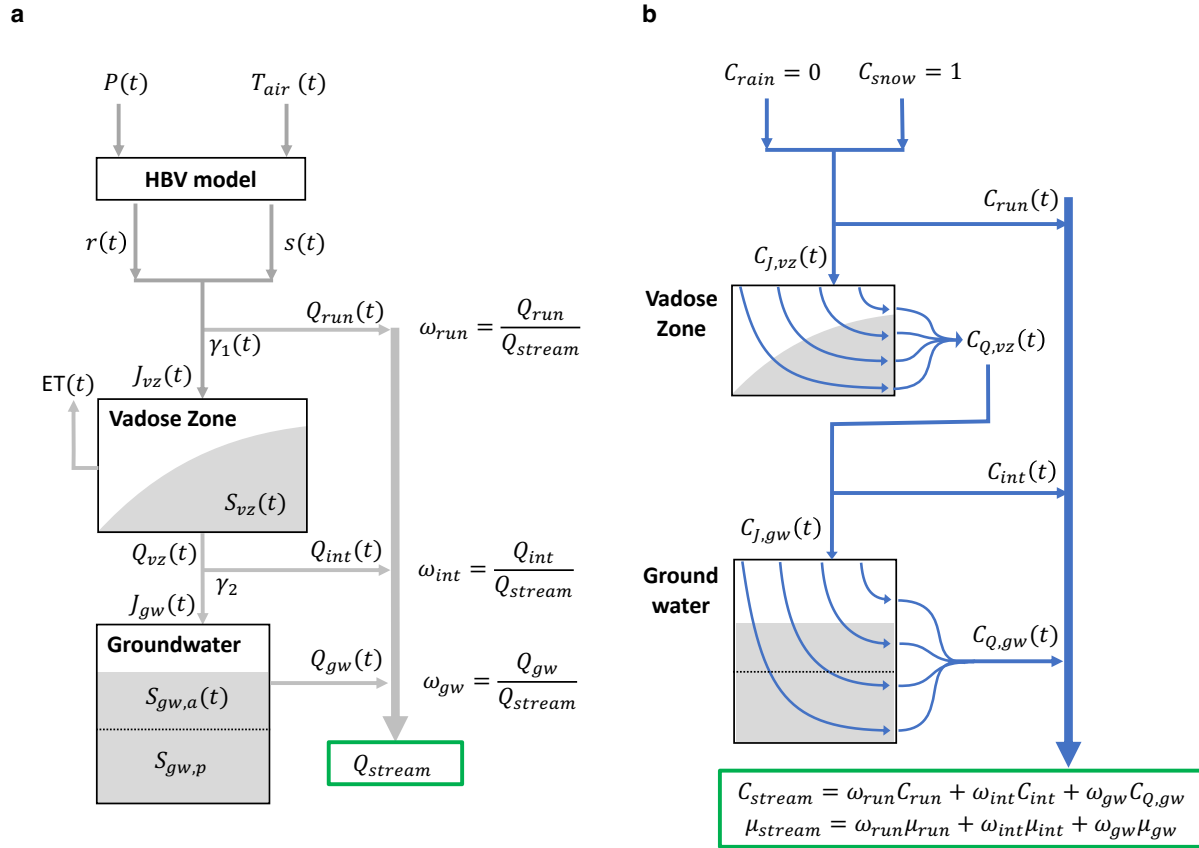


Figure B.1: Conceptual representation of the (a) hydrologic model and (b) transit time distribution model.

parameters  $x$  [-],  $i$  [-], and  $p$  set, respectively, the annual average infiltration, magnitude of the seasonal signal, and phase of the seasonal signal. For the top model (with the lowest RMSE, see Table 3.1), the set of values inferred for  $x$ ,  $i$ , and  $p$  suggest that the fraction of inflow that enters the vadose zone through infiltration is higher in the winter (as high as 94%), and lower in the summer (as low as 22%).

We hypothesized that most of this cyclicity arises from seasonal variations in the intensity of storm events; specifically, if summer storms are frequently more intense than winter storms, a larger fraction of summer-time rainfall would enter the stream as direct runoff, and a smaller fraction would enter the vadose zone through infiltration. An analysis of output

from the HBV model (i.e., hourly estimates of inflow to the catchment from either rainfall or snow melt) supports this hypothesis. From the HBV model, we obtained ten years of hourly estimates for inflow to the catchment from either rainfall or snow melt ( $N=87672$ ). We started our analysis by removing from this timeseries all instances where the HBV model predicted zero inflow (i.e., we removed all dry weather periods). From the remaining non-zero inflow intensity values ( $N=7250$ ) we constructed three probability distributions, one for inflow during the summer (June, July and August), one for inflow during the winter (December, January, February), and one for inflow year round. Consistent with our hypothesis, the distributions for winter and summer inflow intensities peak around  $0.2$  and  $0.5 \text{ mm h}^{-1}$ , respectively, and very intense storms (up to  $6 \text{ mm h}^{-1}$ ) are more frequent in the summer (Figure B.2). The seasonal difference in inflow intensities can also be documented by examining the raw data. Over the ten year time period, the number of hours when summer and winter inflow intensities exceeded  $2 \text{ mm h}^{-1}$  were  $N=320$  and  $253$ , respectively. Conversely, the number of hours when summer and winter inflow intensities were below  $2 \text{ mm h}^{-1}$  were  $N=685$  and  $2479$ , respectively. Put another way, lower intensity inflow events are more frequent in the winter than the summer, while higher intensity inflow events are more frequent in the summer than the winter. Thus, as hypothesized, the bulk of the seasonal variation in  $\gamma_1(t)$  probably reflects runoff generation associated with intense summer rain events.

Once water enters the vadose zone, it can accumulate with time,  $S_{vz}(t)$  [L], leave by evapotranspiration,  $ET(t)$  [ $\text{L T}^{-1}$ ], or leave by discharge,  $Q_{vz}(t)$  [ $\text{L T}^{-1}$ ]:  $\frac{dS_{vz}}{dt} = J_{vz}(t) - Q_{vz}(t) - ET(t)$ . Reflecting the influence of capillary forces on transiently saturated flow, the discharge-storage relationship for the vadose zone is presumed to be non-linear [116, 158]:  $Q_{vz}(t) = K_{\text{sat}} \left( \frac{S_{vz}(t)}{S_{vz,\text{max}}} \right)^g$ , where  $K_{\text{sat}}$  [ $\text{L T}^{-1}$ ],  $S_{vz,\text{max}}$  [L] and  $g$  [-] represent, respectively, the saturated hydraulic conductivity of the vadose zone, maximum depth of the vadose zone, and a power-law exponent. Evapotranspiration was calculated from the product of vadose zone

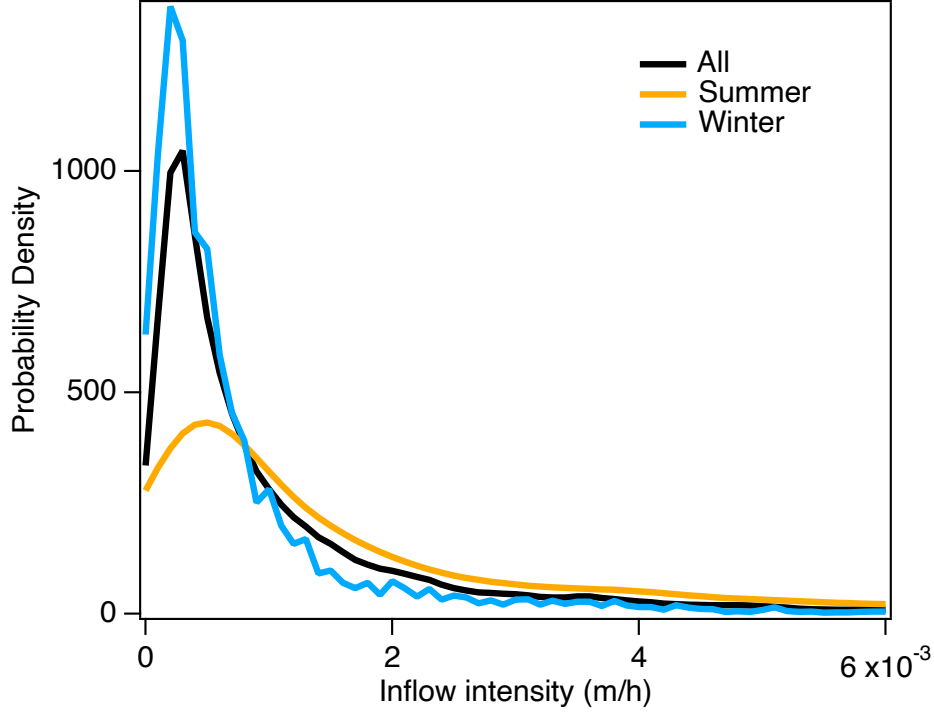


Figure B.2: Probability distributions for inflow intensities for summer (June, July, August), winter (December, January, February) and all days of the study period. During summer, probability for high intensity ( $> 2 \times 10^{-3}$  m/h) inflows is greater (yellow curve) than during winter (blue curve), suggesting higher runoff generation (and consequently lower infiltration) during summer months.

saturation and hourly estimates of potential evapotranspiration,  $PET(t)$  [ $L T^{-1}$ ], obtained from the NASA Land Surface Model [158]:  $ET(t) = \frac{S_{vz}(t)}{S_{vz,max}} PET(t)$ . A fixed fraction  $\gamma_2$  of outflow from the vadose zone infiltrates to groundwater,  $J_{gw}(t) = \gamma_2 Q_{vz}(t)$  [ $L T^{-1}$ ], while the rest flows to the stream as interflow,  $Q_{int}(t) = (1 - \gamma_2) Q_{vz}(t)$  [ $L T^{-1}$ ].

Water entering groundwater can accumulate with time,  $S_{gw}(t)$  [ $L$ ], or flow to the stream,  $Q_{gw}(t)$  [ $L T^{-1}$ ]:  $\frac{dS_{gw}}{dt} = J_{gw}(t) - Q_{gw}(t)$ . Groundwater storage is divided into an active portion that influences streamflow,  $S_{gw,a}(t)$  [ $L$ ], and a fixed passive portion,  $S_{gw,p}$  [ $L$ ], that does not influence streamflow but is hydrologically connected to the stream [97]:  $S_{gw}(t) = S_{gw,a}(t) + S_{gw,p}$ . The groundwater discharge-storage relationship depends linearly on active storage [29]:  $Q_{gw}(t) = k_{gw} S_{gw,a}(t)$  where  $k_{gw}$  [ $T^{-1}$ ] is a response rate constant for the active

portion of groundwater storage. The coupled set of differential equations for storage in the vadose zone and groundwater were numerically integrated within Wolfram Mathematica (v. 12.3).

### B.3 Transient-Transit Time Distribution (T-TTD) Model

T-TTD theory was used to estimate, on an hourly basis, the mean age of water in the stream and the fraction of streamflow derived originally from snow melt, assuming that outflow from the vadose zone and groundwater is selected randomly by age; i.e., a uniform storage selection function was adopted for both the vadose zone and groundwater control volumes (Figure B.1) [90, 176]. These calculations are described in turn.

#### B.3.1 Deriving Solutions for the Mean Age of Water

The mean age of water in the stream,  $\mu_{\text{stream}}(t)$  [T], was calculated from the expected value of the stream's age distribution,  $\mu_{\text{stream}}(t) = \int_0^\infty T p_{\text{stream}}(T, t) dT$ , where the variable  $T$  represents water age and  $p_{\text{stream}}(T, t)$  [T<sup>-1</sup>] is the probability density function (PDF) form of the stream's age distribution at any time  $t$ . The latter can be expressed as the flow-weighted sum of age distributions in runoff, interflow and groundwater discharged to the stream:  $p_{\text{stream}}(T, t) = \omega_{\text{run}}(t) p_{\text{run}}(T, t) + \omega_{\text{int}}(t) p_{\text{int}}(T, t) + \omega_{\text{gw}}(t) p_{\text{gw}}(T, t)$ . The weighting functions are defined as follows:

$$\omega_{\text{run}}(t) = \frac{Q_{\text{run}}(t)}{Q_{\text{stream}}(t)}, \quad \omega_{\text{int}}(t) = \frac{Q_{\text{int}}(t)}{Q_{\text{stream}}(t)}, \quad \omega_{\text{gw}}(t) = \frac{Q_{\text{gw}}(t)}{Q_{\text{stream}}(t)}, \quad (\text{B.1})$$

Combining these equations we arrive at the following expression for the mean age of water in

the stream at any time  $t$ , where  $\mu_{\text{run}}(t)$ ,  $\mu_{\text{int}}(t)$ , and  $\mu_{\text{gw}}(t)$  are the expected values of water age in direct runoff, interflow and groundwater, respectively:

$$\mu_{\text{stream}}(t) = \omega_{\text{run}}(t)\mu_{\text{run}}(t) + \omega_{\text{int}}(t)\mu_{\text{int}}(t) + \omega_{\text{gw}}(t)\mu_{\text{gw}}(t) \quad (\text{B.2})$$

For this analysis we assumed that runoff has a single age,  $T_{\text{run}}$  [T], when it reaches the stream:  $p_{\text{run}}(T, t) = \delta(T - T_{\text{run}})$ , where  $\delta$  is the Dirac Delta function. Therefore, the mean age of runoff entering the stream is  $\mu_{\text{run}}(t) = T_{\text{run}}$ .

The formulae used to estimate the mean age of water in interflow and groundwater were derived by first constructing a generic solution for the age of water leaving a control volume assuming that: (1) inflow has some prescribed age distribution which can vary with time; (2) outflow from the control volume occurs by both discharge and evapotranspiration; and (3) water leaving the control volume by discharge and evapotranspiration is sampled from storage randomly by age. This generic solution for the mean age of water in, and leaving, a control volume was then tailored to yield separate formulae for the mean age of water entering the stream from the vadose zone and groundwater.

### B.3.2 Mean Age of Water Leaving a Generic Control Volume

Consider a control volume drawn around either the vadose zone or groundwater (see below) that receives inflow at rate,  $J(t)$  [L T<sup>-1</sup>], and loses water through discharge at rate,  $Q(t)$  [L T<sup>-1</sup>], and evapotranspiration at rate,  $ET(t)$  [L T<sup>-1</sup>] (all volumes and fluxes are normalized by the catchment area). From volume balance, the change in water stored in the control volume,  $S(t)$  [L], is therefore equal to the instantaneous difference between inflows and outflows:  $\frac{dS}{dt} = J(t) - Q(t) - ET(t)$ . We make the following additional assumptions: (1)

water entering the control volume with inflow  $J(t)$  has an age distribution that varies with time,  $P_{in}(T, t)$  [-], where the variable  $T$  represents the random variable for water age, and the age distribution is expressed as a cumulative distribution function (CDF); and (2) water leaving the control volume by either discharge  $Q(t)$  or evapotranspiration  $ET(t)$  is uniformly sampled from water in storage (i.e., a uniform StorAge Selection (SAS) function is adopted for both discharge and evapotranspiration). Under such conditions, the time evolution of the age distribution of water stored in the control volume,  $P(T, t)$  [-], expressed here as a CDF, is governed by the following Age Conservation Equation (ACE) [25]:

$$\frac{\partial S(t)P(T, t)}{\partial t} = J(t)P_{in}(T, t) - ET(t)P(T, t) - Q(t)P(T, t) - S(t)\frac{\partial P(T, t)}{\partial T} \quad (\text{B.3a})$$

$$P(T = 0, t) = 0 \quad (\text{B.3b})$$

$$P(T, t = 0) = H(T - T_0) \quad (\text{B.3c})$$

$$H(x) = \begin{cases} 0, & x < 0 \\ 1, & x \geq 0 \end{cases} \quad (\text{B.3d})$$

In this equation, the time rate of change in the fraction of water in storage with age less than or equal to  $T$  (left hand side) depends on the inflow of water of age  $P_{in}(T, t)$  (first term on right hand side), outflow of water by evapotranspiration and discharge under uniform selection (second and third terms), and the aging of water in storage with time (fourth term). The boundary condition (Equation B.3b) stipulates that there is no water in storage with age less than or equal to  $T = 0$ , while the initial condition (Equation B.3c) stipulates that water in storage at time  $t = 0$  has a single age equal to  $T = T_0$ , where  $H(\cdot)$  is the unit step or Heaviside function (Equation B.3d). Expanding the left hand side of the equation and substituting the conservation equation for water in storage we obtain the following simplified

form of the ACE:

$$S(t) \frac{\partial P(T, t)}{\partial t} = J(t)(P_{in}(T, t) - P(T, t)) - S(t) \frac{\partial P(T, t)}{\partial T} \quad (\text{B.4})$$

The ACE can also be expressed in terms of probability density functions (PDFs) for the age distributions of water leaving and entering the control volume ( $p(T, t)$  and  $p_{in}(T, t)$ , respectively), by taking the derivative of both sides of Equation B.4 with respect to the age variable  $T$ , where  $p(T, t) = \frac{\partial P(T, t)}{\partial T}$  and  $p_{in}(T, t) = \frac{\partial P_{in}(T, t)}{\partial T}$ :

$$S(t) \frac{\partial p(T, t)}{\partial t} = J(t)(p_{in}(T, t) - p(T, t)) - S(t) \frac{\partial p(T, t)}{\partial T} \quad (\text{B.5a})$$

$$p(T = 0, t) = 0 \quad (\text{B.5b})$$

$$p(T, t = 0) = \delta(T - T_0) \quad (\text{B.5c})$$

The PDF form of the boundary and initial conditions (Equations B.5b and B.5c), follows by differentiating Equations B.3b and B.3c with respect to the age variable  $T$ . Taking the first moment,  $\int_0^\infty T(\cdot) dT$ , of each term in the PDF form of the ACE along with its boundary and initial conditions (Equations B.5a-B.5c) yields, after some manipulation, the following differential equation for the mean age of water in storage:

$$\frac{d\mu(t)}{dt} = \frac{J(t)}{S(t)}(\mu_{in}(t) - \mu(t)) + 1, \quad S(t) > 0 \quad (\text{B.6a})$$

$$\mu(t = 0) = T_0 \quad (\text{B.6b})$$

Here,  $\mu(t)$  represents the mean age (or expected value) of the water in and leaving the control volume at any time  $t$ , and  $\mu_{in}(t)$  represents the mean age (or expected value) of water entering the control volume with inflow at any time  $t$ :  $\mu(t) = \int_0^\infty T p(T, t) dT$  and  $\mu_{in}(t) = \int_0^\infty T p_{in}(T, t) dT$ . The above differential equation can be solved to yield the following exact solution for the mean age of water discharged from the control volume under uniform sampling:

$$\mu(t) = T_0 e^{-\tau_J(t)} + \int_0^t e^{-(\tau_J(t) - \tau_J(x))} \left( 1 + \frac{J(x)}{S(x)} \mu_{in}(x) \right) dx, \quad S(t) > 0 \quad (\text{B.7a})$$

$$\tau_J(t) = \int_0^t \frac{J(\nu)}{S(\nu)} d\nu \quad (\text{B.7b})$$

In the event that the water coming into the tank has a mean age of  $\mu_{in} = 0$ , the above solution simplifies as follows:

$$\mu(t) = T_0 e^{-\tau_J(t)} + \int_0^t e^{-(\tau_J(t) - \tau_J(x))} dx, \quad \mu_{in}(t) = 0, \quad S(t) > 0 \quad (\text{B.8a})$$

### B.3.3 Mean Age of Water in Interflow

From the generic solution presented above, the mean age of water leaving the vadose zone and entering the stream as interflow can be written as follows, where we have assumed the initial age of water in the vadoze zone at time  $t = 0$  is,  $T_{0,vz} = 0$ :

$$\mu_{int}(t) = \int_0^t e^{-(\tau_{J,vz}(t)-\tau_{J,vz}(x))} dx, \quad S_{vz}(t) > 0 \quad (\text{B.9a})$$

$$\tau_{J,vz}(t) = \int_0^t \frac{J_{vz}(\nu)}{S_{vz}(\nu)} d\nu \quad (\text{B.9b})$$

### B.3.4 Mean Age of Water in Groundwater

Accounting for the fact that water entering the groundwater (from the vadose zone) has some time varying mean age,  $\mu_{int}(t)$ , and building on the results presented above, we can write down the following solution for the mean age of water leaving the groundwater and entering the stream:

$$\mu_{gw}(t) = T_{0,gw} e^{-\tau_{J,gw}(t)} + \int_0^t e^{-(\tau_{J,gw}(t)-\tau_{J,gw}(x))} \left( 1 + \frac{J_{gw}(x)}{S_{gw,a}(x) + S_{gw,p}} \mu_{int}(x) \right) dx, \quad S_{gw}(t) > 0 \quad (\text{B.10a})$$

$$\tau_{J,gw}(t) = \int_0^t \frac{J_{gw}(\nu)}{S_{gw,a}(\nu) + S_{gw,p}} d\nu \quad (\text{B.10b})$$

Implementation of this last solution requires that we specify a value for the passive groundwater depth,  $S_{gw,p}$ . All else being equal, the model-predicted mean age of groundwater will increase as the depth of the passive groundwater is increased. Subsurface flow discharged to streams in the Mesozoic Lowland hydrogeomorphic region (HGMR, where Flatlick Branch is located, see Figure 3.1b) is much younger than that in other Chesapeake Bay HGMRs (Figure B.3). For the Flatlick Branch watershed, the median age of subsurface flow discharged to stream is 5.2 years [13] (right panel in Figure B.3).

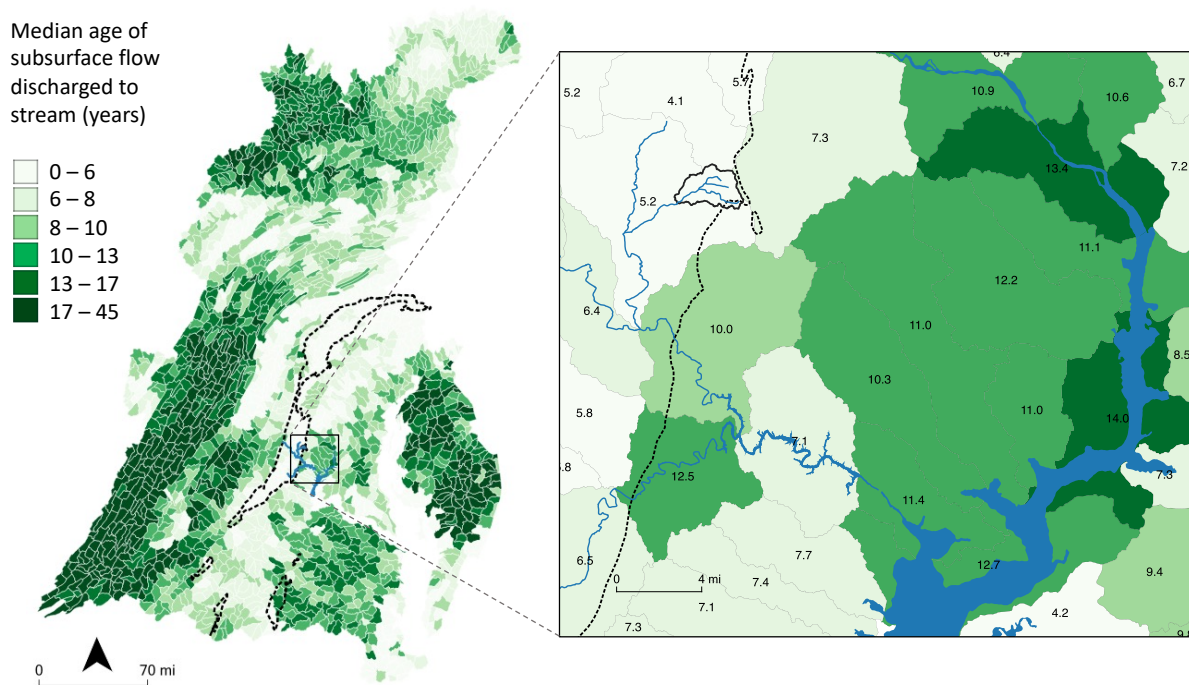


Figure B.3: Median age of subsurface flow discharged to streams in different sub-watersheds within the Chesapeake Bay watershed. Dashed black line denotes the Mesozoic Lowland HGMR. Solid black line (right panel) denotes the Flatlick Branch watershed.

To identify the passive groundwater depth that would yield a similar model-predicted median subsurface flow age, we conducted the following numerical experiment. First, to provide sufficient time for the mean age of groundwater to reach a dynamic equilibrium, we created a 30-year synthetic time series of hourly precipitation, temperature and PET (the inputs to our HBV and Hydrologic models), by repeating the measured ten-year hourly time series for these three climate variables at our site a total of three times. Second, using the parameter values for the top-ranked model (see Table 3.1) we solved the HBV and Hydrologic models (see Sections B.1 and B.2) for the entire 30-year period, yielding hourly estimates for all stocks and flows of water through the catchment. Third, from the 30-year time series of catchment stocks and flows we computed hourly estimates for the mean ages of water discharged to the stream from the vadose zone and groundwater (from equations (B.9a) and (B.10a), respectively). This allowed us to calculate the mean age of subsurface flow using the following equation:

$$\mu_{\text{sub}}(t) = \frac{Q_{\text{int}}(t)}{Q_{\text{int}}(t) + Q_{\text{gw}}(t)}\mu_{\text{int}}(t) + \frac{Q_{\text{gw}}(t)}{Q_{\text{int}}(t) + Q_{\text{gw}}(t)}\mu_{\text{gw}}(t) \quad (\text{B.11})$$

Finally, we computed the median subsurface flow age from the last six years of hourly mean subsurface flow age simulations. The last two steps were then repeated for 5 different choices of the passive groundwater depth, ranging from 0 to 1.5 m. The results of this numerical experiment, which are presented in Figure B.4, indicate that the median groundwater age increases linearly with passive groundwater storage. From this plot we infer that, for the Flatlick Branch site, a median subsurface flow age of 5.2 years corresponds to a passive groundwater depth of  $S_{\text{gw},p} \approx 1.4\text{m}$ . This choice of passive groundwater depth was therefore adopted for all age simulations described in the main text. We also adopted  $T_{0,vz} = 0$  years and  $T_{0,gw} = 15$  years for the initial ages of water in the vadose zone and groundwater, respectively.

### B.3.5 Snow Melt Fraction

In Figure B.1b, the variable,  $C_{\text{stream}}(t) \in [0, 1]$  [-], represents the fraction of streamflow, at any time  $t$ , that originated as snow melt. The end members,  $C_{\text{stream}}(t) = 1$  or  $C_{\text{stream}}(t) = 0$ , therefore represent conditions where the streamflow is 100% derived from snow melt or rainfall, respectively. As noted in the main text, we assumed that direct runoff has an effective age of  $T_{\text{run}} = 0$ . Given this assumption and for the choice of a uniform StorAge Selection (SAS) function for discharge from the vadose zone and groundwater (45), the fraction  $C_{\text{stream}}(t)$  can be estimated directly from solute mass balance and the dynamic water balance calculations presented in Section B.2, as the flow weighted sum of the snow melt fraction of runoff, interflow, and groundwater ( $C_{\text{run}}(t)$ ,  $C_{\text{int}}(t)$ ,  $C_{\text{gw}}(t)$ , respectively):

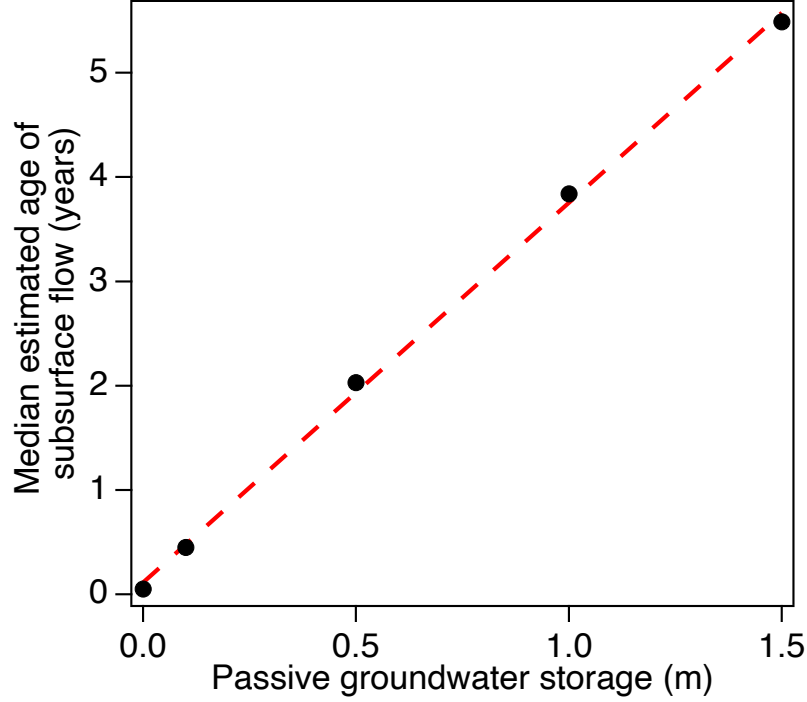


Figure B.4: Model-predicted median subsurface flow age discharged to Flatlick Branch for different choices of passive groundwater storage depth.

$$C_{\text{stream}}(t) = \omega_{\text{run}}(t)C_{\text{run}}(t) + \omega_{\text{int}}(t)C_{\text{int}}(t) + \omega_{\text{gw}}(t)C_{\text{gw}}(t) \quad (\text{B.12a})$$

$$C_{\text{run}}(t) = C_{J,vz}(t) = \frac{s(t)}{s(t) + r(t)} \quad (\text{B.12b})$$

$$C_{\text{int}}(t) = C_{J,gw}(t) = \frac{1}{S_{vz}(t)} \int_0^t C_{J,vz}(t_i) J_{vz}(t_i) e^{-(\tau_{Q,vz}(t) - \tau_{Q,vz}(t_i))} dt_i \quad (\text{B.12c})$$

$$C_{\text{gw}}(t) = \frac{1}{S_{\text{gw},a}(t) + S_{\text{gw},p}} \int_0^t C_{J,gw}(t_i) J_{gw}(t_i) e^{-(\tau_{Q,gw}(t) - \tau_{Q,gw}(t_i))} dt_i \quad (\text{B.12d})$$

$$\tau_{Q,vz}(t) = \int_0^t \frac{Q_{vz}(r) + \text{ET}(r)}{S_{vz}(r)} dr \quad (\text{B.12e})$$

$$\tau_{Q,gw}(t) = \int_0^t \frac{Q_{gw}(r)}{S_{\text{gw},a}(r) + S_{\text{gw},p}} dr \quad (\text{B.12f})$$

The expression for  $C_{\text{run}}(t)$  follows from a mass balance over rainfall and snow melt entering

the catchment with snow melt fractions of  $C_{rain} = 0$  and  $C_{snow} = 1$ , respectively (Equation B.12b and top of Figure B.1b). The integrals appearing in Equations B.12c and B.12d represent the sum over all snow melt entering the vadose zone and groundwater control volumes, respectively, from time  $t_i \in [0, t]$ . The exponential terms appearing in these integrals account for the outflow of snow melt under uniform sampling, the rate of which depends on outflow-weighted time  $\tau_Q(t)$  [-]. The latter takes on different functional forms for the vadose zone (where snow melt can leave the control volume by both discharge and evapotranspiration, Equation B.12e) and groundwater (where snow melt leaves the control volume by discharge alone, Equation B.12f). As described above, for these calculations we set the volume of passive groundwater to  $S_{gw,p} = 1.4\text{m}$ .

## B.4 Model Calibration

### B.4.1 Data Sources

HBV and hydrologic model predictions of catchment hydrology are driven by hourly measurements of precipitation, air temperature, and potential evapotranspiration (PET) (Figure B.1a and Figure 3.2a). Ten years (water years 2008-2017) of measured hourly precipitation (with a heated gage) and air temperature at Dulles International Airport (station ID WBAN:93738, located approximately 6 km north of the Flatlick monitoring station, see Figure 3.1a) were downloaded from the National Oceanic and Atmospheric Administration website ([www.ncei.noaa.gov](http://www.ncei.noaa.gov)). Hourly estimates of local PET (for a pixel ( $0.125^\circ \times 0.125^\circ$ ) centered on the nearby Occoquan Forest) were obtained from NASA's land surface model (NLDAS-Noah) using the Data Rods Explorer ([apps.hydroshare.org/apps/data-rods-explorer](http://apps.hydroshare.org/apps/data-rods-explorer)). Daily groundwater elevation (in feet to groundwater from land surface, for compar-

ison with model-predictions of active groundwater depth, see Figure B.9) were obtained for USGS well (#385638077220101), located approximately 10 km northeast of the USGS stream monitoring station on Flatlick Branch (Figure 3.1). The hydrologic model was calibrated and validated with ten-years (water years 2008-2017) of hourly streamflow measurements at a USGS monitoring station on Flatlick Branch (USGS Station ID 01656903 Figure 3.1). T-TTD predictions of mean stream age and snow melt fraction (Section B.3) were compared with hourly in situ measurements of specific conductance, which was collected at the same location on Flatlick Branch (USGS Station ID 01656903), and over the same ten-year time period (water years 2008-2017) as the streamflow measurements described above.

## B.4.2 Parameter Inference

The hydrological component of our modeling framework includes seven parameters, which were inferred from streamflow measurements at Flatlick Branch as described in Section 3.2. Preliminary evaluation indicated that the posterior distributions of all parameters were well constrained (see Figures 3.2 c,d), with the exception of the active groundwater response rate for which the posterior values were more uniformly distributed, a problem also noted by Bertuzzo et al. [29]. As noted in the main text, we fixed the active groundwater response rate to  $k_{\text{gw}} = 0.011 \text{ day}^{-1}$ , based on the slope of log-transformed measurements of stream flow at Flatlick Branch against time for the master recession curve (Figure B.5). Posterior distributions were derived for the remaining six parameters conditioned on this single value for the active groundwater response rate.

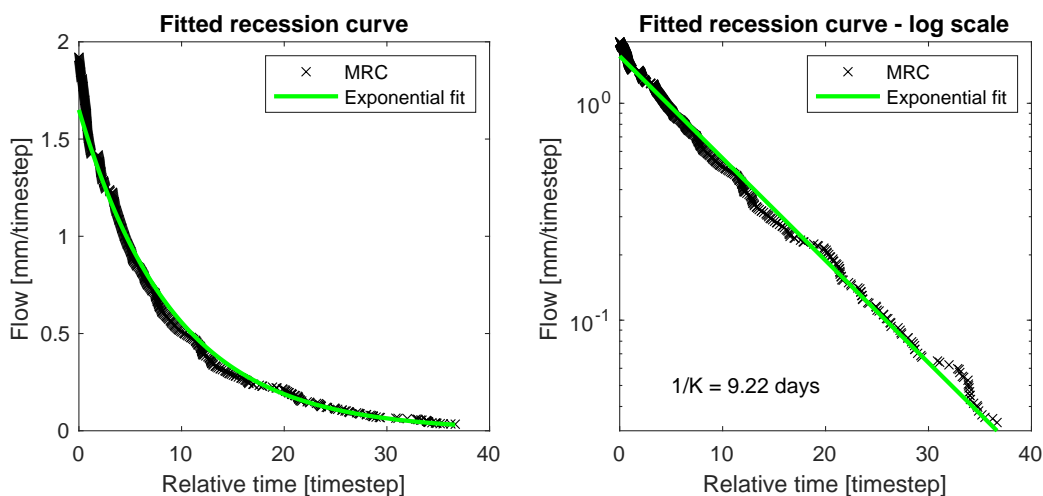


Figure B.5: Master recession curve for the Flatlick Branch watershed.

## B.5 Estimating Deicer Application Rates

In Northern Virginia, winter maintenance responsibilities fall under the jurisdiction of both public sector agencies (e.g., on roads, parking lots, etc.) and private sector companies (e.g., on private properties) [140]. Virginia Department of Transportation (VDOT) guidelines for deicer application rates in this area (which are based on Salt Institute’s standard road salt (as NaCl) application rates) are keyed to winter-weather mobilization levels, which range from a Mobilization Level 1 (corresponding to a recommended daily road salt application to impervious surfaces of  $0.025 \text{ kg m}^{-2}$ ) to Mobilization Level 5 (corresponding to a recommended road salt application of  $0.048 \text{ kg m}^{-2}$ ) (Table B.2). The mobilization levels, in turn, depend on forecasts of precipitation probability, snow accumulation depth and ambient temperature (Table B.2, see also Appendix D.a in Moltz et al. [140]). We re-constructed a ten-year timeseries of daily mobilization levels at Flatlick Branch based on historical weather data recorded at Dulles Airport (i.e., we used actual historical weather data as a proxy for historical weather forecasts, which were not available for the ten year period of interest here).

To evaluate how well these simulated mobilization levels comport with reality, we obtained from VDOT the actual daily mobilization levels recorded for the Northern Virginia region during the winter seasons of 2019 and 2020. Mobilization levels predicted with measured climate data at Dulles (black bars Figure B.6) compare favorably with actual mobilization levels recorded by VDOT (red bars Figure B.6), although there are many cases where the actual mobilization level was higher than the predicted mobilization level, and more infrequently cases where the actual mobilization level was lower than the predicted mobilization level. These differences are due to weather forecast inaccuracies (e.g., that might predict precipitation when no precipitation in fact occurred) and the fact that the conditions listed for each mobilization level in Table B.2 are just recommended guidelines; other factors, such as professional judgement [191], often influence the mobilization levels adopted on any particular winter day (personal communication, VDOT staff).

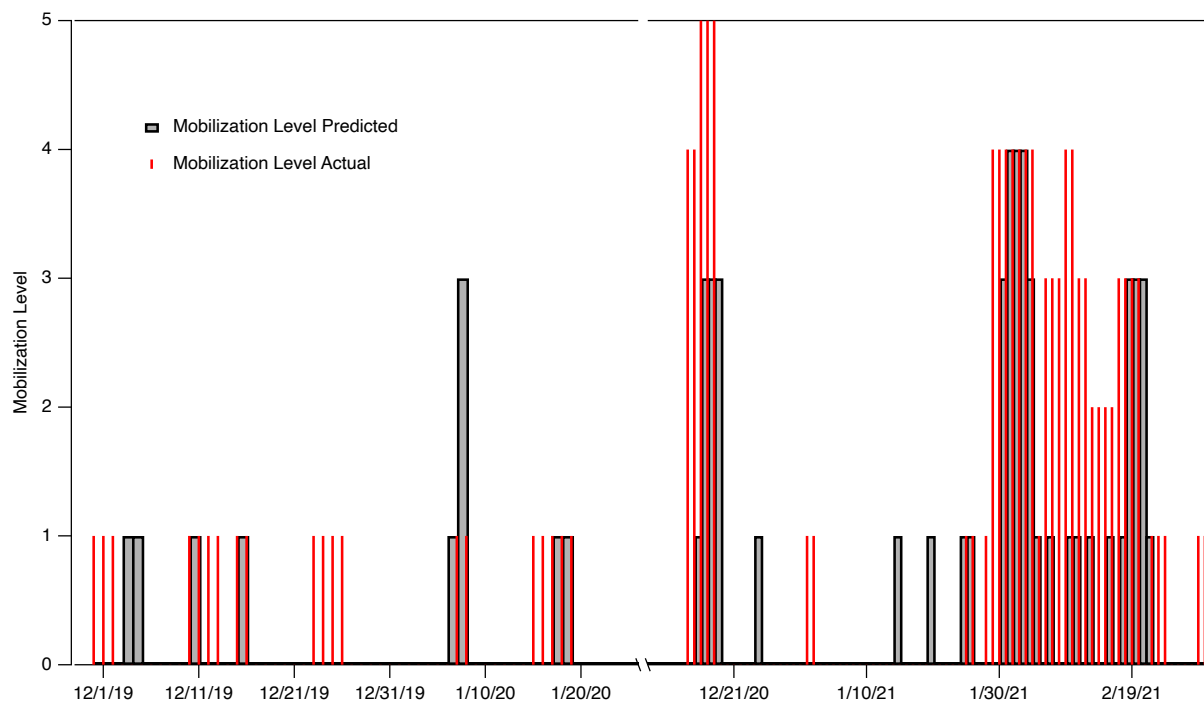


Table B.2: Salt Institute’s standard road salt (as NaCl) application rates

Weather Forecast	Winter-Weather Mobilization Level	Road Salt (NaCl) Application Rate (kg/m <sup>2</sup> )
P: >20%; S: possible; T: 30-36	Anti-ice	0.025
P: 20-49%; S: possible; T: 30-36	1	0.025
P: 50-100%; S: < 1 inch; T: 25-29	2	0.031
P: 50-100%; S: < 2 inch; T: 20-24	3	0.037
P: 50-100%; S: < 6 inch; T: 15-19	4	0.042
P: 50-100%; S: > 6 inch; T: 10-14	5	0.047

P: Chance of precipitation; S: Snowfall; T: Temperature (°F).

## B.6 Inferring Chloride Concentrations from Specific Conductance

To contextualize the specific conductance (SC) measurements on Flatlick Branch, we estimated from the SC measurements stream chloride concentrations which can, in turn, be directly compared to the U.S. Environmental Protection Agency’s 1988 Ambient Water Quality Criteria for stream chloride concentration (chronic and acute thresholds of 230 and 860 mg L<sup>-1</sup>, respectively) (EPA 1988). To convert SC measurements into chloride concentrations we utilized USGS measurements of SC and chloride on 27 grab samples collected at our field site on a monthly basis for the past three calendar years (2020-2022). Regressing log-transformed chloride against log-transformed SC we obtain the following power-law relationship between the two:  $[Cl] = 10^a \times SC^b$ , where  $a = -1.89 \pm 0.48$  and  $b = 1.41 \pm 0.18$  ( $R^2=0.91$ ) (Figure B.7). Using this relationship, we inferred in-stream chloride concentrations corresponding to the peaks in measured specific conductance (Figure 3.8).

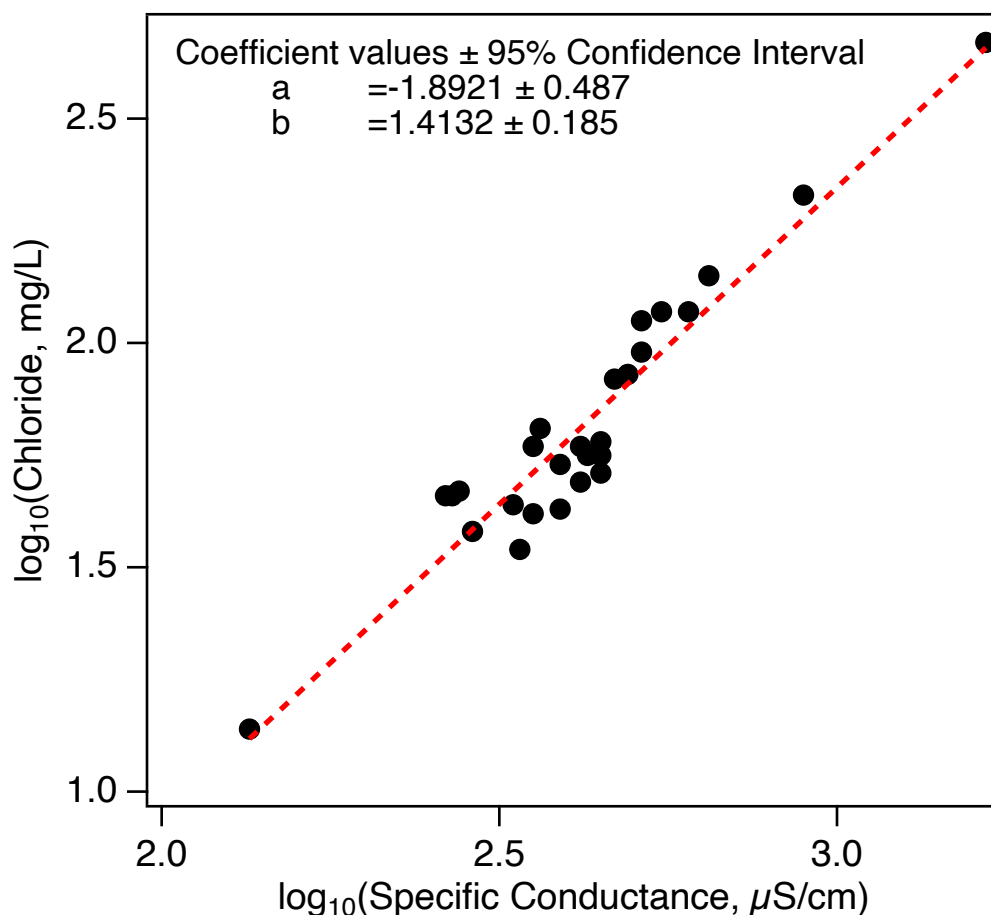


Figure B.7: Measured chloride vs in-stream specific conductance at Flatlick Branch.

## B.7 Groundwater Specific Conductance in the Mesozoic Lowland HGMR

We compiled historical data [72, 164] and data available through the National Groundwater Monitoring Network ([cida.usgs.gov/ngwmn](http://cida.usgs.gov/ngwmn)), on specific conductance measured in groundwater wells (depths ranging from 80-1000 feet) in the Mesozoic Lowland hydrogeomorphic (HGMR) region of Virginia. Measured specific conductance in deep groundwater ranged from 62-4500  $\mu\text{S/cm}$ , with a median value of 542.5  $\mu\text{S/cm}$  (Figure 3.5). These data are compiled in Tables B.3-B.5.

Table B.3: Groundwater Specific Conductance for Wells in the Mesozoic Lowland HGMR Reported in Posner and Zenome, 1983

USGS Local Reference No.	Date	Depth of Well (feet)	Specific Conductance (uS/cm)
EC-10	11/27/79	858	970
51V-3E	7/30/75	100	780
51V-3E	7/30/75	520	750
51V-3E	7/30/75	900	4500
51V-24H	7/20/79	500	560
51V-24H	7/26/79	760	2000
50U-83C	6/24/80	-	2140
50U-84F	6/24/80	-	644
50T-16B	7/30/80	153	433
50S-2D	5/02/80	205	439
48R-3A	6/17/80	-	2710
DC-31	10/18/78	285	355
DB-47	10/18/78	600	275
51V-14F	10/24/78	423	295
51V-14F	10/25/88	880	290
51V-23H	7/09/79	1000	640
51V-5J	1/13/77	289	150
49U-11C	4/28/80	500	254
48R-4A	6/17/80	100	414
47R-11G	8/12/80	-	412

Table B.4: Groundwater Specific Conductance for Wells in the Mesozoic Lowland HGMR Reported in Froelich and Zenome, 1985

USGS Local Reference No.	Date	Depth of Well (feet)	Specific Conductance (uS/cm)
385320077251701	7/05/79	743	931
385320077251701	7/09/79	1000	538
384810077284501	4/18/77	320	600
384918077281201	4/17/77	290	437
385321077234001	12/21/76	309	160
385311077234501	1/13/77	289	150
385157077275301	4/20/77	400	398
385543077271901	8/18/75	860	1170
385617077271201	7/30/75	100	780
385617077271201	7/30/75	530	750
385617077271201	7/30/75	900	4500
385048077320001	4/20/77	-	585
385656077241201	10/04/74	-	215
390130077210801	10/04/74	-	320
390109077210701	10/04/74	-	188
385657077232701	11/12/74	-	200
385350077272501	7/20/79	500	547
385350077272501	7/26/79	500	2050
385205077275501	6/20/79	650	570
385205077275501	8/09/76	650	849

Table B.5: Groundwater Specific Conductance for Wells in the Mesozoic Lowland HGMR in Virginia from the National Groundwater Monitoring Network ([cida.usgs.gov/ngwmn](http://cida.usgs.gov/ngwmn))

USGS Local Reference No.	Date	Depth of Well (feet)	Specific Conductance (uS/cm)
385930000000000	7/22/03	120	551
385930000000000	7/22/03	120	507
385930000000000	2/03/05	120	330
385930000000000	2/03/05	120	432
385930000000000	5/05/05	120	482
385930000000000	5/05/05	120	445
385930000000000	8/01/05	120	520
385930000000000	8/01/05	120	523
385930000000000	8/07/07	120	599
385930000000000	8/07/07	120	606
385930000000000	7/28/09	120	698
385930000000000	7/28/09	120	712
385930000000000	8/17/11	120	795
385930000000000	8/17/11	120	784
385930000000000	8/12/15	120	977
385930000000000	8/12/15	120	946
384956000000000	7/23/03	80	62
384956000000000	7/23/03	80	66
384956000000000	7/28/15	80	72
384956000000000	7/28/15	80	74

## B.8 Deconvolution Framework

As noted above, the T-TTD model produces time-varying estimates for the age-distribution of water in the stream,  $p_{\text{stream}}(T, t)$  (units inverse age) where  $T$  is water age and  $t$  is time (units of age and time, respectively). The increment of salt mass discharged from the stream per unit time with age in the range  $T$  to  $T + \Delta T$  at time  $t$  is therefore  $\Delta \dot{M}_Q(T, t) = \dot{M}_Q(t) p_{\text{stream}}(T, t) \Delta T$ . Here  $\dot{M}_Q(t)$  (units of salt mass per time) is the measured salt mass discharged from the stream at time  $t$  (equal to measured salt concentration times measured stream discharge) and  $\Delta \dot{M}_Q(T, t)$  is the portion of that discharged salt mass with age  $T$  at time  $t$ . The rate at which salt was added to the catchment (e.g., as deicers) at “injection” time  $\tau = t - T$  is therefore the sum over all  $\Delta \dot{M}_Q(T, t)$  for which the difference of  $t$  and  $T$  equals  $\tau$ :

$$\dot{M}_J(\tau) = \sum_{\tau=t-T} \Delta \dot{M}_Q(T, t) \quad (\text{B.13})$$

This can be visualized graphically by imagining a matrix in which the rows and columns represents time  $t$  and stream water age  $T$ , respectively, and the entries are our estimate of  $\Delta \dot{M}_Q(T, t)$  obtained from the measured stream salt mass loading rate and our T-TTD theory estimates for the age distribution,  $p_{\text{stream}}(T, t)$  (see above). The salt mass loading rate to the catchment at time  $\tau$  is simply the sum over all cells in the matrix that fall along the line,  $t = \tau + T$  [37, 149].

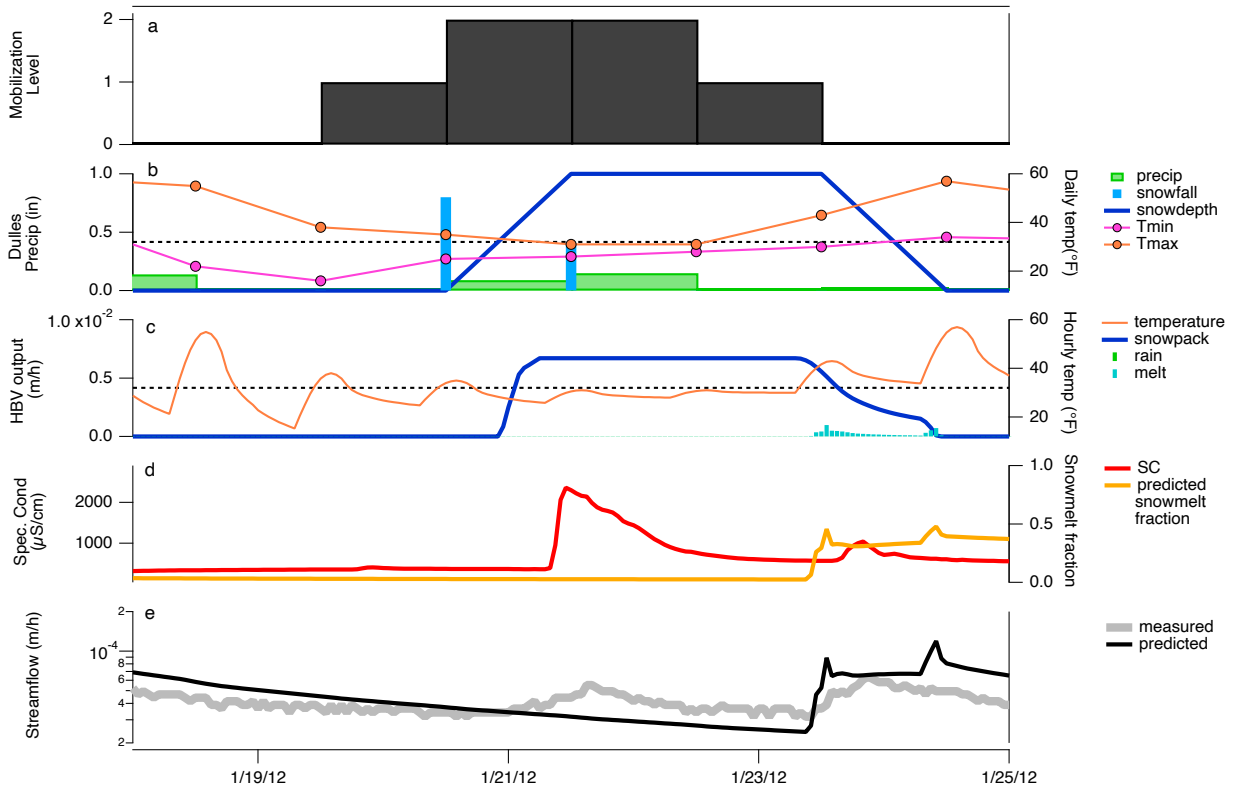


Figure B.8: **An illustrative one week period when a peak in measured stream specific conductance did not align with our model-predicted snow melt fraction.** (a) Model predicted winter weather mobilization level based on the Salt Institute Guidelines (see Table B.2). (b) Measured daily total precipitation, snowfall, accumulated snow depth and minimum and maximum temperature recorded at Dulles Airport. (c) HBV model input hourly temperature and HBV model-predicted rainfall, accumulated snowpack and snowmelt. (d) Measured specific conductance (SC) at Flatlick Branch and model-predicted fraction of streamflow originating as snowmelt (note that measured SC in the stream peaks several days before the HBV model predicts a snow melt event). (e) Measured and model-predicted streamflow at Flatlick Branch. When the temperature at Dulles is just below freezing (orange curve in panel c), the HBV model assumes precipitation as snowfall and accumulates the snowpack (blue curve in panel c) whereas Dulles weather records indicate a mix of snowfall and rainfall (blue and green sticks in panel b) that likely washed away the applied deicers resulting in a peak in SC (red curve in panel d) and a slight increase in streamflow (grey curve in panel e), an event that the HBV model failed to capture (black curve in panel e).

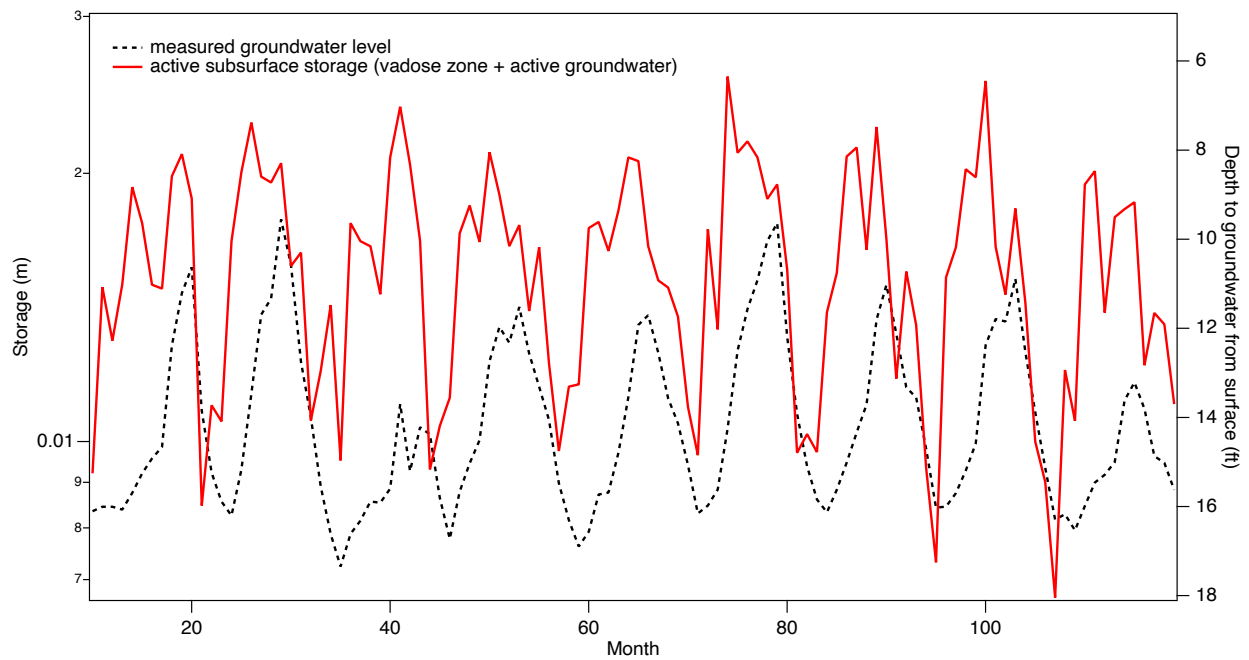


Figure B.9: Model-predicted storage (monthly averaged) in the vadose zone and groundwater (red curve) follows a seasonal pattern similar to that of the monthly groundwater level observed at a nearby USGS monitoring well (USGS well #385638077220101, see Figure 3.1)

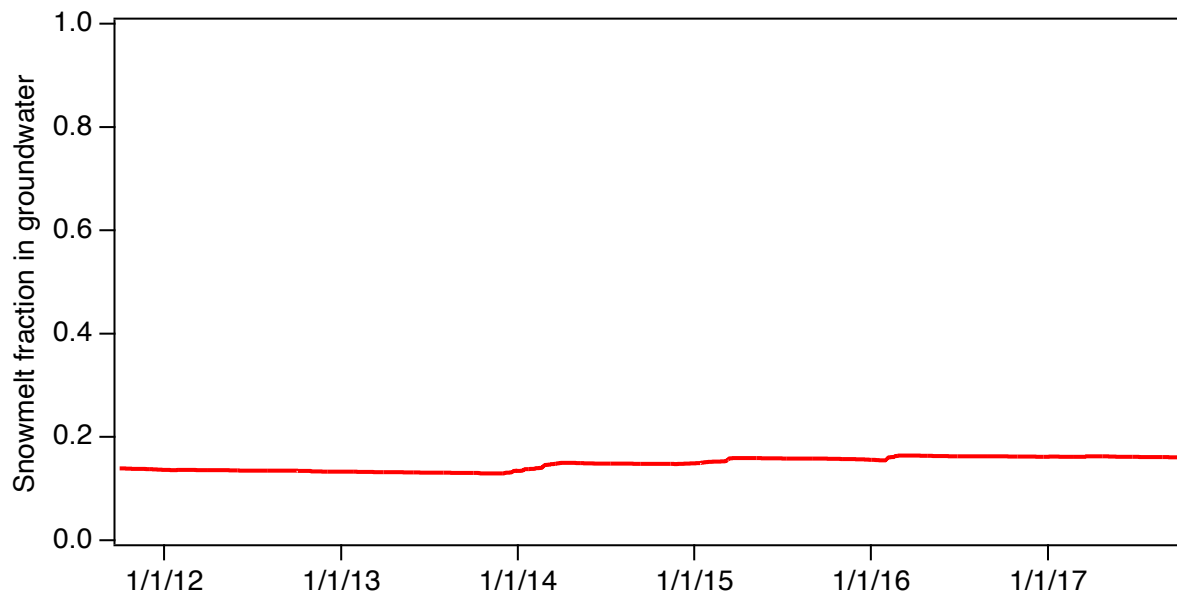


Figure B.10: Model-predicted fraction of snowmelt in groundwater for the validation period.

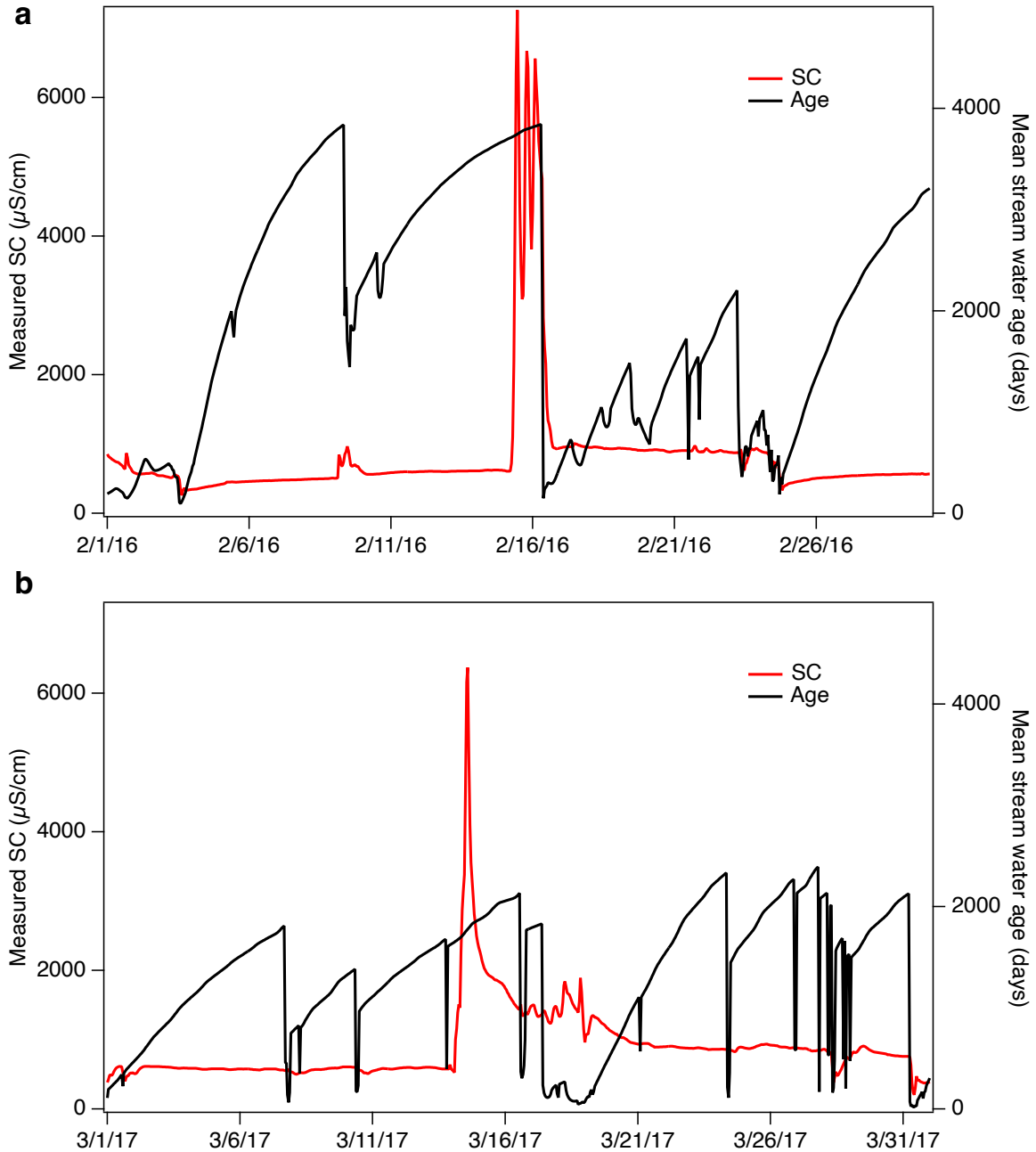


Figure B.11: Illustrative examples of periods when peaks in measured stream specific conductance (SC) do not perfectly align with reductions in the mean stream water age (reflecting contribution from younger direct runoff and/or interflow). SC pules either arrive early (panel a) or are delayed (panel b) with respect to younger flows from direct runoff and/or interflow.

# Appendix C

## Supplementary Information for Chapter 4

### C.1 TTD model calibration procedure

#### C.1.1 Evaluation of Water Balance Error

As noted in Chapter 4, we calculated the daily ungaged inflow to the reservoir over a period of 11 years, from measured daily inflows and outflows, along with the change in water storage with time (see water balance equation at the top of Figure 4.2). As a check on these calculations, we: (1) integrated up daily inflows and outflows over the eleven year period (referred to here as “cumulative inflows” and “cumulative outflows”); and then (2) computed the net volume of water lost from the reservoir by numerical error over the 11-year period from the difference of cumulative inflows and outflows. From these calculations we find that numerical error resulted in a cumulative loss of water from the reservoir of approximately  $10^7$  cubic feet of water, which corresponds to 0.003% of the cumulative inflow of approximately  $3 \times 10^{11}$  cubic feet over the same period of time. Thus, our calculations close water balance over the reservoir to a very high degree of precision.

### C.1.2 Shifted-uniform SAS

From the daily water balance over the reservoir, we numerically evaluated a set of functions that are required for estimating solute breakthrough concentration under Shifted-Uniform sampling (see Grant and Harman [83] for details): (1) cumulative volume of water transferred between Tanks 1 and 2,  $\bar{Q}_\Delta(t)$ , (2) time required to drain all original water in Tank 1 (critical time),  $t_c$ , and (3) maximum age of water in Tank 1,  $T_{m1}(t)$  [83]. The solution for sodium concentration in reservoir outflow (Equation 4.5) was then implemented in Mathematica as follows:

1. Create a null two-dimensional  $m \times n$  matrix A, where  $m = n =$  number of days in the timeseries. Let  $m$  represent time,  $t$  whereas  $n$  represents the time at which solute breakthrough begins,  $t_{BT}$ . Here  $A_{m,n}$  is the matrix element in the  $m^{\text{th}}$  row and  $n^{\text{th}}$  column.
2. Replace every element below the main diagonal of the matrix with  $A_{m,n} = e^{(-\bar{\tau}^*(m)+\bar{\tau}^*(n))}$  where  $\bar{\tau}^*(t) = \int_0^t \frac{Q_{OUT}(x)}{S(x)} dx$ .
3. Sodium concentration in reservoir outflow at time  $t_k$  can be calculated using the following equation:  $C_Q(t_k) = \frac{\sum [M_{in}][A]^{\frac{1}{1-p}}}{(1-p)S(t_k)}$ , where  $[M_{in}]$  is a vector for daily sodium mass loading to the reservoir (Equation 4.3) from  $t = 1$  to  $t = t_k$  and  $[A]$  is a vector of elements below the main diagonal in the matrix's  $t_k^{\text{th}}$  row.

This procedure significantly reduced the computational time required to estimate solute breakthrough (e.g., for the purposes of model optimization, and real-time simulations for participatory modeling exercises). We calibrated the model parameter,  $p$ , and other unknowns in the power law equation for sodium concentration in ungaged flow ( $X, a, b$  in

Equation 4.2a), as follows: (a) For every choice of  $X$ , create all possible realizations of parameter sets by combining  $a \in (0, 1)$ ,  $b \in (0, 2)$  and  $p \in (0, 1)$  in steps of 0.1, (b) For every realization, calculate  $C_Q(t_k)$  (using Step 3) for all days in the timeseries,  $t_k$ , when measurements of sodium concentration are available at Station 8 in Figure 4.1a and evaluate root mean squared error (RMSE), log-likelihood and AIC. The parameter set for the realization with lowest RMSE and AIC is used to generate daily predictions of sodium concentration in reservoir outflow.

### C.1.3 Gamma distribution SAS

The Gamma distribution SAS solution was implemented using the *mesas.py* python module [89]. Inputs to the module include: (1) parameters specifying the SAS function, solute properties and other model settings, specified using a nested data structure that can be stored and read from a JSON-formatted text file; and (2) timeseries of reservoir inputs (both flow and sodium ion concentration) and outflows provided as a .csv text file (see Harman and Xu Fei [89] for details). We assumed initial water concentration,  $C_{old} = 0$  mg/L and allowed sufficient model spin-up (10 years) to eliminate the effect of initial conditions. Also, we set the partitioning coefficient  $\alpha_q = 1$  for reservoir outflow (flow over the dam + abstraction) and  $\alpha_q = 0$  for evaporation, which means that sodium cannot leave the reservoir through evaporation (see Harman and Xu Fei [89] for description of the partitioning coefficient). The model output includes a timeseries for sodium ion concentration in outflow.

The scale parameter,  $\beta(t)$ , was set equal to the total storage in the reservoir,  $S(t)$  [88]. A value for the shape parameter,  $\alpha$ , was inferred as follows: (1) For every choice of  $X$ , create all possible realizations of parameter sets by combining  $a \in (0, 1)$ ,  $b \in (0, 2)$  and  $\alpha \in (0, 5)$  in steps of 0.1; (2) For every realization, run the *mesas.py* module (as described above), generate

a timeseries of sodium ion concentration in outflow and calculate RMSE, log-likelihood and AIC.

## C.2 Identifying deicer wash-off events

In Northern Virginia, winter maintenance responsibilities fall under the jurisdiction of both public sector agencies (e.g., on roads, parking lots, etc.) and private sector companies (e.g., on private properties) [140]. Virginia Department of Transportation (VDOT) guidelines for deicer application rates in this area (which are based on Salt Institute’s standard road salt (as NaCl) application rates) are keyed to winter-weather mobilization levels, which range from a Mobilization Level 1 (corresponding to a recommended daily road salt application to impervious surfaces of  $0.025 \text{ kg m}^2$ ) to Mobilization Level 5 (corresponding to a recommended road salt application of  $0.048 \text{ kg m}^2$ ). The mobilization levels, in turn, depend on forecasts of precipitation probability, snow accumulation depth and ambient temperature (see Appendix D.a in Moltz et al., 2020). We re-constructed an eleven year timeseries of daily mobilization levels in the Occoquan watershed based on historical weather data recorded at Dulles Airport (i.e., we used actual historical weather data as a proxy for historical weather forecasts, which were not available for the eleven year period of interest here). Deicer wash-off events were identified by comparing peaks in the daily timeseries of flow and sodium concentration ( $C_{BR}(t)$ ,  $C_{OR}(t)$  and  $C_{UG}(t)$ ) that coincide with back-to-back non-zero predicted winter weather mobilization levels (see yellow shaded bars in Figure C.5).

## C.3 Supplementary Tables and Figures

Table C.1: Rating curve for the Occoquan Reservoir.

Pool elevation (ft. msl)	Storage Volume (cf)	Pool Area (acre)
118.0	9.22E+08	1144
120.0	1.03E+09	1218
122.0	1.14E+09	1328
123.0	1.20E+09	1378
124.0	1.26E+09	1480
126.0	1.39E+09	1637
128.0	1.54E+09	1806
130.0	1.71E+09	2089

Table C.2: Top-ranked MLR models of Sodium Concentration at ST10 and ST45.

	ST10	ST45
No. of observations	370	296
F statistic	28.51*** (df=4; 365)	292.4*** (df = 4;291)
<b>Coefficients</b>		
Intercept	3.15***	3.29***
ln(Q, cfs)	-0.12***	-0.09***
Specific conductance (uS/cm)	-	0.0016***
Rainfall (max in the previous two weeks)	-0.09***	-
Snow depth (max in the previous two weeks)	0.03***	0.017***
Seasonality	-	0.0417***
No. of days below freezing in the previous two weeks	0.011*	-
<b>Performance metrics</b>		
Adjusted R <sup>2</sup>	0.24	0.80
RMSE	0.26	0.13
PBIAS	-1.2	0.3
BIC	113	-319
LOOCV prediction error	0.215	0.091

Table C.3: Optimal SAS function based on RMSE.

SAS function	$X$	RMSE	$a$	$b$	$p$	$\alpha$	AIC
Gamma distribution SAS	$C_{OR}(t)$	5.31	0.1	1.9	-	1.1	4673.45
	$C_{BR}(t)$	5.07	0.7	0.9	-	1.4	1801.47
Uniform SAS	$C_{OR}(t)$	5.02	0.2	1.4	0	-	1793.57
	$C_{BR}(t)$	4.89	0.4	0.9	0	-	1778.51
Plug flow SAS	$C_{OR}(t)$	6.85	1.8	0.9	1	-	1943.55
	$C_{BR}(t)$	6.98	1.8	0.7	1	-	1946.23
Shifted uniform SAS	$C_{OR}(t)$	5.03	0.4	1	0.01	-	2543.63
	$C_{BR}(t)$	4.96	0.4	0.9	0.01	-	2549.39

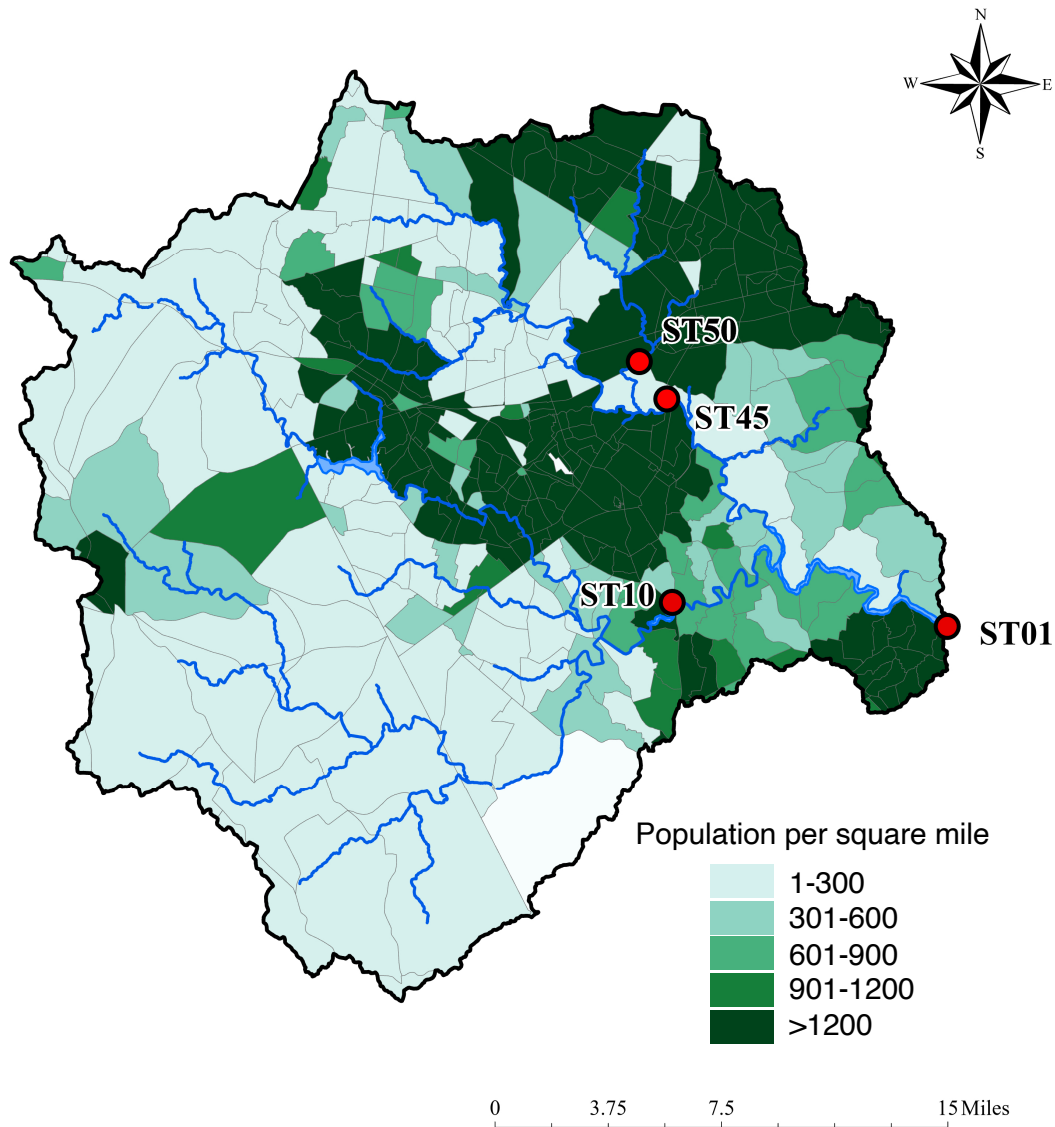


Figure C.1: The Occoquan Reservoir, its tributaries and the surrounding watershed (delineated by the thick black line). Internal polygons represent Metropolitan Washington Council of Governments (MWCOG) delineated Transportation Analysis Zones, colored by population density. Also shown are locations of Virginia Tech Occoquan Watershed Monitoring Laboratory's long-term monitoring stations on the Occoquan Reservoir (ST01), Occoquan River (ST10), Bull Run (ST45) and Cub Run (ST50), a major tributary of Bull Run upstream of UOSA.

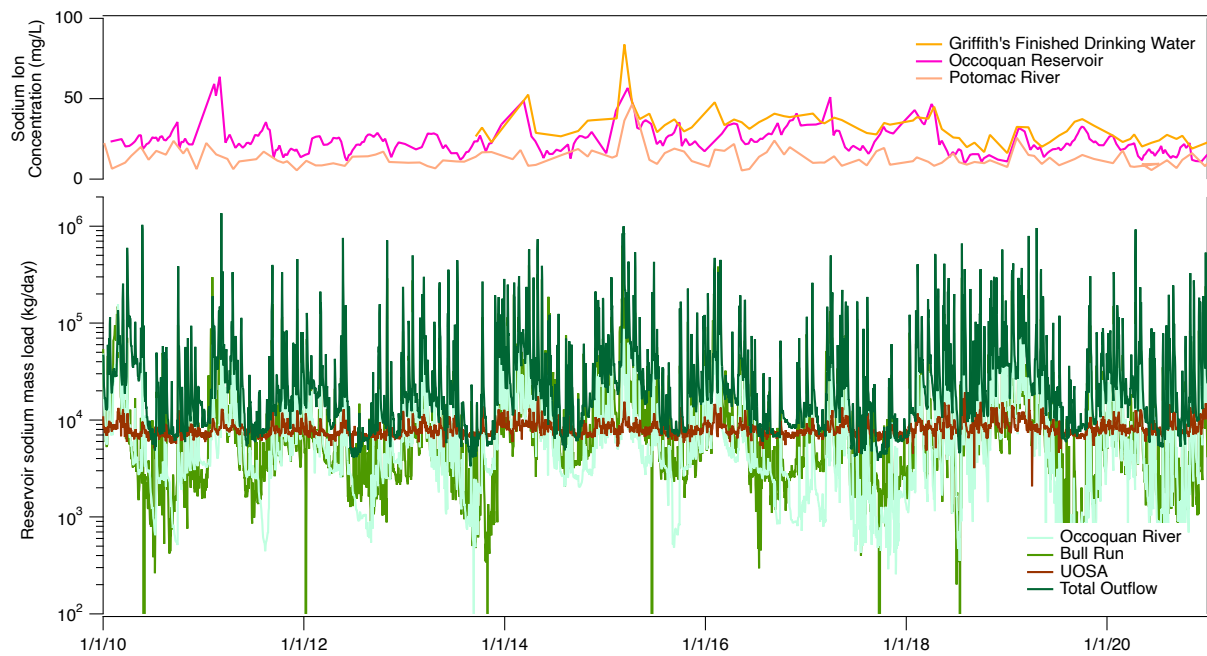


Figure C.2: Top panel: measured sodium ion concentrations in the Potomac River, Occoquan Reservoir and Griffith's finished drinking water. Bottom panel: daily sodium mass load balance for the Occoquan Reservoir. Daily sodium mass loads are calculated by multiplying the daily sodium ion concentration by the daily inflow volume.

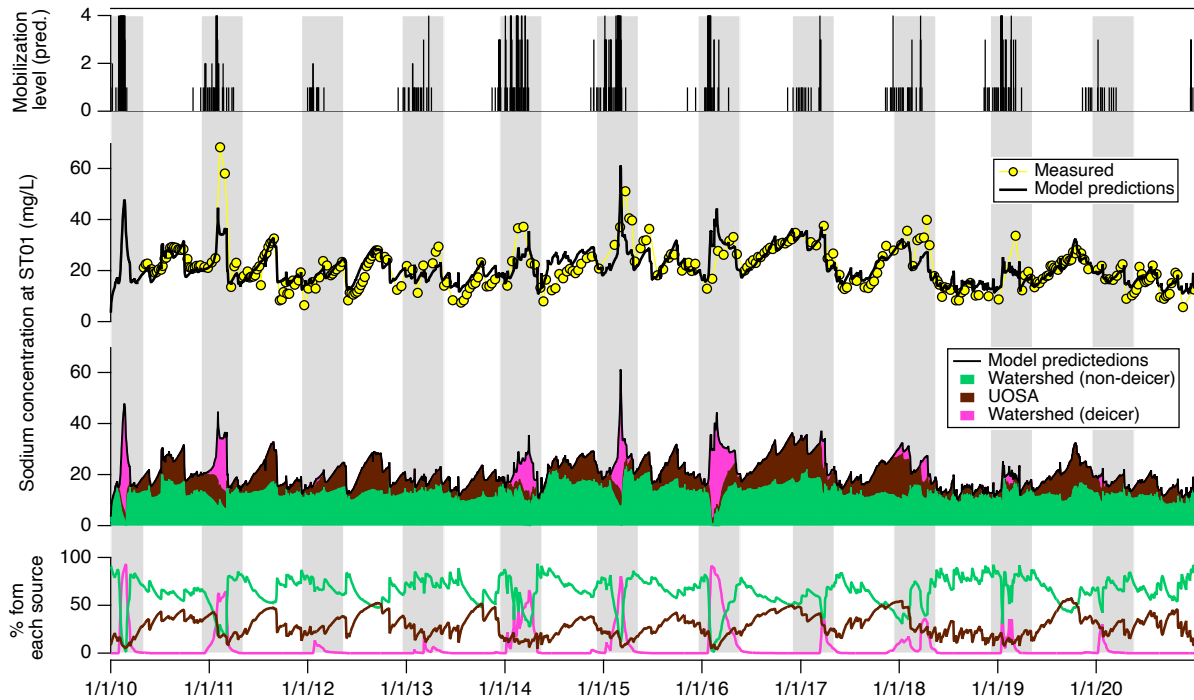


Figure C.3: Top panel: predicted daily winter weather mobilization levels in Northern Virginia. Second panel: measured vs model predicted sodium ion concentrations at ST01. Third panel: source breakdown for the predicted sodium ion concentrations. Bottom panel: percentage of daily sodium concentration from each source. Grey bars denote winter months (December-April).

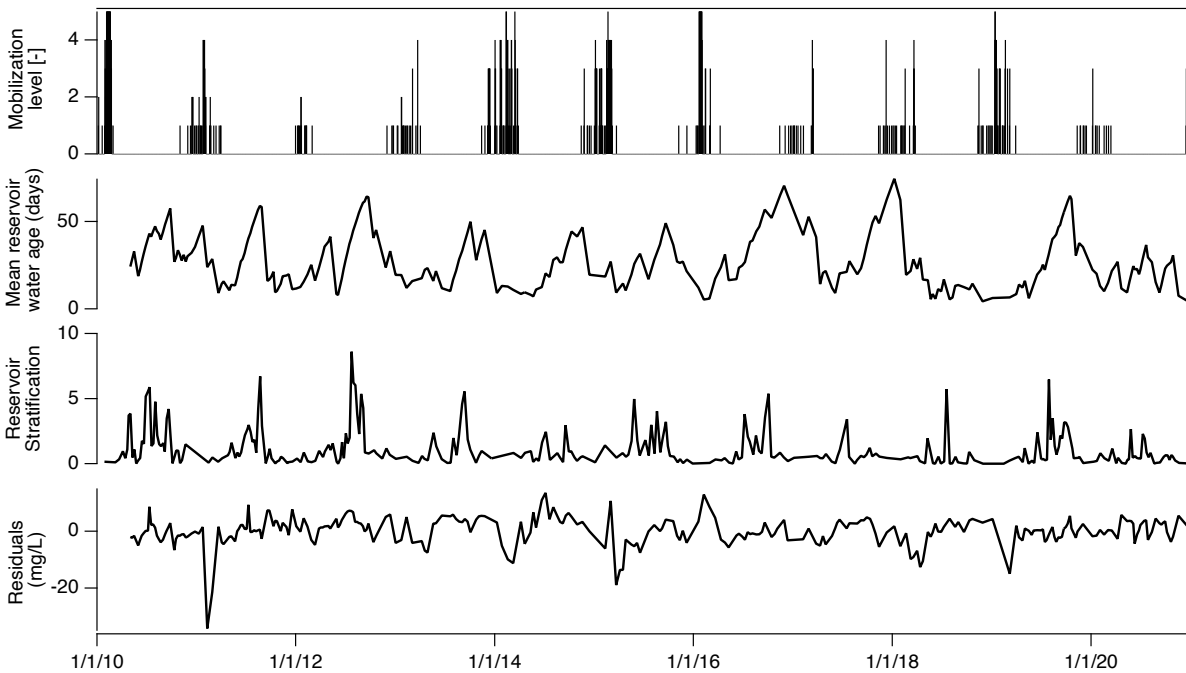


Figure C.4: Top panel: predicted daily winter weather mobilization levels in Northern Virginia. Second panel: mean age of water (in days) stored in the reservoir. Third panel: standard deviation of the reservoir buoyancy frequency calculated from conductivity, temperature and depth profiles near ST01. Higher value indicates greater reservoir stratification. Bottom panel: model residuals computed by subtracting model predictions of sodium ion concentration from measurements. It can be clearly seen that model residuals do not reveal any clear seasonal patterns in relation to reservoir stratification, mean age of water in the reservoir or deicer wash-off events.

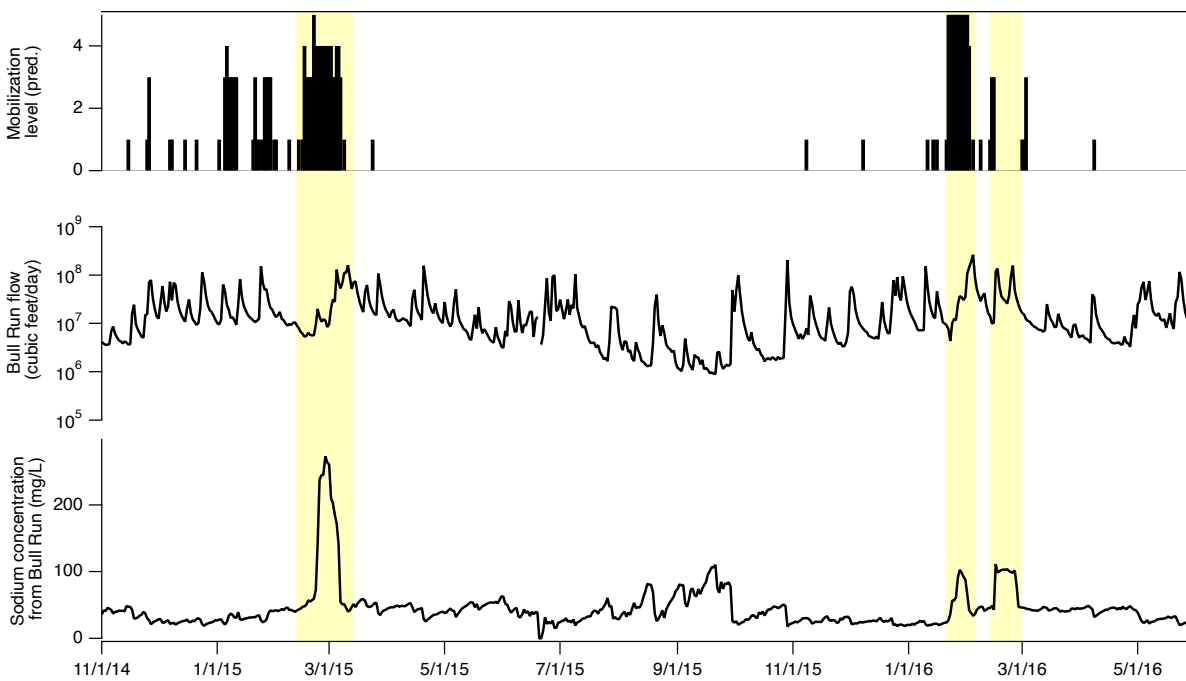


Figure C.5: Predicted daily winter mobilization levels (top panel), daily flow from Bull Run upstream of UOSA (middle panel) and daily sodium concentration from Bull Run upstream of UOSA (bottom panel) for an illustrative two year period. Yellow shaded areas represent events identified as deicer wash-off.

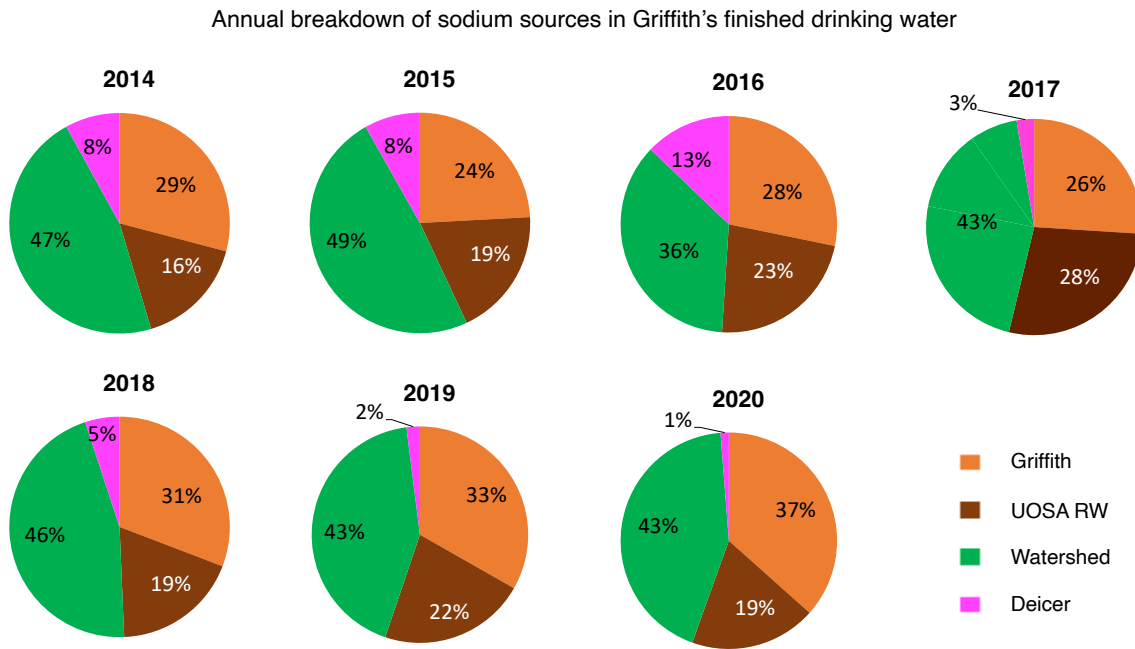


Figure C.6: Annually averaged contributions from different sources to sodium mass load in Griffith's finished drinking water for the years 2014-2020.

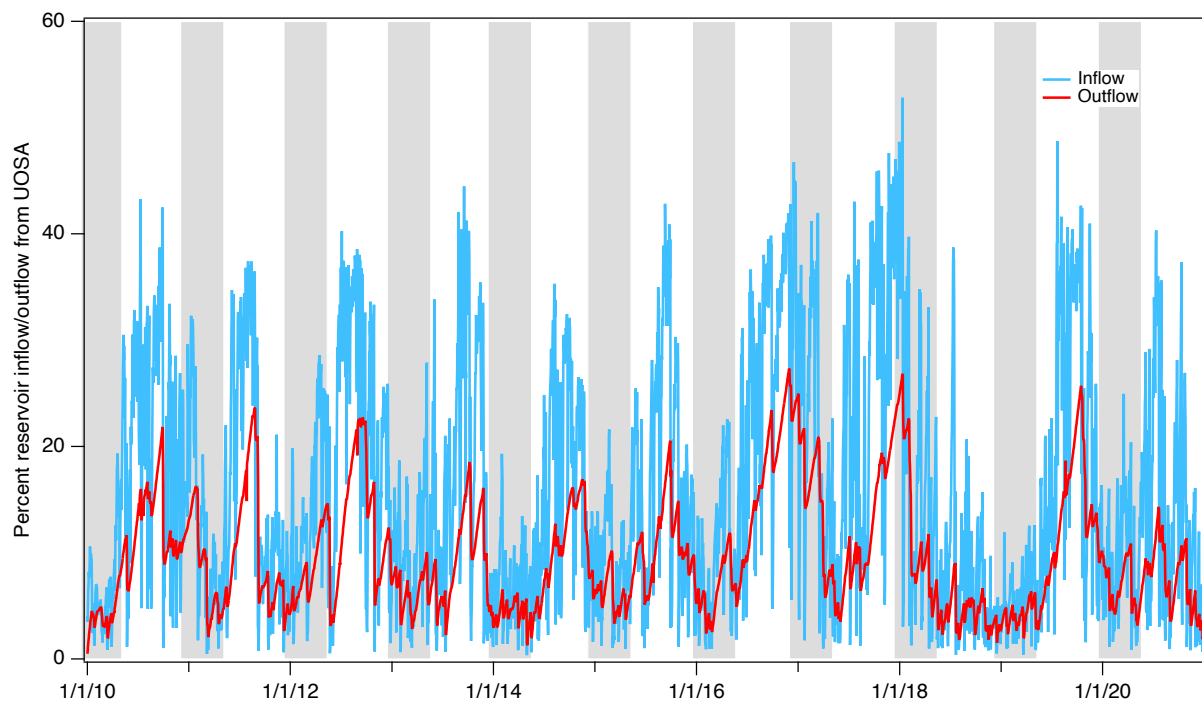


Figure C.7: Fraction of UOSA's flow in daily reservoir inflow and outflow. The latter was calculated by setting  $C_{UOSA} = 1$  mg/L and  $C_{BR} = C_{OR} = C_{UG} = 0$  mg/L in the transit time model.